Role of gangliosides in extracellular vesicle secretion in wild-type and Huntington's disease cell models

by

Vaibhavi Narayan Kadam

A thesis submitted in partial fulfillment of the requirements for the degree of

Master of Science

Neuroscience
University of Alberta

ABSTRACT

Gangliosides are sialic acid containing glycosphingolipids highly enriched in the brain that play vital roles in intercellular communication, cell signalling and calcium homeostasis. A decrease in the ganglioside levels in the brain has been associated with several neurodegenerative diseases. Studies in the Sipione lab have previously demonstrated that the levels of gangliosides, especially ganglioside GM1, are decreased in Huntington's disease (HD). HD is a monogenic neurodegenerative disease characterized by motor impairment and cognitive and psychiatric decline. It is caused by an abnormal expansion in the CAG trinucleotide repeat in the exon 1 region of the huntingtin (*HTT*) gene, which in turn encodes for an abnormally elongated polyglutamine stretch near the N-terminus of the huntingtin (HTT) protein. As a result, the mutant (mHTT) protein misfolds, acquires toxic conformations and aggregates, eventually compromising neuronal function and viability. Past work in the Sipione lab has also shown that restoring normal levels of GM1 by its exogenous administration in HD mouse models has profound therapeutic effects and reduces mHTT levels in the brain. Because GM1 does not affect the transcription of the *Htt* gene, the mechanism underlying its effects on mHTT burden may be at the proteostatic level. Proteomics and Gene Ontology analysis of both wild-type and HD mouse brains treated with GM1 *in vivo* (compared to untreated controls) revealed that the treatment affects the abundance of various proteins of the extracellular vesicle (EV) pathway. EVs are cell-derived, membrane-enclosed particles (30-1000nm) which are involved in intercellular communication and cell signaling and have been found to carry misfolded proteins.

In this thesis, I investigated the hypothesis that cell treatment with exogenous GM1 increases the secretion of EVs containing mHTT. I further investigated the effects of decreasing endogenous ganglioside levels - as observed in HD and other neurodegenerative conditions – on EV and mHTT secretion. My studies demonstrate that cell treatment with GM1 promoted EV release in both normal and HD cells of both neuronal and peripheral origin, without affecting particle size. Furthermore, GM1 restored normal EV secretion in a neuronal cell line stably expressing mHTT (N2a 72Q) that displays reduced GM1 levels compared to wild-type control cells and lower levels of EV secretion. In N2a 72Q cells, GM1 treatment increased the export of mHTT via secreted EVs. On the other hand, pharmacological inhibition of ganglioside synthesis in neuronal cells resulted in impairment of EV secretion and reduced levels of mHTT in EVs. To confirm the effects of endogenous gangliosides on EV secretion, I used a neuronal cell line where *B4galnt4*, the gene that encodes for a major ganglioside biosynthetic enzyme, was deleted by CRISPR-Cas9. The resulting decrease in cellular levels of complex gangliosides in this model resulted in decreased secretion of EVs, a phenotype that could be attenuated by GM1 administration. Thus, overall, my data suggest that cellular ganglioside levels positively correlate with EV release, highlighting a novel role of neuronal gangliosides in EV and misfolded protein secretion. Of note, modulation of cellular gangliosides was found to influence the GM1 content of EVs. As GM1 is known to mediate cell-cell communication and inflammation, future studies will determine whether the abundance of GM1 on the surface of EVs carrying mHTT may determine their fate, by functioning as a ‘code’ to facilitate EV shuttling to microglia cells for uptake and degradation.

PREFACE

This thesis is an original work of Vaibhavi Kadam.

The data presented in Figs. 10, 11, 16.A, 18 and S6 were generated in collaboration with Dr. Luis Carlos Morales, a former PhD student under the supervision of Dr. Simonetta Sipione (Department of Pharmacology, University of Alberta). Data in Figs. S1 and S3 were generated in collaboration with Ms. Anissa Viveiros, a former MSc student under the supervision of Dr. Elena Posse de Chaves (Department of Pharmacology, University of Alberta).

EV analyses by imaging flow cytometry (IFC) were generated in the Flow Cytometry Facility (Faculty of Medicine and Dentistry, University of Alberta) in collaboration with Dr. Aja Rieger (Faculty of Medicine and Dentistry, University of Alberta) who aided with the setup and optimization of the technique.

Nanoparticle tracking analysis (NTA) was performed under the supervision of Dr. Desmond Pink, in the laboratory of Dr. John Lewis (Faculty of Medicine and Dentistry, University of Alberta).

Dynamic light scattering (DLS) data were generated through a collaboration with Dr. Leonardo Cortez (Dr. Valerie Sim's laboratory, Centre for Prion and Protein Folding Diseases, University of Alberta).

ACKNOWLEDGEMENTS

Close to three years ago, I set foot in a foreign place where I knew no one, with three bags and loads of dreams, all because I wanted to study under the tutelage of my supervisor, Dr. Simonetta Sipione. Thank you for granting me the opportunity to learn, unlearn and relearn under you. You have mentored me in all aspects of science - from developing skills of critical thinking and troubleshooting problems to bettering my scientific writing, presentation and even networking abilities. Thank you for showing me by example that our mindset is our biggest asset.

I also owe my gratitude to Dr. Elena Posse de Chaves and Dr. Satyabrata Kar; thank you for being a part of my supervisory committee, for the constructive feedbacks and advice, and for challenging my ideas and keeping me on track. I truly appreciate your contribution.

To Dr. Elena Posse de Chaves, I consider myself fortunate to have been able to work closely under you during my training. Thank you for the invaluable lessons on research you have so generously given.

I am grateful to all members, past and present, of the Sipione lab, especially Ms. Noam Steinberg, Mr. John Monyror, Ms. Jing Huang, Dr. Danny Galleguillos, Dr. Luis Carlos Morales, Mrs. Mel Horkey, Ms. Aislinn Maguire and Mr. Magnus Stenlund, for the innumerable sessions of brainstorming and troubleshooting ideas, and for teaching me to be a better researcher. Big shout out to Noam, Jing, John, and Danny – I will always cherish our times shared at the bench and beyond.

I would also like to extend my thanks to our collaborators from the Posse de Chaves

lab, Ms. Anissa Viveiros and Ms. Sarah Samuelson, for working alongside with zest to accelerate this project.

Ms. Shveta Rai Chhabra, a buddy-turned-roommate-turned-sister, you have been nothing short of a blessing. Thank you for always being there by my side and cheering me on, through thick and thin.

I am very grateful to my friends in Canada and back home in India for the sheer joy, encouragement and support they have offered.

To Pappa, Aai and Mohit, I am because you are. Thank you for always rooting for me. I am forever indebted to everything you have been to me.

TABLE OF CONTENTS

LIST OF TABLES AND FIGURES

CHAPTER 1: INTRODUCTION

1.1 *Gangliosides – synthesis and occurrence in the brain*

Gangliosides are complex glycosphingolipids containing one or more sialic acid residues. Sialic acids are nine-carbon containing acidic sugars that are biosynthesized from *N*-acetylmannosamine and phosphoenolpyruvate [1]. *N*-acetylneuraminic acid is the most abundant sialic acid found in humans. On the other hand, glycosphingolipids are a subclass of glycolipids that contain a hydrophobic ceramide moiety and a hydrophilic sugar head group. Ceramide is the common precursor of glycosphingolipids and is synthesized on the cytoplasmic leaflet of the endoplasmic reticulum (ER) membrane. Of note, the ceramide moiety can be heterogeneous, in that it may contain different sphingoid bases of which C18- and C20- sphingosines are majorly found on gangliosides. Upon transfer to the Golgi, ceramide is subjected to glycosidation by glycosyltransferases and sialyltransferases in a stepwise manner, to synthesize glycosphingolipids [2, 3]. **Fig. 1** shows a simplified scheme of the ganglioside biosynthetic pathway. GM1, a ganglioside that is a major focus of my studies, has two galactose residues, one glucose residue, one *N*-acetylgalactosamine residue and one *N*-acetylneuraminic acid residue linked to the internal galactose through α(2,3) glycosidic linkage (**Fig. 2**).

After being synthesized, gangliosides are transported to the plasma membrane by exocytosis [4]. As the glycan portion of gangliosides faces the lumen of the Golgi apparatus, their orientation at the plasma membrane is with the glycan headgroup exposed to the extracellular space. Thus, gangliosides are present in the outer leaflet

of the plasma membrane with their ceramide moiety anchored into the membrane and the glycan head group extending into the glycocalyx. They are not distributed uniformly but are organized in membrane microdomains called 'lipid rafts' which also consist of other glycosphingolipids along with cholesterol and certain membrane proteins, viz., GPI-anchored proteins, receptor tyrosine kinases, etc. Although they are mainly present at the plasma membrane [5], they also occur in organellar membranes like the endo-lysosomal system [4, 6], mitochondria where GD3 modulates apoptosis [7] and nucleus [8, 9].

Gangliosides are enriched in neuronal membranes [10-12]. They are particularly abundant in the nervous system [13, 14] and account for 10-12% of the total brain lipid content [6]. The human brain contains more gangliosides than the rest of the organs of the body by 10- to 30-fold [15]. The occurrence of gangliosides in the grey matter is 5-fold higher than in white matter [16]. Interestingly, in the human brain, their total amount increases about 3-fold from the gestational week 10 to infancy (about 5 years of age) [17]. GM1 and GD1a increase 12- to 15-fold during this period [17]. More than 90% of gangliosides in the adult brain are represented by the complex gangliosides GM1, GD1a, GD1b and GT1b [18]. Thus, the expression levels of gangliosides change during development and even during ageing, discussed in detail later.

1.2 *Functions of gangliosides in the brain*

The high expression of gangliosides in the brain underscores their crucial roles in intercellular communication, cell signaling, Ca^{2+} homeostasis, membrane dynamics and survival. Gangliosides can exert their functions either by interacting with molecules

(soluble or membrane-bound) outside the cell (*trans*-interaction), or with molecules within the same membrane (*cis*-interaction). Some ganglioside functions that are relevant to and within the scope of this thesis are described below.

Ganglioside-rich lipid domains have been demonstrated to be separate from caveolae [19, 20] that are abundant in cholesterol [21, 22]. During caveolar invagination, the ganglioside-enriched edges of caveolae may favor a strong positive curvature to link the negative membrane to the flat membrane [10]. Furthermore, GM1, in particular, has been found to play key roles in forming and stabilizing lipid membranes. For example, Patel et al. used 1-palmitoyl-2-oleoyl-sn-glycero-3-phosphocholine (POPC) phospholipid bilayers as a model to study clustering and organization of GM1-rich membranes [23]. The group found that GM1-containing membranes showed a higher preference to have a positive curvature. Moreover, increasing concentrations of GM1 favored higher inter-GM1 carbohydrate-carbohydrate interactions that resulted in tighter lipid packing. On the other hand, by using the same lipid model system, Fricke et al. demonstrated that GM1 in liquid phase softens the lipid bilayer thus decreasing its bending rigidity and allowing its deformation to be an energetically conserved process [24]. Observations in giant unilamellar vesicles (GUV) with asymmetric GM1 distribution across the bilayer, that mimic its distribution in neuronal membranes, have also reported GM1 to influence membrane curvature [10, 25] and therefore, neuronal membrane morphology [26]. These findings may contribute to elucidating the role of gangliosides in flexibility of neuronal membranes that may facilitate membrane deformations to induce neuronal sprouting [27], neuronal growth and development [28, 29], and vesicle formation and budding.

Both in cells [30] and in model lipid membranes [31-33], ceramide tends to form separate gel-phase, 'ceramide-rich domains' [34, 35]. These domains may act as sorting platforms for receptors and other components involved in cell signaling [36]. Chiantia et al. reported the enrichment of GM1 in ceramide-rich domains in model membranes that displayed liquid-ordered (raft-like) and liquid-disordered domains along with ceramide-rich phase domains [37]. Interestingly, ceramide also triggers the secretion of extracellular vesicles (EVs), cell-secreted membrane-enclosed particles [38], discussed in detail later.

Gangliosides in the nervous system are also involved in maintaining Ca^{2+} homeostasis. For example, mice lacking GM2/GD2 synthase (*B4galnt1*$^{(-/-)}$) do not synthesize GM2, GD2 and all gangliotetraose gangliosides and have impaired Ca^{2+} regulation capacity [39], suggesting that complex gangliosides may be playing vital roles in maintaining Ca^{2+} homeostasis. Gangliosides at the plasma membrane are involved in modulating Ca^{2+} flux via several Ca^{2+} channels, viz., T-type Ca^{2+} channels [40-42], plasma membrane Ca^{2+}-ATPase (PMCA) [43-45], L-type Ca^{2+} channel [46], among others. Some of these are described below.

As aging proceeds, the capacity to pump intracellular Ca^{2+} out of neurons decreases resulting in elevated cytosolic Ca^{2+} levels [47, 48]. The elevated levels may be, at least in part, due to the age-associated decreased activity levels of PMCA, an integral membrane protein known to efflux intracellular Ca^{2+}, in synaptic membranes [49-51]. Interestingly, maximum activity levels of PMCA were reported in the raft domains of synaptic membranes [52]. Jiang et al. reported that pharmacological inhibition in

neurons by both, D-threo-1-Phenyl-2-decanoylamino-3-morpholino-1-propanol (D-PDMP), which would decrease mono- and polysialogangliosides and by neuraminidase, which would only decrease polysialogangliosides (and increase the GM1 levels), decreased the PMCA activity without any significant effects on PMCA protein levels [45]. Interestingly, treatment with neuraminidase led to lower enzyme activity levels than with D-PDMP, indicating that polysialogangliosides may be increasing while GM1 may be reducing PMCA activity. In contrast, elevation in endogenous gangliosides induced by L-threo-1-Phenyl-2-decanoylamino-3-morpholino-1-propanol (L-PDMP) showed no significant effect on PMCA activity. However, it must be noted that while D-PDMP and L-PDMP will only affect gangliosides, neuraminidase treatment would also affect sialic acid residues on glycoproteins along with gangliosides, potentially influencing the PMCA environment and hence its activity. On the other hand, treatment of neuronal cells with neuraminidase showed that the resulting GM1 enrichment potentiates T-type Ca^{2+} channel activity by increasing Ca^{2+} influx and subsequent neuritogenesis, a process that is inhibited by amiloride, a selective T-type Ca^{2+} channel blocker [40-42].

The neurotrophin family of neurotrophic factors consists of nerve growth factor (NGF), brain-derived neurotrophic factor (BDNF), neurotrophin-3 and neurotrophin-4/5. These are small molecules that are crucial for the survival, growth, and differentiation of cells of the nervous system [53]. Several studies claim that gangliosides, especially GM1, may be exhibiting neurotrophic effects by mimicking endogenous neurotrophins and activating neurotrophic receptors (reviewed in [54]). For example, in rat pheochromocytoma PC12 cells [55] as well as in C6-2B glioma cells overexpressing

the TrkA receptor [56], it was demonstrated that GM1 enhances NGF activity by directly binding to TrkA receptor, which is also a natural receptor of NGF, and enhances NGF-mediated TrkA tyrosine phosphorylation, a measure of its activity levels. Also, GM1 as well as its substrate analogue LIGA20 have been reported to prevent excitotoxicity in cerebellar granule cells by binding to TrkB receptors and mimicking the activity of BDNF [57].

1.3 *Lessons from animal models that lack gangliosides*

Neurological impairments resulting from a decrease in gangliosides highlights their significant role in the brain. Genetically engineered mice with defects in ganglioside biosynthesis at specific steps has enabled understanding the functions of gangliosides [58]. For example, mice with the gene *UDP-glucose ceramide glucosyltransferase* (*UGCG*) disrupted die around day 7.5 of embryonic development and do not show any differentiation beyond development of primitive germ layers [59]. Similarly, *B4galt5* null mice are also embryonically lethal as death occurs at around embryonic day 10.5 [60, 61]. Moreover, mice deficient in *B4galnt1* (GM2/GD2 synthase) mentioned before also show subtle impairment of brain functions and exhibit defects like axonal degeneration [62], myelination defects [62], motor impairment [63] and present with Parkisonian symptoms which were corrected by L-dopa or the membrane permeable GM1-analog LIGA20 [64]. They also have altered lipid raft composition, slower motor nerve conduction, disrupted paranodal junctions and, aberrant ion channel distribution and functioning [65]. Additionally, they have been reported to be sterile and show testicular morphological and functional impairment [66].

Interestingly, mice lacking *St8Sia* (GD3 synthase) do not form GD3 and b-series gangliosides, but yet have a normal life without any developmental defects [67]. This could be likely due to the compensation by other complex gangliosides that are synthesized and functionally replace depleted gangliosides. In another study, however, these mice showed heightened sensory responses to mechanical and chemical stimuli but a reduced response to the formalin test, a model to measure acute pain [68], thus suggesting the crucial role that some or all of the depleted gangliosides play in inflammation and in the sensory nervous system [69]. Double mutant mice developed by crossing these mice with *B4galnt1* gene knock-out (KO) mice express only GM3 as their major ganglioside and are extremely susceptible to sound stimuli, display lethal seizures and sudden death phenotype [67]. A separate study on the double KO model developed showed that although the mice did not present with seizures, they had motor dysfunction, reduced fear response and peripheral nerve loss leading to decreased sensory responses [70]. These mice also showed abnormal neuronal morphology and progressive neuronal degeneration in the cortex [70]. Overall, these studies suggest that GM3 alone cannot functionally replace other gangliosides that may be vital players in the nervous system. Mice lacking *St3gal5* (GM3 synthase) only form 0-series gangliosides and show complete auditory loss due to selective and complete degeneration of the organ of Corti, the auditory sensor located in the cochlea of the inner ear, [71] and enhanced insulin sensitivity [72]. These mice crossed with *B4galnt1* null mice produce double KO mice that do not express any gangliosides and as expected, accumulate LacCer. Although viable, they develop severe neurodegenerative conditions resulting in death at 3 months of age for most

and by 5 months of age for the rest [73]. Thus, these findings highlight the importance of gangliosides in the maintenance, stability, and the overall functional integrity of the nervous system.

1.4 *Gangliosides in ageing and in neurodegenerative diseases*

As mentioned before, the profile and expression levels of gangliosides change throughout development. For instance, the ganglioside profile of the rodent brain during early stages of development majorly includes simple gangliosides like GM3 and GD3. As development progresses, a shift from simple gangliosides to complex gangliosides, viz., GM1, GD1a, GD1b and GT1b, occurs resulting in their predominance in the brain [74, 75]. Moreover, changes in gangliosides also take place during the ageing process.

During normal ageing, analysis of mice whole brains shows an age-associated decrease in GD1a and GT1b and an increase in GM1 [76-78]. LC-MS studies performed to assess age-related changes in gangliosides levels on the synaptic plasma membranes of rat brains also showed that when compared to 6 month old rats, GD1a and GT1b significantly decreased in 23 month old rats while GM1 increased in 34 month old rats [45]. Furthermore, high-performance thin-layer chromatography analysis of whole brains of nine healthy individuals (males) ranging from 25 to 85 years of age showed a decrease in the total abundance of all complex gangliosides with age [79]. Another study investigating ganglioside levels in the post-mortem substantia nigra from 20 healthy subjects (including males and females) between 70 and 90 years of

age showed a decrease in the levels of all complex gangliosides, especially GM1 and GD1a [80].

Several studies have also associated altered brain ganglioside levels to neurodegenerative diseases. A decrease in ganglioside levels is observed in neurodegenerative diseases like Alzheimer's disease (AD) [81, 82], Parkinson's disease (PD) [80, 83], and Huntington's disease (HD) [84, 85], which are protein-misfolding diseases characterized by the misfolding and accumulation of certain proteins leading to their pathological aggregation, eventually compromising neuronal functionality and leading to cellular dysfunction and death.

More specifically, the involvement of gangliosides in neurodegeneration, especially in HD, the focus of my studies, is elucidated in further detail below.

1.5 *Neurodegeneration and Huntington's disease*

HD is characterized by progressive motor dysfunction, cognitive impairment, and psychiatric decline. Motor symptoms can be observed as choreiform movements that include impaired gait followed by bradykinesia and rigidity. Cognitive and emotional deficits are also observed which include cognitive slowdown, decline in attention, frequent experiences of depression and, irritability and apathy.

Although the disease is present in all human populations in the world, its prevalence may vary based on the ancestry of the population. While Asia has the lowest prevalence of HD (0.4 individuals per 1000) [86], populations with European descent have the highest [87]. Of note, North America and the United Kingdom recorded 7.33

and 6.68 cases per 1000 individuals as of 2016, the highest prevalence in the world [86].

Striatal neurons, especially the medium spiny projection neurons, are most susceptible in HD, resulting in striatal atrophy [88-90]. Severe atrophy is also observed in the cerebral cortex [91-93]. A decrease in the volume of the striatum and the cortex can be observed as early as a decade before symptoms develop [94, 95]. Other regions of the brain like the lateral tuberal nucleus of the hypothalamus [96], amygdala [97], thalamus [98, 99], brainstem [100, 101], caudate nucleus and substantia nigra [102] also show degeneration.

1.6 *The Huntingtin gene and protein*

HD is an autosomal dominant disorder caused by the expansion of a CAG repeat in the exon 1 of the huntingtin gene (*HTT*) located on the human chromosome 4. The CAG trinucleotide repeats on the *HTT* gene code for the polyglutamine (polyQ) stretch near the N-terminus of the huntingtin protein (HTT). In normal individuals, the polymorphic CAG trinucleotide repeats 9 – 35 times, with the median being 17 – 20 times [102, 103]. However, in individuals with HD, its repeat number increases to <35 repeats, leading to the encoded mutant HTT protein (mHTT) to have an abnormally elongated polyQ stretch [104], which causes mHTT to misfold and aggregate [105]. Individuals with repeat lengths ranging from 36 to 39 have reduced penetrance and higher age at onset than those with 40 repeats or more [102, 103]. The mean age at onset of the disease is 40 years [106] and death occurs after about 20 years from it. In patients with juvenile onset HD (onset earlier than 20 years of age), the number of

inherited CAG repeats is over 60, however, in some rare cases, the repeat lengths can be in the 40s [107, 108]. Although the CAG repeat length is inversely proportional to the age at onset [109], a significant variance exists in the age at onset for lower CAG repeats, which is likely due to other genetic factors [110, 111].

The *HTT* gene has 67 exons that result in two mRNA transcripts, one of 10,366 bp while the other of 13,711 bp [112]. The latter transcript is more abundant in the brain and differs from the former by a 3' UTR sequence of 3,360 bp [112]. A third transcript has been identified in HD patients, which results from the alternative splicing of the *HTT* mRNA that includes the first exon of the *HTT* gene containing the CAG repeat and thus encodes a shorter N-terminal fragment of mHTT [113-115].

The HTT protein (**Fig. 3**) consists of 3144 amino acids and is about 348kDa in molecular weight. The protein is highly conserved among vertebrates [116-118]. It is ubiquitously expressed in all cells [119] and although predominantly localized to the cytoplasm, it can also be found in the nucleus [120]. Moreover, its expression is highest in the brain [121-124] where it is more abundant in neurons than in glia [121, 123]. HTT is made of several HEAT repeats which are named after the proteins in which they are found, viz., HTT, Elongator factor 3, Protein phosphatase 2A, and TOR1. HEAT repeats consist of two anti-parallel α-helices arranged separated by a non-helical region, and function as scaffolds to mediate intra- and intermolecular protein-protein interactions [125, 126].

The N-terminal domain encoded by exon 1 is the best characterized region of the protein because it contains the polyQ tract that is expanded in HD [127]. The polyQ

tract is preceded by an N-terminal region consisting of 17 amino acids (N17) that form an amphipathic α-helix and can be post-translationally modified by acetylation, ubiquitination and SUMOylation at lysines 6, 9, 15 and phosphorylation at Tyr3, Ser13 and Ser16 that affect mutant HTT toxicity, clearance and localization [128-131]. Gu et al. demonstrated that phosphorylation at Ser13 and Ser16 decreases toxicity and aggregation of mHTT [132]. The N17 domain also contains a nuclear export sequence (NES) and is involved in the intracellular trafficking of mHTT [133, 134]. It is followed by the polyQ region which is larger in mammals compared to other vertebrates, especially humans [127]. The length of the polyQ stretch is directly proportional to the aggregation propensity of the protein [135]. A polyproline (polyP) region follows the polyQ. This region has recently evolved and is only seen in mammals [117]. It forms a proline-proline helix which is vital to maintain the solubility of the protein and thus, influences the propensity of mHTT aggregation [136]. It is also involved in many protein-protein interactions, especially with vesicle-associated proteins [137].

HTT also contains four relatively unstructured PEST (amino acids proline, glutamic acid, serine, threonine) domains [138] that are susceptible to proteolytic cleavage by caspases, cathepsins, calpain, and matrix metalloproteinase MMP10 [139-147]. While the first PEST domain contains the N17 region, the other three are located between HEAT repeats [148]. Proteolysis of the first PEST domain generates N-terminal fragments that have been found to be more toxic than native full-length HTT [149-152]. As previously mentioned, a fragment encoded by exon 1 is also produced by alternative splicing [113-115]. Aggregates of N-terminal fragments have been observed in post-mortem HD brains [121, 153-155]. These toxic N-terminal fragments

can also aggregate to form inclusions in the nucleus along with the cytoplasm [155-157].

Although the exact functions of HTT are still being determined, this scaffold protein has been found to be multifunctional and has many proteins in its interactome [127, 158]. Disruption of the *Htt* gene in homozygous mice results in abnormal gastrulation and embryonic lethality [159-161], suggesting that *Htt* is an important gene for embryonic development and survival. Importantly, HTT modulates the transport of organelles, viz., autophagosomes [162], endosomes and lysosomes [163, 164], amyloid precursor protein (APP)-containing vesicles [165, 166], and others [167, 168] in anterograde or retrograde directions, and in both dendrites and axons of neurons. Some of its relevant functions within the scope of this thesis are discussed below.

HTT interacts with many binding partners that are important players in endocytosis and vesicular trafficking. For example, it interacts with HTT-associated protein 40 (HAP40) to form a complex that directly binds to Rab5 [169], a GTPase associated to early endosomes that regulates their motility along the microtubule network [170]. This complex is then recruited on early endosomes, where it controls the cytoskeletal affinity of early endosomes [169]. Pal et al. demonstrated that elevated HAP40 levels reduced endosomal motility by shifting their transport from microtubules to actin filaments [169]. They further showed that HD cells had upregulated endogenous levels of HAP40 and impaired endosomal motility, a feature that was rescued by selectively ablating HAP40 by RNAi. HTT also activates Rab11, a GTPase found on recycling endosomes, and is necessary for its membrane localization [171]. Moreover, it

interacts with proteins involved in clathrin-mediated endocytosis like the huntingtin interacting protein 1 (HIP1) and huntingtin-interacting protein 1-related protein (HIP1R) [172-174]. Also, HTT is palmitoylated by a palmitoyl transferase, huntingtin-interacting protein 14 (HIP14) [169, 175]. Yanai et al. has reported that expansion of the polyQ stretch decreases HTT interaction with and subsequent palmitoylation by HIP14, and results in elevated neuronal toxicity and inclusion body formation [176].

HTT is also reported to associate with proteins important in synaptic transmission. For example, HTT binds to the Src homology 3 (SH3) domain of postsynaptic density 95 (PSD95) protein, a member of the membrane-associated guanylate kinase family of proteins that binds to NMDA and AMPA receptors to regulate their localization and trafficking [177]. The interaction of HTT with PSD95 is weakened due to the pathological polyQ stretch [178] leading to localization of PSD95 at extrasynaptic sites instead of postsynaptic sites [179], thus affecting glutamate receptor activity and resulting in their excitotoxicity [178].

Importantly, HTT is involved in the formation of autophagosomes and in the regulation of autophagy, a major intracellular degradation pathway that directs cellular contents including misfolded proteins to lysosomes for clearance [180-185]. Autophagosomes generated constitutively at distal axons of neurons are retrogradely trafficked to the cell body [186] by the HTT-HAP1 complex [162]. In HD, mHTT inactivates mTOR, a serine/threonine kinase which suppresses autophagosome formation in nutrient-rich conditions [187], thus initiating autophagosome formation [188]. However, HTT also disrupts cargo recognition by autophagosomes and therefore, although generated in

abundance, they are devoid of any contents [189]. Moreover, mHTT also abrogates the fusion of autophagosomes with lysosomes by impairing the former's motility [162]. Thus, autophagy is dysfunctional in HD. On the other hand, the ubiquitin proteasome system (UPS), another major protein degradative pathway in mammals [180-183], is also compromised in HD [190-194]. As a result, the cellular proteotoxic burden due to the lack of clearance of misfolded proteins like mHTT as well as damaged organelles increases. Of note, mHTT also causes defects in other vital cellular machineries like gene transcription [195, 196] and in mitochondrial regulation and transport [197, 198], discussions on which are beyond the scope of this thesis. Thus, overall, HTT is associated with a loss-of-function as well as a gain-of-function phenotype in HD (**Fig. 4**).

1.7 *Prion-like spreading in HD*

Like AD, PD and HD, prion diseases are also protein-misfolding, neurodegenerative diseases which, however, are characterized by the presence of 'infectious' prions (PrP^{Sc}), the pathogenic form of the normal prion protein (PrP^{c}) [199] expressed in several cell types [200]. PrP^{Sc} is considered an infectious agent because on encountering a non-pathogenic PrP^{c}, it interacts with the normal protein and induces it to misfold through a process termed 'templated conformational change' [201]. In other words, the pathogenic protein can function as a 'seed' to self-perpetuate and spread pathology. The presence of PrP^{c} is necessary for prion spreading in neuronal cells [202]. Indeed, PrP^{Sc} has also been found to propagate from one cell to another where it may recruit PrP^{c} and act as a template for its conversion to a pathogenic

species [203]. Mechanisms identified for facilitating this spread include transfer through EVs [204] and tunneling nanotubes [205-208].

Interestingly, in the recent years, a mounting body of evidence has also reported prion-like propagation in neurodegenerative diseases like AD, PD and HD. As discussed earlier, these diseases share a common pathological hallmark: misfolding and aggregation of certain proteins in and among specific subsets of vulnerable neurons or glial cells. For example, PD is characterized by α-synuclein and its accumulation into Lewy bodies (LB), HD by mHTT and its inclusion bodies and AD by Aβ and tau aggregating into amyloid plaques and neurofibrillary tangles, respectively. Of note, although protein aggregates in neurodegenerative diseases were initially considered pathogenic, recent studies indicate that they may be protective, acting as 'molecular sinks' to sequester more toxic oligomers [209-211]. Moreover, oligomeric intermediates of these toxic proteins have been reported to cause toxicity [211-218]. In other words, neuropathological species of proteins develop at certain loci in the brain and then spread to other areas of the brain resulting in disease progression. The pathological spreading in these diseases can also be supported by their predictable pattern of disease progression (**Fig. 5**). For example, in AD, the trans-entorhinal region is affected first, followed by the entorhinal cortex and then the hippocampus, amygdala and neocortex [219]. Thus, fibrils of Aβ, α-synuclein, mHTT, tau may also spread pathology either by functioning as 'endogenous seeds' to misfold wild-type (WT) proteins and/or by cell-to-cell spreading. Self-propagating fibrils have been reported *in vitro* for Aβ [220], α-synuclein [221] as well as tau [222]. Furthermore, prion-like spreading has also been reported *in vivo* in AD [223-226] and in PD [227-233] by

administering the misfolded proteins involved. For instance, in AD, brain homogenates derived from patients or aged APP-transgenic mice directly administered to young APP-expressing transgenic mice induced Aβ accumulation in the brain [234-237]. Furthermore, by inoculating the same mice with purified brain-derived Aβ fibrils or with synthetic Aβ aggregates, Stöhr et al. demonstrated that Aβ alone is sufficient to induce its accumulation [226]. The authors further reported that brain-derived aggregates showed higher bioactivity than synthetic Aβ aggregates, perhaps due to their higher ability to template, or due to them having a different “strain” (conformation) that leads to faster propagation [226].

Similarly, in PD, patient brain-derived LB extracts injected in WT mice and macaque monkeys induced the conversion of WT endogenous α-synuclein into the pathogenic form and resulted in PD pathology [230]. Synthetic α-synuclein fibrils injected into WT mice also induced cell-cell spread of α-synuclein accompanied by Parkinson-like pathology [227].

Based on the dual hit theory proposed by Hawkes et al. [238, 239], now called the Braak hypothesis [240], PD is caused via the nasal or gastric entry of a pathogen because the early sites of LB pathology reported are the olfactory bulb and the foregut. On the basis of this hypothesis, Rey et al. showed that human α-synuclein injected into the olfactory bulb of WT mice spreads to the brain regions connected to it [229]. Interestingly, in stark contrast with studies that claim α-synuclein fibrils induced LB pathology in mice brains [227, 228, 233], the group found that monomeric and oligomeric, but not fibrillar forms of α-synuclein caused LB pathology. These

discrepancies could be explained by the difference in the strains formed or even by differences in the injected dose and duration of the experiment [229].

A mounting body of evidence has also reported that mHTT can be secreted extracellularly. Jansen et al. have demonstrated the presence of both SDS-soluble as well as insoluble mHTT in media derived from PC12 cells stably expressing mHTT (exon1-74Q-GFP) by western blotting [241]. Polyglutamine aggregates have also found to be internalized by both neuronal and peripheral cells [242].

Importantly, mHTT may also be spreading in a prion-like fashion. Tan et al. showed that exogenous mHTT as well as HD patient- and BACHD transgenic mice-derived CSF (containing mHTT) can seed aggregation in Htt14A2.6 PC12 cells (that express mHTT) and requires the mHTT template [243]. Moreover, on exposing a human neuroblastoma cell line to N-terminal HTT fragments with 25Q (wtHTT) or 48Q (mHTT), immunohistochemistry results suggested the presence of mHTT in more number of cells with greater puncta compared to wtHTT [244]. To test the prion-like behaviour of mHTT fibrils, the cells were further incubated with fibrils of wtHTT and mHTT for 5 days, after which increased aggregation of mHTT was observed over wtHTT by filter retardation assay, a method used to capture and measure protein aggregates, and by immunohistochemistry [244]. mHTT aggregates also colocalized with endogenous HTT, thus suggesting the recruitment of the WT protein into aggregates, in line with other studies [242, 245, 246]. Surprisingly, by filter retardation assay, the cells exposed to wtHTT also showed the presence of HTT aggregates. However, wtHTT cannot self-aggregate by itself [247]. Therefore, the presence of

wtHTT aggregates in those experiments could be a consequence of sonicating the sample before loading it on the membrane, as sonication causes protein aggregation [248].

Herrera et al. provided further evidence to show the intercellular spreading of mHTT by transfecting cells with wtHTT (exon1-25Q) or mHTT (Exon1-103Q), both of which were fused to non-fluorescent halves of the Venus protein which fluoresces when it is fully reconstituted, i.e., when HTT dimerizes. By measuring this fluorescence by flow cytometry, the group observed cell-cell mHTT propagation and speculated that monomers and oligomers may diffuse more easily than their inclusion bodies to 'infect' neighbouring cells [249]. Cicchetti et al. also demonstrated the presence of mHTT in normal, genetically unrelated fetal neural allografts transplanted into the brains of HD patients [250]. Pecho-Vrieseling and colleagues observed transneuronal mHTT spreading in human stem-cell derived neurons functionally integrated into organotypic brain slices derived from R6/2 mice, a transgenic HD model [150]. They also showed propagation of mHTT in a mixed-genotype model, wherein mHTT spread from R6/2 cortical neurons to WT medium spiny neurons as well as through *in vivo* systems in the corticostriatal pathway where mHTT was observed in medium spiny neurons after its viral delivery to the cortex. Finally, they showed that in their *ex vivo* systems, spreading was largely blocked upon botulinum toxin treatment that inhibits synaptic vesicle fusion. These findings suggest that mHTT propagation may be dependent on synaptic activity or one or more of the components of the synaptic machinery. Nonetheless, the potential off-target effects of the toxin treatment on mHTT propagation should not be ruled out [251].

Interestingly, Jeon et al. found that implantation of either human HD fibroblasts or induced pluripotent stem cells (iPSCs) into cerebral ventricles of normal and genetically unrelated neonatal mice transmitted mHTT aggregates to the host tissue resulting in the onset of both motor and non-motor HD phenotypes [252]. Importantly, they were the first group to show the presence of mHTT in EVs, discussed later.

1.8 *Gangliosides in HD*

Previously published studies from the Sipione Lab have demonstrated a decrease in the levels of GM1 and other gangliosides (GT1b and GD1a) in the striatum and cortex of YAC128 mice [85], a transgenic model of HD that expresses full-length human *HTT* gene with 128 CAG repeats [253]. The levels of GM1 were also reduced in rat striatal cell lines as well as in human HD fibroblasts. A downregulation in the expression of genes encoding enzymes involved in the ganglioside biosynthetic pathway in HD cell models was also observed, suggesting that decreased ganglioside levels in HD are due to decreased synthesis [85]. Treatment of striatal STHdh$^{111/111}$ HD cells with GM1 restored normal cellular ganglioside levels and increased their survival in growth factor deprivation conditions, at least in part, by activating the AKT pathway and by reducing mHTT toxicity by increasing its phosphorylation at serine 13 and 16 [85, 254]. The latter is a post-translational modification that was shown to affect mHTT folding and clearance [128, 132]. On the other hand, inhibition of cellular gangliosides in WT striatal STHdh$^{7/7}$ cells increased cell death in apoptotic conditions to levels observed in HD, suggesting that gangliosides modulate the susceptibility of cells to growth factor deprivation and potentially to other stress stimuli [85]. Importantly, the *in vivo* effects

of GM1 were also investigated in three different genetic mouse models of HD, namely the previously mentioned transgenic YAC128 [253], R6/2, a transgenic model that expresses exon 1 of human *HTT* gene with 150 CAG repeats [150] and Q140, a knock-in model in which the exon 1 of human *HTT* with 140 CAG repeats is inserted into the mouse *Htt* gene by replacing its exon 1 [255]. Accordingly, intracerebroventricular (ICV) infusion of GM1 corrected motor impairments in all three models, cognitive and psychiatric dysfunctions in YAC128 and Q140 mice, and slowed down neurodegeneration and improved neuropathology in R6/2 mice [254, 256] (**Fig. 6**). Of note, the treatment reduced both SDS-soluble mHTT and its SDS-insoluble aggregate levels [254, 256] (**Fig. 6**). Past studies in the lab to investigate the mechanism behind the disease-modifying effects of GM1 in HD have found that GM1 does not cause changes in the transcription of the *Htt* gene [256]. Thus, the decrease in cellular mHTT levels must be due to proteostatic mechanisms that enhance its clearance.

Previous studies in our lab have ruled out the involvement of autophagy, a major protein degradation pathway [180-183], in the GM1-mediated clearance of mHTT (Dr. L.C. Morales, unpublished data). Instead, interestingly, preliminary proteomics analysis of HD mouse brains treated with GM1 compared to untreated controls revealed that the EV pathway is one of the pathways most significantly affected by treatment with GM1 *in vivo* in both WT and HD brains (**Fig. 7**). Based on these data, a main hypothesis in my thesis is that GM1 promotes the export of mHTT via EV secretion as a mechanism to reduce mHTT in vulnerable neurons.

1.9 *Extracellular vesicles*

1.9.1 *Background*

EVs are membrane-bound, nano-sized particles that play key roles in intercellular communication, cell signaling, maintaining cellular homeostasis and proteostasis. They can transfer information by carrying various biomolecules such as proteins, lipids, and nucleic acids. EV release by cells is an evolutionarily conserved phenomenon seen in both prokaryotes and eukaryotes [257].

EVs were first reported in 1946 by Chargaff and West when they observed that high speed centrifugation of blood plasma resulted in lipid-rich sediments with procoagulant factors [258]. These were later referred to as ‘platelet dust’ in 1967 by West [259]. The term “extracellular vesicle” was first used in a manuscript in 1971 [260]. Many research groups have found EVs to be present in most biological fluids like urine, cerebrospinal fluid (CSF), saliva, breast milk, plasma, seminal fluid, synovial fluid, etc. [257]. In the CNS, EVs are important for neurobiological functions like synaptic neurotransmission and synaptic plasticity [261].

EVs are a heterogenous group of vesicles that, based on their origin and pathway of biogenesis, can be classified as exosomes, microvesicles or apoptotic bodies (**Fig. 8**). Apoptotic bodies are vesicles shed by cells due to membrane blebbing during apoptosis. Both exosomes and microvesicles are shed by living cells and have overlapping properties even though their pathways of biogenesis are distinct, which makes it impossible to discriminate them from each other with the currently available

methods [262-264]. Thus, we will use the term EV to refer to both exosomes and microvesicles.

1.9.2 *Exosomes*

The existence of these EVs was demonstrated while studying reticulocyte formation [265, 266] and the word ‘exosome’ was coined to describe them [267]. Their secretion was later described in neurons [268], immune cells [269, 270] and others [271, 272]. Exosomes (30 – 120nm in size) originate from the endocytic pathway by the intraluminal budding of the membrane of multivesicular bodies (MVBs) to form intraluminal vesicles (ILVs). MVBs subsequently fuse with the plasma membrane to release these ILVs as exosomes into the extracellular environment.

The mechanisms behind exosome biogenesis and secretion have not yet been completely elucidated, however, the evolutionarily conserved Endosomal Sorting Complex Required for Transport (ESCRT) machinery [273] has been extensively described to be involved in their formation [274-276]. It comprises of about 20 proteins assembled into four ESCRT (ESCRT-0, -I, -II, -III) complexes along with associated proteins. The complexes are numbered in the order in which they participate in the yeast ESCRT pathway [277]. The ESCRT-0 complex localizes to endosomes by interacting with phosphatidylinositol-3-phosphate (PI3P), a lipid enriched on endosomes, and is responsible for the recognition of ubiquitinated proteins as cargo and their recruitment to the endosomal membrane. It also recruits ESCRT-I by interacting with its component TSG101. The ESCRT-I complex further interacts with and recruits ESCRT-II and both complexes together induce membrane budding with

sequestered cargo. Next, ESCRT-III, recruited by accessory protein ALG-2-interacting protein X (Alix) via interaction with TSG101 of ESCRT-I and CHMP4 of ESCRT-III [278, 279] is responsible for vesicle scission into the MVB lumen. Recent findings showed that Alix orchestrates ILV formation through the syndecan-syntenin-Alix pathway. According to these studies, heparanase cleaves the heparan sulphate chains on syndecans, which are transmembrane proteoglycans. The cleavage results in the formation of syndecan microdomains that interact with the adaptor protein syntenin and syntenin, in turn, directly interacts with Alix to facilitate ILV formation [280, 281]. Finally, the Vps4 complex, that consists of the type I AAA-ATPase Vps4 and its cofactor Vta1, disassembles and recycles the ESCRT-III complex [282]. Recently, binding of Vps4 ATPase to ESCRT-III has also been demonstrated to induce membrane neck constriction for ILV biogenesis [283].

Many studies have demonstrated that depletion of specific components of the ESCRT machinery did not inhibit the formation of MVBs, thus suggesting the involvement of ESCRT-independent mechanisms in ILV formation and exosome biogenesis [284]. These mechanisms involve proteins like tetraspanins and heat shock proteins and/or lipids. For example, tetraspanins, like CD9, CD63, CD81, are transmembrane proteins that form clusters of tetraspanin-enriched microdomains (TEMs) which interact with a large number of proteins, are highly enriched in EVs [285-288], and have been implicated in ECRT-independent exosome biogenesis. For example, bone marrow dendritic cells derived from CD9 KO mice showed impaired exosome secretion compared to WT [289]. In melanoma cells, the sorting of PMEL, a transmembrane melanosomal protein, to ILVs occurs in an ESCRT-independent manner [290] by the

participation of CD63, a tetraspanin mainly localized on late endosomes and lysosomes [291]. Several studies on cancer cells have also highlighted that increasing intracellular Ca^{2+} levels enhances EV secretion [292-295].

Other than proteins, lipids are also instrumental in exosome biogenesis and sorting. By silencing specific enzymes, many studies have demonstrated specific lipids to be important players in exosome formation. For example, mouse oligodendroglia exosomes are enriched in ceramide. In these cells, treatment with GW4869, an inhibitor of neutral sphingomyelinase2 (nSMase2), an enzyme that catalyses the hydrolysis of sphingomyelin into phosphocholine and ceramide, resulted in decreased exosome secretion of the proteolipid protein (PLP). The authors proposed that ceramide formation triggers the release of exosomes and that the conical shape of ceramide likely causes intraluminal budding by favoring a negative membrane curvature [38]. Supporting the role of ceramide in exosome secretion, Yuyama et al. also highlighted the role of sphingolipid metabolism in the secretion of exosomes derived from N2a cells as well as primary neurons, and showed that inhibiting nSMase2 reduced exosome secretion, while blocking sphingomyelin synthase 2 (SMS2), the enzyme that converts ceramide to sphingomyelin, increased it [296]. Many groups now use nSMAse2 inhibitors to determine whether EVs are exosomes [289, 297-299]. However, its inhibition does not decrease exosome secretion in all cell lines [272, 300, 301] possibly due to the different subcellular localizations of nSMase that result in ceramide formation at different locations [302, 303].

Phospholipase D2 (PLD2), which catalyses the hydrolysis of phosphotidylcholine to phosphatidic acid and choline, is enriched in exosomes and involved in their biogenesis [304, 305]. Phosphatidic acid enriched in the inner leaflet of the MVB membrane, may induce negative membrane curvature, like ceramide [305, 306]. Also, both siRNA-mediated genetic knockdown or pharmacological inhibition of PIKfyve, the kinase that converts PI(3)P to PI(3,5)P2, inhibits the fusion of lysosomes with MVBs as well as autophagosomes and, increases exosome secretion [307].

Cholesterol is also enriched in exosomes [304, 308, 309]. Genetic and pharmacological approaches to increase cholesterol accumulation in MVBs have shown to stimulate the secretion of exosomes [310]. By using a pulse-chase assay for lipid-raft components, viz., GM1 and transferrin receptor, Tan et al. observed that exosomes from mesenchymal stem cells may be derived from the endocytosis of lipid rafts present on the plasma membrane of parental cells [311].

1.9.3 *Microvesicles*

Microvesicles, also referred to as ectosomes, microparticles or shedding vesicles, are 100 – 1000nm in size. They are formed by the outward budding and subsequent pinching of the plasma membrane. The first EVs reported were microvesicles [258]; they were referred to as ‘platelet dust’ [259] as mentioned before. The distribution of phospholipids on the plasma membrane influences microvesicle biogenesis. Phospholipids are asymmetrically distributed across the plasma membrane; the outer leaflet is enriched with phosphotidylcholine (PC) and sphingomyelin, while the inner leaflet contains higher amounts of phosphatidylserine (PS) and

phosphatidylethanolamine (PE) [312]. Three type of proteins are important for the biogenesis of microvesicles: aminophospholipid translocases such as flippases (inward-directed pump) and floppases (outward-directed pump) that are responsible for the movement of lipids across the membrane leaflets in an ATP-dependent process, and a Ca^{2+}-dependent scramblase which facilitates bidirectional lipid mixing in an ATP-independent manner. Ca^{2+} Influx into the cytosol not only activates scramblase leading to redistribution of membrane lipids and exposure of PS on the outer leaflet, but also activates a cysteine protease calpain which induces cytoskeletal remodeling, separating the cytoskeleton from the membrane, thus leading to membrane blebbing [313, 314]. The PS present on the surface of microvesicles also functions as an 'eat-me-signal' for immune cells [315]. The presence of PS on EVs is frequently used to identify them as microvesicles [315]. However, recently, cryo-electron microscopy observations in plasma-derived EVs have noted the presence of microvesicles that do not bind to Annexin V, a protein that binds with high affinity and specificity to PS [316], thus suggesting the existence of PS-negative microvesicles [317]. The presence of PS-negative microvesicles in plasma has also been supported by Connor et al. [318]. However, it cannot be excluded that these PS-negative microparticles may in fact be exosomes.

Phosphatidylinositol 4,5-bisphosphate (PIP2) is present on the inner leaflet of the plasma membrane [319] and contributes to anchoring the membrane to the cytoskeleton [320] and to regulate actin dynamics [321]. A decrease in cytoskeleton-membrane anchorage by hydrolysis of PIP2 [320, 322, 323] can induce membrane blebbing and thus, microvesicle release.

Acid sphingomyelinase, an enzyme that converts sphingomyelin to ceramide at acidic pH found in late endosomes and lysosomes, is also involved in microvesicle biogenesis. For instance, in astrocytes, activation of the ATP receptor $P2X_7$ stimulates the phosphorylation of P38 MAP kinase which then induces the recruitment of acid sphingomyelinase from the lumen of lysosomes to the outer leaflet of the plasma membrane to catalyse the hydrolysis of sphingomyelin to ceramide [324]. These studies have also been confirmed in macrophages [325].

Menck et al. investigated the impact of inhibiting nSMases (also known as SMPD2 and 3) on the secretion of EVs by SMPD2/3 inhibition either genetically by RNAi or pharmacologically by GW4869. Of note, EVs were isolated by differential centrifugation. Interestingly, the group found that both approaches decreased the secretion of EVs pelleted at 100,000 x g (*bona fide* exosomes), but increased the secretion of EVs that could be pelleted at 14,000 x g (suggested to be microvesicles) and that also had higher levels than normal of sphingomyelin [326]. Thus, the authors of this study suggested that nSMase inhibition differently alters the lipid composition levels of specific EV subpopulations. However, due to the isolation method employed, which does not allow for the absolute separation of EV subpopulations due to their overlapping sedimentation coefficient and size [326, 327], these data have to be interpreted with caution.

The ESCRT family may also be involved in microvesicle biogenesis. TAT5 is a conserved P4-ATPase that is localized to the plasma membrane to maintain PE symmetry. It is regulated by Class III PI3K, DnaJ protein RME8 and sorting nexin

pathways [328]. Loss of TAT5 activity in *Caenorhabditis elegans* results in PE externalization on the outer leaflet of the plasma membrane and the release of microvesicles through the ESCRT machinery [328]. Also, similar to the interaction between the Gag protein of the human immunodeficiency virus (HIV) and TSG101 that enables Gag to recruit TSG101 and other ESCRT proteins from the endosomal membranes to the plasma membrane for viral budding [329-331], microvesicle budding can also occur by the direct interaction of TSG101 with the plasma membrane localized Arrestin domain-containing protein 1 (ARRDC1) which recruits it to the plasma membrane [332]. The authors claim that the vesicles are distinct from exosomes because they lack late endosomal markers like CD63 and LAMP1. However, CD63 has been found on microvesicles [333], although expression of EV markers in general may vary based on cell-type [333-335].

1.9.4 *Crosstalk between EV release and autophagy: An overview*

Autophagy is an essential cellular pathway vital for the maintenance of proteostasis and delivers damaged as well as misfolded proteins to the lysosome for degradation [184]. This pathway is impaired in neurodegenerative diseases [336-338]. Interestingly, several studies have demonstrated a close association of the autophagic machinery with EV biogenesis. The two pathways co-ordinate with each other to remove proteins destined for degradation and thus, contribute to alleviate proteotoxic stress [339]. Furthermore, defects in the autophagy-lysosomal pathway have been shown to enhance EV secretion to attenuate proteotoxic stress [339-342]. For example, bafilomycin A_1 -mediated inhibition of the autophagy-lysosomal pathway in

α-synuclein-expressing cell and animal models increased the secretion of α-synuclein through exosomes [343]. Thus, in neurodegenerative conditions, which are marked by autophagic dysfunction, cells may enhance the employment of the EV machinery as a compensatory mechanism to secrete the toxic protein out of the cell and thereby reduce its proteotoxic load. The secretion of these EVs carrying misfolded proteins may have detrimental as well as beneficial effects as outlined below.

1.10 *EVs in neurodegeneration and HD*

As mentioned before, EVs secreted by brain cells in protein misfolding diseases have been found to carry the pathogenic proteins that are the hallmark of those conditions [344-347]. The secretion of EVs carrying these misfolded proteins could be a mechanism to increase disease pathogenesis by spreading the toxic proteins in a cell-to-cell manner [348-350]. On the other hand, it could also function as a pathway to export them out of the cell to reduce proteotoxic stress [348, 351, 352]. Thus, in the context of neurodegenerative diseases, EVs are considered a double-edged sword.

Rajendran et al. first reported that in AD, Aβ is packaged in exosomes and released into the extracellular environment [346]. Several studies have also shown that Aβ and tau accumulate and spread in a prion-like manner through EVs [345, 353, 354]. Furthermore, Aβ plaques in mouse brains and autopsied brains of AD-affected patients were found to be enriched in exosome markers [346, 355].

EVs have also been shown to be involved in the pathogenesis of PD. The first evidence to point out that α-synuclein oligomers are packaged in EVs was given by Danzer et al. [356]. These findings have been supported by other research groups [345, 357,

358]. Moreover, PD patient plasma-derived EVs carrying monomeric and oligomeric α-synuclein stereotaxically injected *in vivo* in the striatum of mice are taken up by microglia [359], immune cells of the CNS which surround neurons and survey the environment to clear out damaged and obsolete material [360, 361]. Similar results were observed when these EVs were administered to the microglial cell line, BV-2 and to human microglia *in vitro* [359]. Exosome uptake resulted in increased microglial proliferation and elevated secretion of proinflammatory cytokines and nitric oxide [359], thus potentially contributing to neurotoxicity [362, 363].

In the case of HD, Jeon and colleagues were the first group to demonstrate that EVs transfer mHTT from cell to cell by injecting EVs derived from human HD fibroblasts into cultures of mouse neural stem cells *in vitro* and into neonatal WT mice *in vivo*. Moreover, in the mice exposed to EVs *in vivo*, mHTT could be detected in the striatum three weeks after implantation and HD manifestations were observed as early as eight weeks post-implantation [252]. Zhang et al. also showed the presence of mHTT-GFP and the expanded repeat RNA in EVs derived from human 293T cells overexpressing mHTT-GFP [364]. Importantly, by co-expressing N-terminal fragments (571 amino acids) of wtHTT (25Q) or mHTT (72Q) in mouse neuroblastoma Neuro2a (N2a) cells, Trajkovic et al. showed that mHTT is preferentially secreted over wtHTT in the culture medium. Moreover, most of the mHTT secreted extracellularly was in the free form and only about 8% was found in the EV pellet [365]. However, in their studies, EVs were isolated by ultracentrifugation which, as discussed in detail later, only sediments less than 10% of the total EVs in the medium. Thus, we cannot rule out the possibility that a significant portion of EVs and hence, mHTT associated to them, must have been

retained in the supernatant, thereby confounding the results. The group also observed that the secretion of mHTT was diminished by cell treatment with GW4869, an nSMase2 inhibitor as mentioned before, and was regulated by phosphatidylinositol 3-kinase (PI3K) [365].

While EVs containing misfolded aggregates such as mHTT, α-synuclein, Aβ and tau may be playing a role in the pathogenesis of neurodegenerative diseases, their release from their cell of origin can in fact serve a neuroprotective function by increasing the export of the toxic protein to alleviate the proteotoxic burden of the cell. For example, in conditions of cellular stress, transglutaminase 2 recruits mHTT, BCL2-associated athanogene 3 (BAG3, a co-chaperone involved in mHTT clearance [366]), and the EV markers Alix and TSG101 into EVs which are released in the extracellular environment [367, 368]. CSPα, a synaptic chaperone that aids in presynaptic protein folding [369], is secreted via EVs and enhances the export of mHTT in EVs [370], a finding that has been extended to other neurodegenerative diseases [370, 371]. Of note, the inactive mutant $CSP\alpha_{HPD\text{-}AAA}$ does not promote the export of the pathogenic protein.

Hong et al. claimed that mHTT impairs EV secretion in astrocytes by comparing the levels of EV markers, Alix and Flotillin-1, released into the medium of cultured astrocytes from WT and HD knock-in mice, by immunoblotting [372]. Of note, immunoblotting analyses were performed by normalizing EV marker signals in EV fractions over their corresponding signals in parent cell lysates, and both WT and HD astrocytes showed same levels of marker proteins. However, normalization of data performed in this manner could lead to potentially confounding results since EV marker

levels can differ based on cell type [333-335]. In other words, equivalent marker levels in parent cell lysates does not necessarily imply that the EVs secreted would also have similar expression levels as their parent cells. Thus, the lower EV marker levels in HD astrocytes compared to WT are not sufficient to imply decreased EV secretion and call for further investigation on the 'number' of EVs released. In this study, mHTT could not be detected in EVs isolated by ultracentrifugation, therefore it remains unclear whether it would be secreted via EVs. Interestingly, the authors of this study showed that EV secretion is inhibited in cells expressing mHTT by inhibition of expression of αB-crystallin, a heat shock protein enriched in astrocytes [373] that is known to prevent fibril formation and aggregation in HD, AD and PD [374-377], and also to mediate exosome secretion [378]. Of note, overexpression of αB-crystallin rescued the low EV secretion phenotype and decreased mHTT aggregates as well as reactive astrocytes, an early pathological feature in HD [372].

Furthermore, exosomes from adipose stem cells significantly decreased the accumulation of mHTT aggregates in R6/2 neuronal cultures *in vitro* as measured by western blotting and immunocytochemistry [379]. Also, p-CREB-PGC1α pathway, a mitochondria-associated pathway downregulated due to mitochondrial dysfunction in HD [380] is also activated, in line with other studies that highlight the therapeutic potential of upregulating the pathway in HD [381, 382].

The protective role of EVs has also been reported in other neurodegenerative diseases like AD and PD. For example, in PD, Tomlinson et al. reported that microvesicles from PD patient-derived sera have a protective effect on primary rat cortical neurons

subjected to cellular stress [383]. Interestingly, Grey et al. have demonstrated that exosomes derived from neuroblastoma cells promote α-synuclein aggregation, and the aggregation kinetics depended on the lipid composition of the vesicles [384]. Furthermore, small unilamellar vesicles (SUV) prepared of GM1 or GM3 promoted α-synuclein aggregation in a concentration-dependent manner, suggesting the role of exosomal lipid components in driving α-synuclein aggregation [214]. This could perhaps be a compensatory protective mechanism, given that aggregates are reported to be less toxic than oligomers [209-211].

On the other hand, in the context of AD, An et al. showed that *in vivo* intracerebroventricular administration of N2a- or human CSF-derived EVs to rats rescued the Aβ-mediated impairment of long term potentiation (LTP), primarily through the sequestration of Aβ oligomers with PrP^{c}, an exosomal surface protein [385]. Importantly, EVs carrying pathogenic proteins may be secreted extracellularly to subsequently degrade the pathogenic material outside the parent cell. Indeed, recent studies by Yuyama and colleagues have demonstrated that both rat primary microglia and BV-2 internalize extracellular Aβ to a greater extent in the presence of N2a-derived exosomes compared to their absence. Moreover, in BV-2 cells, the internalized exosomes along with Aβ colocalized in the lysosomal compartment, thus destined for clearance [296]; these findings would be discussed in detail later.

1.11 *Methods for the characterization of EVs*

Although the field is rapidly advancing, the isolation and the analysis of EVs is still quite challenging due to the small size of EVs and the complexity of EV phenotypes

and subpopulations. Numerous methods have been developed in recent years to improve EV isolation and characterization. However, every method has some drawbacks [386, 387]. Presently, there is not one single method that can be employed to accurately determine the number, size, phenotype, and other characteristics of EVs [387]. Moreover, data variability can be a major challenge in the field of EV biology [388]. Hence, it is of utmost importance to use multiple, complementary techniques to corroborate findings [389]. At the same time, methods used to analyse EVs must be considered and chosen carefully depending on the scientific question [389]. Due to the complex heterogeneity of the EV population, increasing emphasis is being given to technologies that allow single-particle analysis [390, 391].

EVs can be characterized based on their number, size, and density. They can also be characterized based on phenotypic markers present on them, which might provide insight into their cellular origin and/or function and fate [333, 392]. Such methods employed to generate data documented in this thesis are discussed below. They include nanoparticle tracking analysis (NTA), dynamic light scattering (DLS), imaging flow cytometry (IFC), Cytoflex flow cytometry and, iodixanol density gradient centrifugation.

1.11.1 *Investigating EV particle size*

Nanoparticle Tracking Analysis (NTA) allows for the determination of the size distribution of EVs in a liquid suspension by monitoring their Brownian movement [387, 393, 394]. First, a laser beam incident on the sample illuminates it and the particle Brownian motion is recorded as a video sequence in real-time by a charge-coupled

device (CCD) camera which is oriented at a 90° angle to the illumination plane. Through the camera, the NTA program identifies and tracks the center of each individual particle simultaneously to calculate the mean particle velocity. Using this information and knowing the sample temperature and solvent viscosity, the program determines the particle hydrodynamic diameter using the Stokes-Einstein equation. According to the manufacturer (NanoSight Instruments, Mavern, UK), NTA can detect particles ranging in size from 10nm to 1000nm in solution. However, due to the low refractive indices of EVs, their limit of detection for NTA is 30 – 50nm [394]. The accuracy of NTA size measurements is within 5% of the expected particle size range [395].

On the other hand, by knowing the sample measurement volume, the particle concentration can also be calculated by the program. However, due to the high variation between the particle number detected between video replicates captured for the same sample, NTA particle concentration measurements are considered to have low precision [394]. Using a statistical bootstrapping approach, Parsons et al. have demonstrated using three EV containing biological fluids that, for particles in the range of 50 and 120 nm, the precision of particle concentration measurements can be significantly improved by increasing the number of video replicates for each sample [396].

Like NTA, **Dynamic Light Scattering (DLS)** is another remarkable technique to measure particle size distribution [387, 397]. On being illuminated by a monochromatic light source, the fluctuations in the bulk scattered light intensity due to the Brownian

movement of particles are measured over time. Using the Stokes-Einstein equation, this information is used to calculate the particle hydrodynamic diameter. Of note, the detectors recording the scattered light can be oriented either forward at 90° or backward at 173°. For our experiments, we used 90° as the detection angle as it is ideal for weakly scattering samples like EVs. DLS has a detection range of 1nm to 6μm [397]. However, unlike NTA, DLS does not measure each particle individually and hence is more suited for measuring particles in a monodisperse population [397]. Moreover, according to Rayleigh theory, the intensity of the light scattered is proportional to the sixth power of the diameter. Thus, small differences in EV diameters would lead to larger differences in the scattered light intensities. Hence, DLS is sensitive to the presence of larger particles in the suspension [387]. Also, DLS is not suitable to measure particle concentration as determining this value depends on many factors like the particle diameter, concentration and refractive index [387].

Filipe et al. [394] analysed polystyrene beads of known sizes (60 to 1000nm) by NTA and DLS to compare the two techniques. The group observed that for monodisperse samples, the mean size values determined using both techniques were similar to the expected sizes. Moreover, the values measured by NTA were closer to the expected size than those measured by DLS; however, DLS recorded lower standard deviation than NTA. Next, the group prepared polydisperse samples by mixing of the beads in fixed proportions. They found that NTA was able to resolve peaks of populations more accurately while DLS appeared biased toward the larger sized beads. However, the NTA program compromised on the number of smaller particles when the sample

contained larger particles. The requirement of small EV sample quantity also makes NTA a preferable method of EV characterization over DLS.

1.11.2 *Investigating EV particle number*

Flow cytometry has been conventionally used for the analysis of cells. However, conventional flow cytometers lack sensitivity and resolution to detect particles with diameters less than 500nm [398-402]. To detect and measure EVs, highly sensitive flow cytometers like the Cytoflex and imaging flow cytometer have been introduced.

Imaging flow cytometry (IFC) enables the analysis of heterogeneous EV populations by combining the power of flow cytometry with the resolution of fluorescent microscopy [387, 403]. The cytometer uses CCD camera instead of photomultiplier tubes, thus reducing the 'noise' and increasing light signal detection sensitivity. Also, the readout mode used is Time Delay Integration (TDI), which when paired with slower flow rates, leads to higher sensitivity than that observed in traditional flow cytometry [404, 405]. The instrument has a 100% duty cycle, which means that every particle that flows through the cell is imaged [405]. Perhaps, the most important advantage of IFC is the ability to image all particle events; hence, coincidence events (if any) or events that appear non-EV-like can be easily removed from the analysis [406]. Of note, Lannigan et al. has reported that no coincidence events are detected up to particle concentrations of 10^{10}/mL [403], in stark contrast to traditional flow cytometers that suffer at concentrations greater than 10^{7}/mL [407].

IFC can measure particle concentrations in liquid suspensions. Also, EV phenotypes (subpopulations) can be determined by using fluorescently conjugated antibodies. The

use of proper controls when analysing this data holds paramount importance [387, 400, 408, 409] as there is usually no wash step prior to acquisition and thus, any antibody aggregates formed in the suspension may appear EV-like and confound analysis [387, 410]. A major limitation of IFC is the challenge to concentrate samples into small volumes to collect number of objects similar to traditional flow cytometry measurements in a reasonable amount of time. Also, sizing of EVs is a challenge but fluorescent calibrators can be used to estimate size ranges [411, 412].

Cytoflex flow cytometry, on the other hand, can also be employed to determine EV particle number. Cytoflex is a semiconductor-based flow cytometer which employs avalanche photodiodes that have higher light detection sensitivity across a broader wavelength range [413] in comparison with traditional photomultiplier tubes [414]. These diodes are paired with wavelength division multiplexing design that eliminates the use of dichroic mirrors or light filters - components used in traditional flow cytometers that can cause signal losses of about 20-50% [413]. Thus, maximum signal can be collected using the Cytoflex. The Cytoflex has the option of using violet side-scatter (VSSC, 405nm) for detecting particles. Using VSSC over SSC is advantageous as the former has a shorter wavelength leading to higher light scatter from particles. Using VSSC, the Cytoflex could resolve 98.6nm of silica beads with a refractive index of 1.44 [413]. Importantly, the device can detect EVs isolated from plasma that are as small as 65nm [413]. However, it is difficult to discriminate true EV particle population from background/instrument noise. This issue can be overcome by using fluorescent markers to label EVs.

1.11.3 *Investigating EV density*

In my studies, it was essential to determine the density of EVs in order to evaluate the efficiency of the methods in use to isolate EVs. The density of EVs may differ based on their parental cells [415]. **Iodixanol density gradient centrifugation** is a method used to isolate EVs and determine their densities while maintaining their physical integrity and separating them from protein contaminants [416]. It results in the sedimentation of EVs in the region of the gradient where their density is equivalent to that of the surrounding medium [417].

1.12 *Hypothesis and objectives*

The Sipione lab previously demonstrated that GM1 exerts disease-modifying effects in HD mouse models [254, 256]. These effects are accompanied by a significant decrease in the levels of both soluble and insoluble mHTT [256]. Since GM1 treatment does not alter *Htt* mRNA [256], the mechanism by which it reduces mHTT may be at the proteostatic level. Furthermore, our preliminary proteomics and gene ontology analyses of WT and HD mice treated with GM1 *in vivo* (compared to untreated controls) shows the enrichment of proteins involved in the EV pathway (**Fig. 7**). Thus, this calls for investigating the role of GM1 (and potentially other gangliosides) in the secretion of EVs in HD as well as in healthy cells. In addition to that, the role of gangliosides in EV release has not been elucidated before, to the best of my knowledge, although studies have reported that EVs contain GM1 and other components of lipid rafts [308, 418-421] and that lipid rafts are involved in EV biogenesis [311, 419]. In this thesis, **I will investigate the hypothesis that**

exogenously administered GM1 and endogenous ganglioside levels modulate the secretion of EVs and mHTT.

The main objectives of this thesis are:

1. To determine the role of exogenously administered GM1 in the secretion of EVs and mHTT
2. To determine the role of endogenous gangliosides in the secretion of EVs and mHTT

CHAPTER 2: MATERIALS AND METHODS

2.1 *Chemicals, reagents, and materials*

Purified porcine GM1 was provided by TRB Chemedica Inc, Switzerland. Genz-123346 was purchased from Toronto Research Chemicals, Canada. Vybrant™ DiI and Vybrant™ DiD Cell-Labeling solutions were from Thermo Fisher Scientific, USA. L-Glutamine, sodium pyruvate, Geneticin®, N2 supplement, B27 supplement, GlutaMAX™ supplement, Opti-MEM® I reduced serum media (with phenol red), Opti-MEM® I reduced serum media (phenol red-free), Dulbecco's Modified Eagle Medium (DMEM) – high glucose (phenol red-free), Minimum Essential Medium (MEM) (with phenol red), MEM (phenol red-free), MEM Non-Essential Amino Acids Solution, Hank's Balanced Salt Solution (HBSS) and Neurobasal™ media were purchased from Gibco™, Thermo Fisher Scientific, USA. DMEM – high glucose (with phenol red), cell-culture grade phosphate buffered saline (PBS), Penicillin/Streptomycin were purchased from HyClone™, GE Healthcare, USA. Cell-culture grade DMSO, Tween-80, fetal bovine serum (FBS), EDTA, EGTA, MG132, bovine serum albumin (BSA), BSA free of fatty acids were purchased from Sigma Aldrich, USA. Complete® Protease inhibitor cocktail and PhosStop® phosphatase inhibitor cocktail were purchased from Roche, Switzerland. IGEPAL® CA-630 (Sigma Aldrich, USA) was used in place of Nonidet P-40 (NP-40) detergent as the latter is no longer commercially available. Nitrocellulose membranes were purchased from Bio-Rad, USA while PVDF membranes (Immobilon®-FL) were from Merck Millipore, USA. Pre-lubricated pipette tips 1-200µL and 100-1000µL (Maxymum Recovery™, Axygen®, Corning Life

Sciences, USA) and microcentrifuge tubes (CoStar, Corning Life Sciences, USA) were used for the isolation and analysis of EVs. All polystyrene and polypropylene tubes were from Falcon™, Thermo Fisher Scientific, USA.

2.2 *Cell models*

Neuro2a mouse neuroblastoma cells (N2a) were kindly donated by Dr. Satyabrata Kar (University of Alberta, Canada). N2a cells were cultured in DMEM:Opti-MEM I (1:1) supplemented with 10% heat inactivated FBS, 2mM L-Glutamine and 0.11g/L sodium pyruvate (N2a growth media) and maintained at 37°C with 5% CO_2.

Embryonic rat cortical neurons were isolated from E18 embryos and maintained in neuronal growth media (Neurobasal™ containing 200µM Glutamax®, 100U/mL penicillin, 100µg/mL streptomycin and 1X B27® supplement) on plates coated with poly-L-lysine (molecular weight ≥ 300.000, Sigma Aldrich, USA). All procedures were approved by the University of Alberta's Animal Use Committee and the Canadian Council on Animal Care (CCAC). Pregnant dams (Sprague Dawley) were subjected to isoflurane-anesthesia followed by decapitation. Thereafter, the uterus was transferred to a petri dish on ice and embryos were isolated, decapitated and the brains were dissected to isolate cortical tissue under a dissecting microscope. The cortical tissue was resuspended in 0.25% trypsin-EDTA (Thermo Fisher Scientific, USA) in a 50-mL polystyrene tube and incubated for 20 min at 37°C in a water bath. Digestion was stopped by centrifugation of the suspension at 300 x g for 2 min. The supernatant was discarded, and the pellet was resuspended in trituration media (DMEM + 10% heat inactivated FBS + 1% penicillin/streptomycin). Thereafter, the tissue was passed 10

times through a fire-polished glass Pasteur pipette and the supernatant obtained after tissue sedimentation was transferred to a new polystyrene tube. Trituration was performed three times in total. The cell suspension was then filtered through a 40µm pore-sized nylon cell strainer (Thermo Fisher Scientific, USA). Cells were counted using a haemocytometer and plated at a density of $0.13x10^6$ cells/cm^2 in trituration media. After cells had attached, i.e. 1.5 to 2 h after seeding, the trituration media was replaced with neuronal growth media. On DIV2, cells were treated with cytosine arabinoside (3µM, Sigma Aldrich, USA) for 48 h to block the proliferation of glial cells and reduce their presence to less than 1% [422]. Thereafter, 50% of the media was replaced with fresh media every 4 days. The culture was maintained at 37°C with 5% CO_2. Experiments were performed on DIV 15.

Primary human fibroblasts, purchased from the Coriell Institute for Medical Research, USA, were derived from one male HD donor (HD35M, Coriell code GM04208) and one age-matched control male donor (WT36M, Coriell code AG07573). A complete characterization of these cells is available in the Cell Line Inventory of the Coriell Institute for Medical Research website. Cells were maintained in MEM (with non-essential amino acids) supplemented with 15% heat inactivated FBS, 2mM L-Glutamine and 0.11g/L sodium pyruvate (fibroblast growth media) and maintained at 37°C with 5% CO_2. Cell passaging was performed by trypsinization in 0.05% trypsin-EDTA (Corning Life Sciences, USA), after cell washing and incubation in HBSS (Ca^{2+}/Mg^{2+} free) containing 0.53mM EDTA for 2 min at r.t. to decrease trypsinization time. Cells were passed before they could reach 80% confluence as the levels of gangliosides change upon reaching confluence [423]. Media collected from four

100mm dishes, each seeded with 0.15 x 10^6 cells cultured for 22 h, were pooled and processed to isolate EVs for immunoblotting.

2.3 *Generation of N2a cells stably expressing mHTT-EGFP*

N2a cells were stably transfected with the cDNA for mHTT Exon 1 (containing 72 glutamines) tagged with enhanced green fluorescent protein (HTT-Exon1 (72Q) EGFP). The plasmid was created by D. Housman (Massachusetts Institute of Technology, USA) by subcloning the mHTT-GFP construct (size 1450 bp) into pcDNA3.1 (size 5428 bp). Cell transfection was performed using Lipofectamine 3000® reagent (Thermo Fisher Scientific, USA). After confirming successful transfection by detection of GFP fluorescence by microscopy, 800µg/mL Geneticin® was added to the medium to select stably transfected cells. GFP-fluorescent cells were further sorted using FACS Aria™ III cell sorter (BD Biosciences, USA), at the Faculty of Medicine and Dentistry Flow Cytometry Facility, University of Alberta, Canada. Expression of mHTT-GFP was confirmed by immunoblotting. The selected stably transfected cell population, referred to as N2a 72Q, was maintained in N2a growth media with 400µg/mL of Geneticin® at 37°C with 5% CO_2. Geneticin was added to the media only in the first week after thawing cells, after which cells were maintained in the absence of the selection agent. Cells were routinely checked for GFP fluorescence by microscopy and were periodically re-sorted by FACS when the percentage of fluorescent cells fell below 80%. They were maintained at 37°C with 5% CO_2. To isolate EVs for immunoblotting studies, media from three to six 100mm dishes each seeded with 0.9-2.0 x 10^6 cells and grown for 24-48 h were pooled.

2.4 *Generation of N2a cells transiently expressing wtHTT-EGFP and mHTT-EGFP*

N2a cells were transiently transfected with the cDNA for either wtHTT Exon 1 (containing 25 glutamines) tagged with enhanced green fluorescent protein (HTT-Exon1 (25Q) EGFP) or with HTT-Exon1 (72Q) EGFP. The plasmids were created by D. Housman (Massachusetts Institute of Technology, USA) by subcloning the HTT constructs for 25Q (size 1300 bp) or 72Q (size 1450 bp) into pcDNA3.1 (size 5428 bp). To generate cells transiently expressing the plasmid, 2-2.5x10^6 N2a cells along with 4-5µg of plasmid DNA were resuspended in Nucleofector® solution (Lonza, Switzerland) and were carefully transferred to a Nucleocuvette® (Lonza, Switzerland). Transfections were performed using the DS-137 program on a 4D-Nucleofector® X unit (Lonza, Switzerland) by a former PhD student (Dr. L.C. Morales) in the Sipione lab.

2.5 *Generation of knock-out cells lacking B4galnt1*

N2a Δ*B4galnt1* cells were generated in collaboration with Dr. Basil Hubbard (University of Alberta, Canada). Guide RNAs were designed to target the *B4galnt1* gene as previously described [424] and mixed with equimolar quantities of Cas9 to construct ribonucleoprotein complexes which were then transfected into N2a cells using Lipofectamine CRISPRMAX (Thermo Fisher, USA) according to manufacturer's instructions. After 24 h of incubation, cells were sorted for the presence of the ATTO 550 fluorescent marker on the tracrRNA, using FACS Aria™ III cell sorter (BD Biosciences, USA), at the Faculty of Medicine and Dentistry Flow Cytometry Facility,

University of Alberta, Canada. To generate clonal cell lines, positive cells were sorted one cell per well into a 96-well plate and further expanded. Confirmation of gene knock-out was achieved by immunoblotting and PCR.

2.6 *Fluorescent labelling of cells for EV detection*

Indirect fluorescent labelling of EVs was performed to detect and quantitate EVs by fluorometry or flow cytometry. Cells were labelled with the lipophilic membrane stain DiI (1,1'-dioctadecyl-3,3,3',3'-tetramethylindocarbocyanine perchlorate; $\lambda_{Ex}/\lambda_{Em}$ = 549/565 nm) or its longer wavelength analogue DiD (1,1'-dioctadecyl-3,3,3',3'-tetramethylindodicarbocyanine, 4-chlorobenzenesulfonate salt; $\lambda_{Ex}/\lambda_{Em}$ = 644/665 nm), which distribute to all cell membrane and therefore also to EV membranes, according to the manufacturer's instructions (Invitrogen™, Thermo Fisher Scientific, USA). Briefly, 5µL of the dye solution (1mM) was added to each 1mL of cell suspension consisting of $1x10^6$ cells in serum-free media, in a polypropylene tube. This suspension was incubated for 15-20 min in the dark at 37°C and then centrifuged at 400 x g for 5 min at r.t. The stained cell pellet obtained was further subjected to two rounds of centrifugation in growth media to remove unbound dye. The cells were then resuspended in plating media and seeded in 100mm dishes. The seeding densities were determined such that the confluence of the cells at the time of harvesting was ≅ 80%.

2.7 *Preparation of EV Collection Media*

The cell-culture media used for cell conditioning and collection of EVs in our initial experiments was serum-free media supplemented with heat inactivated EV-depleted FBS (EVD complete medium). To prepare EV-depleted serum, heat inactivated FBS was transferred to 26.3mL thickwall polycarbonate bottles (Beckman Coulter, USA) and subjected to centrifugation at 100,000 x g for 16 h at 4°C using a Type 70 Ti Fixed-angle rotor (Beckman Coulter, USA) in an Optima L-70 ultracentrifuge (Beckman Coulter, USA) [425]. The supernatant thus obtained was filter-sterilized with a 0.22µm PVDF filter (Millipore, USA) and stored at -20°C until further use.

In later experiments, phenol red-free serum-free medium supplemented with N2 supplement (SFM+N2) was used for EV collection.

2.8 *Cell treatment with ganglioside GM1*

Porcine ganglioside GM1 was dissolved in cell-culture grade PBS to a stock concentration of 10mM and stored at -80°C until use. It was added to cells in growth media or SFM+N2 upon cell seeding or after cell attachment to the growth plate (2-4 h after seeding). GM1 was administered to cells at a final concentration of 50µM (the critical micellar concentration of GM1 in aqueous solutions is 29µM [426]). After incubation with GM1 for 6-18 h, cells were washed once with HBSS (with Ca^{2+}/Mg^{2+}), followed by one wash with HBSS (with Ca^{2+}/Mg^{2+}) supplemented with 0.2% fatty acid-free BSA to remove any free GM1, and one last wash with HBSS (with Ca^{2+}/Mg^{2+}).

2.9 *Inhibition of ganglioside synthesis with Genz-123346*

Genz-123346 was solubilized in 100% cell-culture grade DMSO to a stock concentration of 10mM and stored at -20°C until use. It was added to cells in growth media at the time of cell seeding to a final concentration of 1µM (final concentration of DMSO was 0.01%). DMSO at the final concentration of 0.01% was added to control groups. After 24 h of treatment, cells were washed with HBSS (with Ca^{2+}/Mg^{2+}) and the treatment was replenished in EV collection media.

2.10 *Collection of EVs in cell-conditioned media*

After cell treatment, medium was replaced with EV collection medium and allowed to be conditioned by cells for 16-24 h. The conditioned medium was collected in polypropylene tubes and centrifuged at 2,000 x g for 10 min at 4°C in an Eppendorf® Centrifuge 5810 R, using an A-4-62 swinging bucket rotor, to remove the pellet containing any loose cells, apoptotic bodies, and cell debris. The supernatant retrieved is called Cleared Conditioned Media (CCM).

2.11 *Isolation of EVs from the CCM*

To avoid EV loss, pre-lubricated low protein-binding pipette tips and microcentrifuge tubes were used at all steps of EV isolation and analysis. Depending on the experiments, several methods were used to isolate EVs from the CCM. These include:

2.11.1 *Ultracentrifugation (UC)*

The CCM was first subjected to centrifugation at 100,000 x g for 90 min at 4°C in a 10.4mL thickwall polycarbonate bottle (Beckman Coulter, USA) using an MLA-55 fixed angle rotor (Beckman Coulter, USA) in an Optima™ MAX-XP tabletop ultracentrifuge (Beckman Coulter, USA). Depending on the downstream application, the supernatant was either stored at -80°C or discarded. The pellet was washed by resuspending it in 0.6mL PBS in a 1mL open-top thickwall polycarbonate tube (Beckman Coulter, USA) and centrifuging it at 100,000 x g for 90 min at 4°C using an MLA-130 fixed angle rotor (Beckman Coulter, USA). The final pellet was resuspended in 100µL of PBS.

2.11.2 *Ultrafiltration*

Amicon® Ultra-15 Centrifugal Filters (10,000 MWCO or 100,000 MWCO) (Millipore Sigma, USA) were employed to concentrate large volumes of CCM. The filter device was used and maintained following the manufacturer's instructions. To minimize EV loss, the filter membranes were first blocked by centrifuging them with 5% Tween-80 [427] in PBS at 2,608 x g (Eppendorf™ Centrifuge 5810 R, A-4-62 swinging bucket rotor) for 10 min at 4°C, followed by three PBS centrifugation washes of 5 min each. Once blocked, the membrane was kept in PBS until use to prevent drying. The CCM was concentrated by centrifugation at 2,608 x g at 4°C. The time required to concentrate the material depended on the initial CCM volume, the final (required) retentate volume, the composition of the media being filtered and the MWCO of the filter used. The concentrated CCM (retentate) was immediately and carefully pipetted to a new tube, after which the filter membrane was subjected to three extensive

washes with fresh PBS each time to recover any EVs adhering to it. To avoid variability, the procedure for washing was kept consistent across filters. Thus, for each wash, PBS was repeatedly passed over each side of the membrane five times using a micropipette, following which the wash volume was added to the tube with the retentate. The volume of the wash depended on the final retentate volume required, but a minimum of 150µL was used to avoid foaming. The final volume of the retentate depended on the downstream application. As the retentate contains a high percentage of free proteins not associated to EVs, using the retentate for EV analysis would lead to confounding results. Hence, ultrafiltration was usually an intermediate step required for EV isolation. Consequently, if the EVs were to be isolated from the retentate by density gradient centrifugation, the washes with PBS after retentate collection were substituted by those with serum-free media (DMEM:Opti-MEM I (1:1).

2.11.3 *OptiPrep™ density gradient centrifugation*

The protocol was adapted from various sources [410, 428-430]. First, iodixanol solutions (OptiPrep™ Density Gradient Medium, Axis-Shield, Norway) were diluted in serum-free medium (DMEM:Opti-MEM I 1:1) to prepare 5%, 10%, 20% and 40% iodixanol solutions to make the gradient. They were gently mixed on a rotisserie rotator for 30 min at 4°C. A discontinuous gradient was carefully prepared in a 13.2mL open-top thinwall polyallomer tube (Beckman Coulter, USA) by gently adding 3mL of 40%, 3mL of 20%, 3mL of 10% and 2mL of 5% solutions from bottom to top. The retentate was concentrated using Amicon Ultra-15 centrifugal filters (100,000 MWCO) as indicated previously, and its final volume was brought to 1mL with serum-free media

(DMEM:Opti-MEM 1:1). The retentate was carefully overlaid on top of the gradient. The tubes were centrifuged at 100,000 x g for 18 h at 4°C, using a SW41 Ti swinging-bucket rotor (Beckman Coulter, USA) in an Optima L-70 ultracentrifuge (Beckman Coulter, USA). After centrifugation, 12 fractions of 1mL each were collected from the top and the density of each fraction was measured. All steps were performed at 4°C. The distribution of EVs across the fractions was determined by measuring the fluorescence of each fraction ($\lambda_{Ex}/\lambda_{Em}$ = 540/580 nm for DiI).

2.11.4 *Size-exclusion chromatography (SEC)*

qEV original Size Exclusion Columns (iZON Science®) were used for the isolation of EVs more than 70nm in size. SEC columns were stored in PBS containing 0.05% sodium azide, at 4°C and used according to the manufacturer's instructions. After column equilibration at r.t., 10mL of PBS was first eluted through it and the elution time was recorded to ensure the optimal functioning of the column. Then, 0.5mL of the retentate obtained by ultrafiltration was loaded on top of the column and PBS was used as the elution buffer. 22 fractions, each of 0.5mL, were collected and analysed. The presence of EVs in the various fractions was determined by measuring DiI ($\lambda_{Ex}/\lambda_{Em}$ = 540/580 nm) or DiD ($\lambda_{Ex}/\lambda_{Em}$ = 644/674 nm) fluorescence in each fraction. The protein content of each fraction was determined by measuring the absorbance at 280nm using Nanodrop™ 2000c (Thermo Fisher Scientific, USA). The fractions enriched with EVs (which were generally between fractions 5 and 11 inclusive, referred to as the EV fractions) and proteins (which were generally between fractions 12 and 22 inclusive) were pooled and concentrated using Amicon® Ultra-2mL Filters (10,000 MWCO) that

were blocked with Tween-80 as previously described. The filters were used as per manufacturer's instructions to concentrate the samples by centrifugation at 2,608 x g (with an A-4-62 swinging bucket rotor in an Eppendorf™ Centrifuge 5810 R) at 4°C.

2.12 *Storage and handling of EV samples*

All EV samples were kept on ice at any time and analyzed immediately after isolation for the determination of their number, size distribution and phenotype by imaging flow cytometry, Cytoflex flow cytometry, nanoparticle tracking analysis and dynamic light scattering. For other applications, EV samples were stored at -80°C until use. Repeated freeze-thaw cycles were avoided. To limit EV particle damage, EV samples were mixed by gently pipetting up and down or by tube inversion, and never vortexed.

2.13 *Normalization of EV volume*

EV secretion was normalized over the total cellular protein content to ensure that all downstream EV analyses were performed on EVs secreted from the same number of cells across treatment groups. Of note, the total cellular protein content was similar across treatment groups. To normalize EV secretion over the corresponding cellular protein levels, only an aliquot of the sample (CCM or EV fraction) from the treatment group with the highest cellular protein content was used, the volume of which was calculated based on the formula:

$$V_X = P_L / P_H \times V_H$$

Where, P_L is the cellular protein value of the group with lower cellular protein content, P_H is the cellular protein value of the group with higher cellular protein content,

V_H is the volume of the sample (CCM or EV fraction) with higher cellular protein content, and V_X is the volume to be **used** from V_H.

In experiments where the fluorescence associated to EV membranes was compared between cell types, EV secretion was normalized to cellular dye content to rule out differences in cellular incorporation of the dye as a potential confounding factor.

2.14 *Determination of EV number, phenotype, and size*

2.14.1 *Fluorometry*

DiI or DiD fluorescence was measured in cell lysates and EVs using a SpectraMax® i3x multi-mode microplate reader (Molecular Devices, USA). Ex/Em for DiI is 540/580nm while that for DiD is 644/674nm. The bandwidth of all excitation and emission wavelengths was set to 15nm. Fluorescence was measured in 96-well black-bottom plates by well-scan reading. 100µL of the sample were loaded in each well in triplicates.

2.14.2 *Imaging Flow Cytometry (IFC)*

IFC was used to determine EV number and phenotype (subpopulations). All samples were acquired on an Amnis® ImageStream mkII instrument, at the Faculty of Medicine and Dentistry Flow Cytometry Facility at the University of Alberta. This equipment has 4 excitation lasers (120mW 405nm, 200mW 488nm, 150mW 642nm and 785nm Side Scatter (SSC)). All data were acquired with lasers set at maximum powers, with 60x magnification, low flow rate and high sensitivity. Data were acquired after 1 min of sample loading into the instrument to allow for the flow or particles to stabilize. The DiI

signal associated with EVs was acquired using a 560-595nm filter (channel 3) while the DiD signal was acquired using a 642-745nm filter (channel 11). Channel 1 (435-480nm filter) was used for brightfield imaging and channel 6 (745-780nm filter) was used for SSC measurements. GFP fluorescence in the EVs of cells stably expressing mHTT-GFP was also detected using a 480-560nm filter (channel 2). D-PBS pH 7.4 (BioSure® Sheath Solution, BioSure, UK) was used as sheath fluid. If required, samples were diluted with PBS to avoid coincidence events. For most experiments, 3-10 technical replicates were acquired for each sample and data were averaged. In each experiment, all samples were measured for the same time with a minimum of 10,000 events collected by gating for events with a side scatter lower than the speedbeads (Amnis® SpeedBead® Kit for ImageStream®, Luminex Corporation, USA). The controls used were detergent (NP-40) controls. Unstained samples, unconditioned media, and buffer control samples were used for noise/background signal quantitation/subtraction. To confirm that the particles detected were membrane-bound EVs, 0.05% NP-40 (filtered through 0.1µm PVDF filter) was added to all samples for 30 min at r.t. to destroy membranes. Data were analysed using IDEAS® software v6.2. Any speed beads that may have been captured during the acquisition were gated out and masks were made to identify positive particles as described below:

- DiI : Intensity(M03,Ch03_DiI, 50-4095)
- DiD : Intensity(M11,Ch11_DiD, 60-4095)
- GFP : Intensity(M02,Ch02_GFP, 17-4095)

As DiI or DiD were the fluorescent pan-EV markers, the spot count feature was added to their analysis to detect single particles. Gates were made using unstained or

unconditioned media samples and compensation was applied wherever necessary. The mean pixel intensity of DiI or DiD generated by the software to measure the amount of dye in the particles was also recorded as part of the analysis.

2.14.3 *Cytoflex flow cytometry*

In a subset of experiments, EV particle number in the CCM (1 ml) derived from DiD-labelled cells was determined by flow cytometry using a Cytoflex “S” system (Beckman Coulter, USA), at a “Slow” (10μL/min) flow rate, to avoid coincidence events. Events were collected for 30 s. The trigger channel selected was VSSC-H (Violet Side Scatter-Height). The threshold and gain levels were manually set and kept the same within experiments. The VSSC gain was set to 500 or 600 while the VSSC threshold was set to 2500. Unstained controls were first run to gate out any background noise. All samples were measured in triplicates. As previously described, detergent (0.05% NP-40)-treated samples were run to confirm the membranous nature of the particles detected. Data were analysed using CytExpert v2.3.

2.14.4 *Nanoparticle Tracking Analysis (NTA)*

EV number and size distribution was determined using the NanoSight LM10 system (405nm laser, software version 3.3 – Sample Assistant Dev Build 3.3.203) (NanoSight, United Kingdom). The instrument was calibrated using 200nm polystyrene beads (Nanosphere, USA) resuspended in 10mM potassium chloride (KCl). CCM samples were diluted 1:4-1:7 with PBS to acquire 20-90 particles/frame. 300μL of the sample was injected into the NanoSight chamber with a 1mL syringe. Five serial measurements were taken for each sample, and each measurement was taken for 1

min. PBS was injected into the chamber to wash the system in between samples. The exact sample temperature was manually entered into the system to avoid confounding particle analysis. The camera level was set at 13 while the detection threshold was set at 2 for all sample measurements.

2.14.5 *Dynamic Light Scattering (DLS)*

Freshly prepared retentate obtained by ultrafiltration of the CCM was used for DLS measurements to determine EV size distribution. An aliquot of the retentate corresponding to 350µg of proteins (measured by BCA protein assay) was subjected to asymmetrical flow field-flow fractionation on an AF2000 Postnova system using PBS pH 7.4 as running buffer. Samples were focussed for 5 min before elution at a flow rate of 0.5mL/min. A slot pump was run at 0.3mL/min to concentrate the samples before passing them through detectors. Fractions of 0.2mL were collected and analyzed by an in-line DAWN HELEOS II detector (Wyatt Technology) and using ASTRA software v6.1.

2.15 *Protein quantification*

Protein concentration in cell lysates and EV samples was measured with a Pierce™ BCA Protein Assay and with a Pierce™ Enhanced BCA Protein Assay (Thermo Fisher Scientific, USA), respectively, according to manufacturer's instructions. The latter has a lower working range than the former assay and requires incubation of samples at 60°C for 30 min. All samples for protein measurements were loaded in triplicates. The absorbance of each sample was measured by endpoint reading at 562nm, using a SpectraMax® i3x multi-mode microplate reader (Molecular Devices, USA).

2.16 *Detection and quantitation of ganglioside GM1*

GM1 in cell lysates and EV samples was quantified by dot-blotting. Cells lysed in 1X NP-40 lysis buffer (20 mM Tris-HCl at pH 7.4, 1% NP-40 v/v, 1 mM EDTA, 1 mM EGTA, 50μM MG132, 1X protease/phosphatase inhibitor cocktail) were passed through a 27-G needle ten times, incubated on ice for 30 min and then sonicated at intensity 2.0 for 10 s, prior to sample immobilization onto a 0.45μm pore size nitrocellulose membrane (Millipore, USA) using a 96-well Bio-Dot® apparatus (Bio-Rad, USA). EV samples were either sonicated at intensity 2.0 for 10 s or lysed with 0.01% NP-40. 1.0μg of protein from cell lysate was loaded in each well, in triplicates. EV samples were loaded in duplicates or triplicates. Membranes were blocked for 1 h with Odyssey® blocking buffer (LiCor Biosciences, USA) or Intercept® blocking buffer (LiCor Biosciences, USA), and then incubated overnight at 4°C or for 2 h at r.t. with biotinylated cholera toxin B (Thermo Scientific, USA) diluted in Odyssey® or Intercept® blocking buffer at a final concentration of 0.25μg/mL, to detect GM1, and with anti-α-tubulin antibodies (2125, Cell Signaling, USA) to control for equal loading of cell lysates. Membranes were then washed with TBS-T (20mM Tris-HCl, 137mM NaCl, pH 7.4-7.6 containing 0.1% Tween-20) and incubated with IRDye800®-conjugated Streptavidin (LiCor Biosciences, USA) diluted 1:5000, and the appropriate fluorescent secondary antibody diluted 1:10000, with Odyssey® or Intercept® blocking buffer:TBS-T (1:3) for 1 hour at r.t.. Finally, membranes were washed once with TBS-T and once more with TBS (20mM Tris-HCl, 137mM NaCl, pH 7.4-7.6) before scanning in an Odyssey® near-infrared scanner (LiCor Biosciences, USA). Signal was quantified using Odyssey® Application Software v3.0 (LiCor Biosciences, USA).

2.17 *Immunoblotting*

30-60µg of cell lysate proteins and equal fractions of EV samples isolated by UC or by SEC (not exceeding 60 µg of total EV proteins) were heated in sample loading buffer (62.5mM Tris-HCl pH 6.8, 2% SDS, 10% glycerol, 5% 2-mercaptoethanol, 6.25mg/mL bromophenol blue) for 5 min at 95°C. For full-length HTT detection, samples were heated for 5 min at 60°C. Samples were loaded in 4-20% SDS PAGE gradient gels and run in a Mini-PROTEAN® II electrophoresis chamber (Millipore, USA). Proteins were transferred to a 0.45µm PVDF membrane in standard Towbin buffer (25mM Tris-HCl, 192mM glycine, 20% methanol v/v) using a Mini Trans-Blot® apparatus (Bio-Rad, USA). For transfer of protein aggregates and full-length HTT, a modified SDS-Towbin buffer (25mM Tris-HCl, 192mM glycine, 16% methanol v/v, 0.05% SDS w/v) was used. Amounts of EV samples normalized over the total amount of proteins in the donor cell lysates were loaded.

In some experiments, dot-blotting of EVs was performed. EV samples were loaded in triplicates on a 0.45µm nitrocellulose membrane using a 96-well Bio-Dot® apparatus (Bio-Rad, USA).

The membrane was blocked for 1 h with Odyssey® blocking buffer (LiCor Biosciences, USA) or Intercept® blocking buffer (LiCor Biosciences, USA), and then incubated with primary antibodies dissolved in blocking buffer:TBS-T (1:1) for 2 h at r.t. or overnight at 4°C. A complete list of antibodies used is available in **Table 1**. The membrane was then washed with TBS-T and incubated with the appropriate fluorescent secondary antibodies (LiCor BioSciences, USA) diluted in blocking buffer:TBS-T (1:3) for 1 h at

r.t. The membrane was washed with TBS-T and TBS before scanning in an Odyssey® near-infrared scanner (LiCor Biosciences, USA). Signal was quantified using Odyssey® Application Software v3.0 (LiCor Biosciences, USA) or ImageJ (NIH, USA). Alternatively, the membrane was incubated with HRP-conjugated secondary antibodies (Bio-Rad, USA), detected with Clarity™ Western ECL substrate (Bio-Rad, USA), visualized with a C-DiGit western blot scanner (LiCor Biosciences, USA) or an Amersham Imager 600 (GE Healthcare, USA), and analysed using ImageJ (NIH, USA). Signal from the cell lysates was normalized over Revert™ total protein stain (LiCor Biosciences, USA).

2.18 *ELISA for mHTT-EGFP*

mHTT-EGFP levels in EVs isolated from CCM from N2a 72Q cells by SEC were measured by the GFP SimpleStep ELISA® kit (Abcam, USA), following manufacturer's instructions. All materials and reagents were equilibrated to r.t. before use. 50µL of all samples and standards were loaded in duplicates. The endpoint reading was recorded by measuring absorbance at 450nm using SpectraMax® i3x multi-mode microplate reader (Molecular Devices, USA). Data were normalized over total cellular protein content.

2.19 *Protease protection assay to determine the topology of mHTT associated with EVs*

2 x 10^6 N2a 72Q cells were seeded in each of twelve 100mm dishes. After 2 h to allow for cell attachment, the cells were treated with GM1 (50µM) in SFM+N2 for 6 h or left untreated (control). After 16 h, the conditioned medium was collected to prepare the

CCM. The CCM was concentrated using Amicon® Ultra-15 Centrifugal Filters (100,000 MWCO) and EVs were isolated by SEC. The protein concentration of the EV samples was measured by Pierce™ Enhanced BCA Protein assay. The Proteinase K protection assay was performed on freshly prepared EVs. Three EV aliquots, each corresponding to 20µg of proteins, were prepared from both control and GM1-treated EV samples and used for a Proteinase K digestion assay as indicated below. Proteinase K (Sigma Aldrich, USA) was solubilized in 25mM Tris-HCL, pH 8.0, containing 5mM $CaCl_2$ (Buffer A) to a concentration of 0.1mg/mL. 2.0µg of the enzyme was added to one 20µg-EV aliquot per experimental group and incubated for 1 h at 37°C. Proteinase K was inactivated by sample heating at 95°C for 10 min. Saponin (Sigma Aldrich, USA) was dissolved in MilliQ water to a stock concentration of 5%. It was added to EV samples to a final concentration of 0.1% and incubated at 37°C for 20 min. Treatment groups were:

Group a: 20µg of the EV sample was treated with saponin to permeabilize EV membranes. Then, buffer A was added (same volume as Proteinase K used in groups b and c) and the sample was incubated for 1 h at 37°C followed by heating at 95°C for 10 min. This treatment provided the total mHTT-GFP and total protein signal.

Group b: EVs were first subjected to Proteinase K treatment as indicated above, in order to digest proteins at the EV surface (but not in the EV lumen). The enzyme was inactivated by heat, and saponin was added as indicated above. This treatment allowed to detect luminal EV mHTT and other proteins remaining after digestion of surface proteins.

Group c: 20µg of the EV sample was treated with saponin first. Then, it was treated with Proteinase K followed by heat inactivation. In this sample, both surface and luminal EV proteins are degraded by Proteinase K.

NP-40 was added to all samples at a final concentration of 0.05% and incubated for 30 min at r.t. to lyse EVs completely.

Samples were spotted on a 0.45µm pore size nitrocellulose membrane (Millipore, USA) using a 96-well Bio-Dot® apparatus (Bio-Rad, USA), after dilution with PBS to reduce the final concentration of NP-40 and saponin to less than or equal to 0.01% and 0.0167% respectively, to avoid detergent interference with protein binding to the membrane. NP-40 and saponin final concentrations were kept the same for all groups within the experiment. 5.0µg of EVs were loaded in duplicates or triplicates. The membrane was blocked for 1 h with Intercept® blocking buffer (LiCor Biosciences, USA) and incubated with primary antibodies anti-Alix (611621, BD Biosciences, USA) and anti-HTT N17 NEP (Dr. Truant, University of British Columbia, Canada) overnight at 4°C. The membrane was then washed with TBS-T and incubated with fluorescent secondary antibodies (LiCor Biosciences, USA) for 1 h at r.t. The membrane was washed with TBS-T and TBS before scanning in an Odyssey® near-infrared scanner (LiCor Biosciences, USA). Signal was quantified using ImageJ® software (NIH, USA).

2.20 *Statistical analysis*

All statistical analyses were performed in GraphPad PRISM v6.01. Unless otherwise stated, the two-tailed paired *t*-test was used for all pair-wise comparisons. For

comparing multiple groups with two or more independent variables, two-way ANOVA was used with Tukey's *post-hoc* analysis.

Table 1: List of antibodies used for immunoblotting and imaging flow cytometry

Antibody	Host	Catalogue no.	Company/Provider	Dilution	Application
AIP1 (Alix)	Mouse	611621	BD Biosciences	1:250	Western Blotting
Calnexin	Rabbit	ADI-SPA-860	Enzo	1:2000	Western Blotting
CD9	Rabbit	ab92726	Abcam	1:2000	Western Blotting
CD9	Mouse	ab2215	Abcam	1:2000	Dot Blotting
CD81	Mouse	sc-7637	Santa cruz	1:1000	Western Blotting
Flotillin-1	Mouse	610820	BD Biosciences	1:1000	Western Blotting
GFP	Rabbit	2956	Cell Signaling	1:2000	Western Blotting
HTT mAb2166	Mouse	MAB2166	Millipore	1:5000	Western Blotting
HTT N17 NEP	Rabbit	-	Dr. Truant, University of British Columbia	1:5000	Western/Dot Blotting
TSG101	Rabbit	ab125011	Abcam	1:1000	Western Blotting
α-Tubulin	Rabbit	2125	Cell Signaling	1:10000	Dot Blotting

CHAPTER 3: RESULTS

3.1 *Role of exogenous GM1 in the secretion of EVs and mHTT*

3.1.1 Cell treatment with GM1 increases the secretion of EVs from neuronal cells as determined by EV isolation by ultracentrifugation

The first goal of my thesis was to investigate whether treatment of neuronal N2a cells with ganglioside GM1 increases the secretion of EVs. Due to their small size and low scatter, EVs were detected by labeling them with a lipophilic fluorescent dye, DiI or DiD. Rather than directly labelling isolated EVs, which could result in confounding effects from the presence of free dye or its micelles (non-EV particles) [431], donor cells were labelled prior to EV collection. This strategy enabled washing away non-incorporated dye and labelling of all cell membranes, including EVs prior to their secretion. The DiI or DiD fluorescence signal was used as a surrogate marker to detect and measure EV membranes. After labelling, N2a cells were seeded and treated with vehicle or GM1 after which, EVs were collected by allowing the cells to condition the medium. A flow chart of these experiments and relative timelines is shown in **Fig. 9**. In my initial experiments, FBS depleted of EVs (EVD-serum) by centrifugation at 100,000 x g for 16 h was used to supplement the cell medium (EVD complete medium) during conditioning [425]. EVs secreted by cells were isolated from the cleared conditioned medium (CCM) by ultracentrifugation (UC) at 100,000 x g, a widely accepted method of EV isolation [262, 432, 433]. Fluorometry analysis of the EV pellets isolated by UC showed an increase in the DiI fluorescence associated to EV membranes from N2a cells treated with GM1 compared to vehicle (**Fig. 10.A**).

Moreover, dot-blotting of the EV pellet from GM1-treated N2a cells also showed an increased signal for Alix, a well-established EV marker [327, 397], however, the data did not reach statistical significance due to variability between experiments (**Fig. 10.B**). These effects of GM1 were also demonstrated by a former PhD student in our lab (Dr. L.C. Morales) in primary cultures of rat embryonic cortical neurons, as measured by immunoblotting for the EV markers Flotillin-1 [327, 333] and TSG101 [327, 333, 397] recovered in the EV pellet after UC of the CCM (**Fig. 11**). Calnexin, an ER marker, was used to control for the purity of the EV preparations and to exclude the possibility of contamination from cell debris and apoptotic bodies [434] (**Fig. 11**). Overall, these data suggest that GM1 increases the secretion of EVs from primary and immortalized neuronal cells.

3.1.2 Isolation of EVs by ultracentrifugation results in low EV recovery

To determine whether all EVs secreted in the medium are recovered by UC, in collaboration with Anissa Viveiros, a former MSc. student in Dr. Posse de Chaves' laboratory, we performed imaging flow cytometry (IFC) analysis on the CCM and on the supernatant obtained after its UC at 100,000 x g to detect any fluorescent EV particles remaining in suspension after UC. We found that only less than 10% of EV particles secreted in the CCM were recovered in the pellet (**Fig. S1**). Majority of the EVs were still present in the supernatant or were lost, likely due to sample handling and/or EV attachment to the walls of tubes and tips. To improve recovery, I increased the duration of UC, rather than increasing its speed, because UC at 100,000 x g is known to already cause EV aggregation and loss of physical integrity [435], and hence

increasing the speed of UC could further damage EVs. Thus, the supernatant recovered by UC at 100,000 x g for 90 min was further subjected to UC at 100,000 x g for 16 h, similar to the standard protocol used to deplete EVs from FBS [425]. Immunoblotting for the EV markers Alix and CD9 [333, 334] showed that the majority of EVs were still present in the supernatant obtained after 16 h spin (**Fig. S2**). The total signals for Alix and CD9 detected by dot blotting were slightly higher in the supernatant obtained after 16 h UC, compared to the supernatant obtained after 1.5 h UC. The reason for this is not clear, but perhaps EV breaking during prolonged centrifugation might have facilitated antibody access to their specific epitopes, especially considering that samples were loaded onto membranes in the absence of detergents. Of note, while Alix is a luminal protein of EVs [436, 437] that could potentially be released into the supernatant upon EV breakage, CD9 is an integral membrane tetraspanin [288], and therefore its presence in the supernatant indicates the presence of vesicles (whether intact EVs or fragmented membrane particles).

The supernatant fraction from the unconditioned medium (UCM) containing EVD-serum also showed the presence of EV markers after UC for 16 h (**Fig. S2**), supporting previously published studies that claim that EVD-serum is not completely devoid of EVs [438, 439]. This could have important implications on the analysis of EVs secreted into FBS-containing conditioned medium, and in studies that look at the effects of EVs on cells, due to the potential interference of the co-presence of FBS-derived EVs [438-440].

To mitigate this problem, in collaboration with the Posse de Chaves lab, we formulated and optimized an EV collection medium that does not include FBS. This serum free medium contained all components of the growth medium except for FBS, and was supplemented with N2 (SFM+N2) to compensate for the lack of serum and prevent the activation of cell autophagy [441]. Cell incubation in SFM+N2 did not cause cell death and did not significantly affect EV secretion compared to EVD complete medium (data not shown, Viveiros et al., manuscript in preparation).

To better understand the reason why the majority of EVs from N2a cells do not pellet at 100,000 x g, I performed density gradient centrifugation in OptiPrep™, to determine their density. I found that EVs from N2a cells are present in the fractions with density between 1.015g/cm^3 and 1.029g/cm^3 (**Fig. S3**). This is much lower than the density required for efficient EV pelleting by UC at 100,000 x g [442]. Thus, in conclusion, isolation by UC offers poor EV yield, a finding also in agreement with other published studies [432, 443].

3.1.3 Imaging flow cytometry analysis confirms that GM1 treatment increases cell secretion of EVs

As UC offered poor EV recovery and sedimented only a fraction of the total EVs present, it became imperative to investigate if the effects of GM1 treatment observed after EV isolation by UC could be also observed in the total population of EVs secreted by the cells (i.e. in the fraction pelleted at 100,000 x g as well as in the fraction that is not amenable to be pelleted). To this end, EVs were measured directly in the CCM by IFC, using two experimental timelines: one with a shorter GM1 treatment and EV

collection period and the other with longer treatment and EV collection period (**Figs. 12.B, 12.C**). The two timelines were designed to investigate the effects of short- and long-term treatment with GM1. EV particles were visually detected using an imaging flow cytometer as shown in **Fig. 12.A**. For both experimental timelines, IFC analysis of the CCM showed an increase in the number of DiD or DiI positive EV particles and, in agreement, in the total fluorescence in the medium (measured by fluorometry) upon N2a cell treatment with GM1, compared to vehicle (**Fig. 12**), confirming the results obtained after EV isolation by UC. Of note, GM1 treatment did not affect the amount of dye incorporated into the EVs as determined by measuring the mean pixel intensity by IFC (**Fig. S4**), suggesting that the higher number of EV particles detected after GM1 treatment is not due to higher incorporation of the dye and consequent improved detection. The results obtained by IFC were further confirmed by EV analysis by Cytoflex flow cytometry (**Fig. S5**).

3.1.4 EV isolation by size-exclusion chromatography

In experimental applications that require EV isolation for the analysis of EV biology and/or fate, most studies have performed EV isolation by UC [262, 444, 445]. Our data have clearly shown that this is less than ideal due to poor EV recovery, EV damage, as well as the bias introduced by the potential isolation of specific EV subpopulations. Furthermore, as mHTT is not easily detected in EVs by IFC, probably due to its low abundance, I needed an alternative method to UC to separate EVs from free proteins in the CCM and measure mHTT levels in EV fractions. Therefore, in collaboration with the Posse de Chaves lab, we optimized a method to isolate EVs by size-exclusion

chromatography (SEC) to increase yield and limit EV loss and damage, compared to UC, and to obtain EV fractions devoid of soluble proteins and other components in the medium (data not shown, Viveiros et al., manuscript in preparation) [446-450]. On separating the CCMs by SEC, fractions containing EVs showed a higher fluorescence peak upon cell treatment with GM1 compared to vehicle, as measured by fluorometry (**Fig. 13.A**), and a higher number of DiD positive particles as determined by IFC (**Fig. 13.B**).

3.1.5 GM1 treatment promotes EV secretion in HD cells

To determine whether GM1 treatment also increases the secretion of EVs in HD cells, I generated N2a cells stably expressing mHTT-EGFP (N2a 72Q). In line with our previous data comparing HD models to WT controls [85], N2a 72Q cells also exhibited lower GM1 levels than N2a, however, the data did not reach statistical significance due to inter-experimental variability (**Fig. 14**). Cell treatment with GM1 increased both WT and HD cell GM1 content to similar levels (**Fig. 14**). Interestingly, N2a 72Q cells also showed lower EV secretion than control N2a cells (**Fig. 15**), confirming previous findings in HD astrocytes [372]. To test the effect of GM1 on EV secretion in this model, I used two experimental timelines for GM1 treatment and EV collection, similar to those used for N2a cells (**Fig. 16**). EVs were analysed in the CCM as well as after isolation by UC and measured by fluorometry and by IFC. In all cases, GM1 treatment increased the secretion of EVs by N2a 72Q cells (**Fig. 16**). Similar results were obtained when EVs were isolated by SEC and analyzed by fluorometry or IFC (**Fig. 17**). Of note, DiD

incorporation into EVs did not differ between treatment groups, as measured by IFC (**Fig. S4**).

3.1.6 Cell treatment with GM1 increases the export of mHTT via EVs

The next goal was to investigate whether GM1 treatment increases the export of mHTT via secreted EVs, thus potentially alleviating proteotoxic stress in vulnerable neurons. The presence and the amount of mHTT-EGFP in N2a 72Q-derived EVs was measured by immunoblotting and by ELISA. Attempts were also made to detect GFP fluorescence in the EVs by IFC. However, this could not be achieved as the GFP expression per EV particle was below the threshold level for detection by IFC.

In a preliminary experiment performed by a former PhD student in our lab (Dr. L.C. Morales), EVs were isolated from N2a cells transiently transfected with either HTT-Exon1(25Q)-EGFP (wtHTT) or HTT-Exon1(72Q)-EGFP (mHTT) by UC. Immunoblotting analysis of the EV pellet confirmed increased secretion of the EV marker Alix upon cell treatment with GM1, along with an increase in the secretion of both wtHTT and mHTT. Interestingly, the levels of mHTT exported were higher as compared to wtHTT, even though the cellular levels of transfected mHTT were lower, perhaps suggesting that the mutant protein might be targeted to EVs more efficiently. (**Fig. S6**). Despite this, the cellular levels of mHTT only showed a trend towards a decrease, which did not reach statistical significance due to a high variability of results across different experiments.

To rule out potential confounding effects due to cellular stress caused by transient gene transfection, I performed similar experiments using N2a 72Q cells as they stably

express mHTT-GFP. Immunoblotting analysis of EVs isolated by UC suggested that cell treatment with GM1 increased the secretion of mHTT as well as the EV marker Flotillin-1 in EVs (**Fig. 18**). No statistically significant differences in the levels of mHTT were observed in the cell lysates after treatment with GM1. Here, as in the transiently transfected model, it is possible that overexpression of mHTT might not allow for the detection of significant changes in the intracellular levels of the protein over a short period of time. To confirm that GM1 increases the secretion of mHTT with a technique that allows for higher EV recovery compared to UC, I isolated EVs by SEC and analyzed their mHTT levels by immunoblotting and ELISA (equivalent EV fractions normalized over their corresponding cellular protein content were used) (**Fig. 19**). GM1 treatment increased levels of mHTT in secreted EVs as determined by immunoblotting (**Fig. 19.B**) as well as ELISA (**Fig. 19.D**). Immunoblotting results also indicated that GM1 treatment showed a trend toward increased secretion of CD9 and Alix in EVs (**Fig. 19.B**). However, in all cases, the data did not reach statistical significance due to variability among experiments (**Figs. 19.B, 19.D**). In all experiments, calnexin levels were measured to control for the purity of the EV fractions and to exclude the possibility of contamination from cell debris and apoptotic bodies (**Figs. 18, 19**).

3.1.7 GM1 increases the secretion of EVs in human WT and HD fibroblasts

As the studies performed so far were in mouse neuroblastoma cell lines either in their WT form or overexpressing mHTT, it became imperative to validate the effects of GM1 in a more biologically relevant cell model. Therefore, similar experiments were performed in primary human fibroblast cell models which, although non-neuronal,

express physiological levels of either wtHTT or mHTT under the control of the human *HTT* promoter. In line with my previous findings, analysis of CCMs derived from fibroblasts from one HD male patient and an age-matched male WT control treated with vehicle or GM1 showed that GM1 treatment increased the secretion of EVs in both genotypes as measured by IFC (**Fig. 20.A**). Contrary to N2a 72Q cells, which secreted less EVs than control N2a cells, HD fibroblasts secreted more EVs than WT, as measured by IFC. However, technical issues beyond my control might be responsible for this discrepancy, as the WT fibroblasts consistently incorporated lesser dye than HD cells, for unknown reasons, which resulted in less dye incorporated by their EVs compared to HD EVs (**Fig. 20.B**). The lower fluorescence of WT EVs might have resulted in reduced particle detectability, as some particles may have had signal intensities lower than the threshold required for IFC measurements, thus resulting in lesser events acquired compared to HD EVs. Immunoblotting performed for mHTT in EV fractions isolated by SEC produced a smeared signal for mHTT, which was impossible to quantitate. In cell lysates, the amount of both soluble and aggregated mHTT showed a decreasing trend upon treatment with GM1 in two independent experiments (**Figs. 20.C, 20.D**), in line with our previously published observations *in vivo*, in animal HD models [256]. Of note, the EV markers CD9 and CD81, considered to be canonical EV markers [288, 333, 451], were present in the parent cell lysates but were not detected in the EVs (**Fig. 20.C**). Nevertheless, these studies suggest that GM1-mediated effects on EV secretion can also be extended to human peripheral cells, which also show a decrease in the cellular accumulation of mHTT upon treatment.

3.1.8 Majority of EV-associated mHTT is in the EV lumen

To determine whether mHTT is located on the surface or in the lumen of EVs and whether its topology on EVs is affected upon cell treatment with GM1, I performed a protease protection assay using the protease Proteinase K on EVs from N2a 72Q cells. EVs were permeabilized using the detergent saponin before or after subjecting them to Proteinase K treatment. Proteinase K digestion before detergent permeabilization with saponin would only cleave proteins present on the EV membrane. On the other hand, proteinase K treatment after saponin permeabilization would digest both membranal and luminal proteins. As Alix is a luminal EV marker [436, 437], it was used as a control for proteinase K digestion (**Figs. 21.A, 21.C**). Indeed, signal for Alix did not change much upon Proteinase K treatment before detergent permeabilization, indicating that the protease may not be permeabilizing the membrane by itself. Also, as expected, both Alix and mHTT levels were diminished when EVs were permeabilized before Proteinase K treatment (**Fig. 21**). Importantly, signal for mHTT did not change when Proteinase K treatment preceded saponin permeabilization, thus showing that majority of the mHTT associated to EVs is present in the EV lumen (**Figs. 21.A, 21.B**). Furthermore, the GM1 treatment group shows a higher signal for mHTT compared to the control group, while signal for Alix is unchanged, indicating that GM1 treatment enhances the intraluminal expression of mHTT (**Fig. 21**). These findings suggest that GM1 stimulates cells to load mHTT into EVs rather than promoting its association to the surface of EVs once it has been secreted in the extracellular milieu.

3.1.9 Cell treatment with GM1 does not influence the size distribution of EVs

As the size of EVs can be indicative of their biogenesis and function, I next investigated whether cell treatment with GM1 altered the size distribution profile of the secreted EVs. Analysis of EVs by both NTA (**Fig. 22**) and DLS (**Fig. 23**) showed no significant size differences between treatment groups for both genotypes, thus indicating that GM1 might be increasing the overall secretion of EVs irrespective of size. It must be noted that the values for mean, median and mode for the experimental groups are different across the two methods, likely because of the lower sensitivity of NTA compared to DLS, which might skew the population of EVs detected towards a bigger size [394].

3.1.10 Cell treatment with GM1 increases the GM1 content in EVs and their parent cell lysates

As expected, treatment of N2a and N2a 72Q with GM1 increased its levels in cell lysates (**Fig. 24**). GM1 treatment caused the EVs secreted and isolated by UC to have higher GM1 content as determined by normalizing the total GM1 signal in the EV fraction to the total EV DiI fluorescence (**Fig. 24.A**), the latter being used as a surrogate measure of EV membranes. Similar results were obtained when EVs were isolated by SEC and the signal for GM1 was normalized over the number of DiD positive particles detected by IFC (**Fig. 24.B**).

3.2 *Role of endogenous gangliosides in the secretion of EVs and mHTT*

3.2.1 Inhibition of ganglioside synthesis decreases the cell secretion of EVs

As cell enrichment with GM1 (by administration of exogenous GM1) promotes EV secretion, I hypothesized that depleting GM1, and potentially other gangliosides, would impair EV secretion. Lack or decreased levels of gangliosides have been associated to many neurodegenerative diseases [83-85, 452-454] and hence, decreasing the endogenous levels of gangliosides in cells would mimic the reduction observed in these diseases. Inhibition of ganglioside synthesis in cells was achieved with pharmacological as well as genetic strategies. To test whether pharmacological inhibition of cellular gangliosides decreases secretion of EVs and mHTT, I used Genz-123346 [455], an inhibitor of glucosylceramide synthase (UGCG), the first enzyme in the ganglioside biosynthetic pathway (**Fig. 1**). Preliminary studies in our lab have shown that Genz-123346 used at a concentration of 1μM in N2a cells reduces GM1 and GD1a levels to 25% and 10% respectively and causes minimal toxicity (>10%) (data not shown) after 48 h of treatment. Of note, elevated ceramide levels in cells have been shown to promote EV secretion [38]. However, Genz-123346 decreases cellular ganglioside levels without causing ceramide accumulation [456, 457], thus ruling out potential confounding effects on the secretion of EVs.

To determine the effects of pharmacologically decreasing endogenous gangliosides on the secretion of EVs, N2a and N2a 72Q cells were stained with DiD and treated with vehicle (0.01% DMSO) or Genz-123346 (1μM) for 48 h (**Fig. 25**). As expected, treatment with Genz-123346 effectively decreased GM1 in both N2a and N2a 72Q

cells to similar levels. In basal conditions, N2a 72Q cells had less GM1 than control N2a cells (**Figs. 14, 26**), confirming previous findings in other HD models [85].

Analysis of the CCMs by IFC after 48 h of Genz-123346 treatment showed a decrease in DiD positive EV particles compared to control for both genotypes (**Fig. 27.A**). However, the data did not reach statistical significance due to inter-experimental variability. On the other hand, CCM analysis by fluorometry to measure DiD fluorescence associated to EV membranes showed that Genz-123346 treatment resulted in a statistically significant decrease in the secretion of EVs by both N2a and N2a 72Q cells (**Fig. 27.B**). As the DiD mean fluorescence intensity per EV particle was not affected by the treatment (**Fig. S7**), these data suggest that Genz-123346 might have decreased particle secretion, but that the IFC analysis was not sensitive enough to reveal the changes. This explanation is supported by the fact that lower total levels of DiD fluorescence were measured in the EV fractions separated by SEC (**Fig. 27.C**). Altogether, my data suggest that the impaired EV secretion observed in HD cells by our lab (**Fig. 15**) and by others [458], might be, at least in part, due to the lower cellular GM1 levels in HD cells compared to normal cells.

The finding of decreased EV secretion on cell treatment with Genz-123346 was also confirmed by deleting *B4galnt1*, the gene encoding GM2/GD2 synthase, from N2a cells by CRISPR/Cas9 genome editing (N2a Δ*B4galnt1* cells). This cell line lacks endogenous complex gangliosides, including GM1 (**Fig. 28**), although low levels of GM1 can be detected in cells grown in the presence of serum, presumably due to the presence of gangliosides in the serum [16] and the ability of cells to take them up (data

not shown). DiI fluorescence measured in the EV fractions separated by SEC from the CCMs showed a lower amount of EVs secreted by the N2a Δ*B4galnt1* cells compared to control cells (**Fig. 29**). Importantly, administration of exogenous GM1 increased cellular GM1 levels in N2a Δ*B4galnt1* cells (**Fig. 30.A**) and resulted in a partial restoration of EV secretion (**Fig. 30.B**), suggesting that the low EV secretory phenotype of these cells is, at least in part, due to the lack of GM1 among other gangliosides. Of note, there was no difference between the dye incorporated by EVs across treatment groups, as measured by IFC (**Fig. S4**). Thus, the studies so far, confirm that inhibition of ganglioside synthesis reduces the secretion of EVs from neuronal cells, and lend support to the hypothesis that gangliosides, and GM1 in particular, play an important novel role in the secretion of EVs.

3.2.2 Cellular ganglioside levels positively correlate with EV secretion

To further confirm the role of gangliosides in EV secretion, I performed a correlation analysis between cellular GM1 levels as the independent variable and EV secretion as the dependent variable, using data from N2a and N2a 72Q cells treated with vehicle or Genz-123346 or left untreated. All data were normalized over untreated N2a control values. I found a fairly strong positive linear relationship ($r = 0.77$, $p<0.0001$) between the two variables, strongly suggesting the involvement of cellular gangliosides in the secretion of EVs (**Fig. 31**).

3.2.3 Inhibition of ganglioside synthesis decreases the export of mHTT via EVs

Next, I investigated whether inhibition of ganglioside synthesis would also decrease the secretion of mHTT from EVs, contrary to the effects of exogenously administered

GM1 on cells. To test this, EVs from N2a 72Q cells treated with vehicle or Genz-123346 were isolated by SEC (**Fig. 25**). Aliquots of EV fractions normalized over the corresponding total cellular protein content were analyzed by immunoblotting and ELISA. Immunoblotting results showed that Genz-123346 significantly reduced the secretion of mHTT via EVs (**Fig. 32.A, 32.B**). Of note, the secretion of the EV marker CD9 also showed a decreasing trend (**Fig. 32.B**), but Alix levels did not (**Fig. 32.B**), thus suggesting that specific EV subpopulations might be affected by the treatment. Interestingly, a larger effect of Genz-123346 was determined by measuring mHTT expression in EVs by ELISA (**Fig. 32.D**) as compared to determination by immunoblotting (**Fig. 32.B**), which could be because of the higher sensitivity of the ELISA method. The expression of mHTT-GFP in the cell lysates was not influenced (**Fig. 32.C**), despite decreased secretion. Once again, this is possibly due to the cell model overexpressing the protein. Alternatively, the overall amount of mHTT secreted might be too small compared to the intracellular levels, to result in a detectable change in the latter in a short period of time.

3.2.4 GM1 content in EVs is modulated by ganglioside levels of parental cells

Similar to the increase in GM1 content observed in EVs from cells treated with GM1, cell treatment with Genz-123346 showed a decreasing trend in GM1 levels in EVs secreted by both N2a and N2a 72Q cells (**Fig. 33.A)**. In two independent experiments, EVs from N2a Δ*B4galnt1* cells also contained less GM1 than those from N2a cells (**Fig. 33.B**), in accordance with the trend seen in their parent cell lysates (**Fig. 28**). The potential implications of these observations will be discussed in the next chapter.

CHAPTER 4: DISCUSSION

My studies have highlighted a novel role of gangliosides in the secretion of EVs. While on one hand, exogenous administration of GM1 to cells increases EV release as demonstrated in both neuronal and non-neuronal (human fibroblast) cells, inhibition of cellular gangliosides, on the other hand, either by pharmacologically blocking UGCG, or by genetically inhibiting *B4galnt1*, decreases overall EV secretion. Moreover, exogenously added GM1 to cells with *B4galnt1* deletion restored normal cellular GM1 levels while also promoting EV release. Furthermore, the impact of cellular gangliosides on EV secretion is underscored by the strong positive correlation between them.

The field of EV biology is rapidly advancing but is still relatively young, and hence, experiences a lack of well-established, reproducible standard techniques [408]. Moreover, the small size of EVs coupled with their heterogeneous population make separating and classifying EVs based on their size, cargo, composition, and function, among others, a major challenge that is yet to be resolved [388]. Many methods have been used to isolate EVs. However, every method has its limitations [262]. In general, the methods used for EV isolation can have a major influence on the quantity and quality of EVs isolated for downstream analysis [262, 389, 408, 444]. In my experiments, EVs were initially isolated by UC. However, as discussed previously, my data, in agreement with other studies [432, 443], showed that isolation by UC results in low efficiency of EV recovery (<10%), at least in part due to the fact that the EVs secreted by N2a cells have a density that is lower than the mean threshold density

required for efficient pelleting by UC [442]. Hence, a method to separate EVs from the CCM by SEC was optimized. Although SEC is a superior EV isolation method compared to UC, EV loss during the procedure still occurs. Therefore, in order to analyze the whole population, EVs were measured directly in the unprocessed sample, after the removal of cellular debris and apoptotic bodies, i.e., in the CCM, using complementary techniques that allowed for EV analysis at the single-particle level, including IFC, Cytoflex flow cytometry, NTA [390, 391, 413, 459].

In my studies, GM1 was administered in media without serum to not only avoid potentially confounding effects of gangliosides and other lipids present in the serum but also to 'mimic' the serum-free environment in the brain. EVs were initially collected in medium containing EV-depleted serum, prepared by extended centrifugation of the serum at 100,000 x g. However, my studies and other published work [438, 439]. suggest that this medium still contains EVs. Hence, the collection medium was replaced to SFM+N2 that enabled equivalent secretion levels of EVs without causing cellular toxicity (data not shown, Viveiros et al., manuscript in preparation). As cell confluence has shown to influence EV secretion [444], all cells were seeded to reach a confluence of 80% at the end of the experiments, to avoid cellular quiescence by contact inhibition and ensure healthy conditions in the cellular microenvironment.

In my experiments, I pre-labelled donor cells with fluorescent carbocyanine dyes DiI or its substrate analogue DiD. These dyes intercalate with lipids in biological membranes with no reported specificity for any lipids. Both dyes stain membranes uniformly [460]. However, due to a difference in their excitation and emission spectra

($\lambda_{Ex}/\lambda_{Em}$ for DiI is 549/565nm and for DiD is 644/665nm), DiD is a better fit for the lasers available in the ImageStream machine used for IFC. Therefore, in most experiments, DiD was used to label membranes. More than 90% of the particles were DiD positive in my experiments, as measured by IFC, and the rest were DiD negative (data not shown). The DiD negative population may include EVs that are not labelled with DiD or have dye incorporation levels below the detection threshold level. They could also be 'non-EV' protein aggregates secreted in the media or speed beads out of focus that got included in the analysis. These issues cannot be mitigated completely at present, as current protocols for IFC do not allow for label-free detection of EVs due to the low signal-to-noise ratio and thus, demand for fluorescent EV markers [403, 459]. Detection of EVs without labelling is possible using NTA and DLS [397, 461], with the caveat that non-EV particles may be recognized as EVs [390], thus potentially overestimating the total number of particles.

My studies demonstrate for the first time that in neuronal cells as well as patient-derived fibroblasts, gangliosides are important modulators of EV secretion. The impact of gangliosides on EV release was studied by increasing cellular ganglioside levels with exogenously administered GM1 as well as by decreasing their levels using two complementary approaches, viz., by pharmacologically blocking UGCG, the first enzyme of the ganglioside biosynthetic pathway, or by genetically ablating *B4galnt1*, the gene responsible for the synthesis of complex gangliosides (GM1, GD1a, GD1b, GT1b). Analyses using multiple techniques demonstrated that an increase in the levels of cellular GM1 increased EV secretion, while the opposite effect was observed when the synthesis of gangliosides was blocked. Surprisingly, genetic inhibition of

gangliosides led to a more pronounced decrease in EV secretion as compared to pharmacological inhibition, although both strategies reduced cellular GM1 to similar levels. This difference could be due to off-target effects of both approaches. Alternatively, it could be suggestive of a modulatory role of gangliosides other than GM1 on EV secretion. For example, in the *B4galnt1* KO model, a decrease in the levels of complex gangliosides might be accompanied by an increase in the levels of simple gangliosides like GM3 (**Fig. 1**). The increase in GM3, concomitantly with a decrease in GM1, might perhaps explain the stronger phenotype observed in the *B4galnt1* KO cell model, compared to the pharmacological inhibition of UGCG which would result in the decrease of all gangliosides, including GM3 – suggesting that GM3 and other simple gangliosides might be negative regulators of EV secretion. It is also of interest to note that, in the KO model, exogenously added GM1 could not entirely rescue its low EV secretion phenotype and corrected it only partially, despite restoring cellular GM1 levels. This also hints at the potential involvement of other complex gangliosides in EV secretion, because although exogenously added GM1 will elevate GM1 and potentially its downstream ganglioside, GD1a, other complex gangliosides like GD1b and GT1b will continue to remain low (**Fig. 1**). The lower levels of GD1b and GT1b and/or the higher levels of GM3 could thus explain why GM1 treatment could not fully rescue the low EV secretion phenotype observed in the KO model, thus suggesting a potential role of other gangliosides in EV secretion. Future studies will address this hypothesis and test the effects of administering the various gangliosides, alone or in combination, on EV secretion. Notably, Genz-123346 mediated inhibition of UGCG enhances autophagy in neurons [462], which could thereby influence EV secretion,

potentially decreasing it [339-343]. Hence, it is imperative to confirm that the effects of UGCG inhibition on EV secretion are due to the lack of gangliosides. To this end, in future experiments, cells will be replenished with GM1 or a mix of gangliosides after treatment with Genz-123346 to correct EV secretion.

In physiological conditions, EVs are critical players in ameliorating proteotoxic stress. For instance, inhibition of the quality control, proteostasis-regulator ubiquitin ligase STUB1/CHIP led to the accumulation of proteins intracellularly which concomitantly resulted in an enhanced secretion of EVs enriched with oligomeric proteins and ubiquitinated cargoes [352]. Another recent study showed that neuronal cells secrete exosomes containing heat shock proteins (HSPs) like Hsp40, Hsp70 and Hsp90, which are molecular chaperones important for proper protein folding and maintenance of proteostasis [463], and their secretion levels are enhanced during proteotoxic challenges [464]. Furthermore, exogenous administration of these exosomes to polyglutamine (Q81) expressing cells significantly suppressed inclusion body formation [464]. Thus, due to their essential role in alleviating cellular proteotoxicity, a decrease in EV secretion caused by reducing the levels of cellular gangliosides like GM1 as discussed earlier, may potentially prove detrimental. A reduction in ganglioside levels is observed in several neurodegenerative diseases [80-83], including HD [84, 85]. Thus, overall, my findings raise an important question of whether neurodegenerative diseases exhibiting reduced levels of gangliosides also display impaired/reduced levels of EV secretion, thereby making neuronal cells more susceptible to proteotoxic stress. Indeed, my studies in a neuronal cell model expressing mHTT (N2a 72Q), which has lower levels than normal of GM1, as well as

a published study on HD astrocytes [458] showed that HD cells exhibit a low EV secretion phenotype. In my studies, GM1 treatment promoted EV secretion in HD cells. Importantly, the treatment increased the levels of mHTT in the secreted EV fraction. Conversely, inhibition of cellular gangliosides not only decreased EV secretion but also reduced the export of mHTT in the EVs. These results indicate that GM1 stimulates cells to export mHTT via EVs, to potentially decrease cellular proteotoxicity.

I also demonstrated that the majority of mHTT secreted in EVs is luminal and GM1 treatment increases it without changing its topology. Thus, mHTT appears to be exported into the extracellular environment loaded *within* EVs rather than being associated with EV membranes *after* their secretion. Of note, the localization of Aβ on the surface of exosomes is supported by immunogold labelling studies [346]. Other studies performed to determine the topology of misfolded proteins in EV fractions have provided contradicting results and have been largely unconvincing mostly due to the lack of proper experimental controls. For example, using the protease Proteinase K and its inhibitor 4-(2-aminoethyl) benzenesulfonyl fluoride hydrochloride (AEBSF), Sinha et al. reported the mainly luminal presence of Aβ associated to EVs [465]. However, the study failed to use a *bona fide* membrane EV marker such as CD9 [288] as a control to show that the enzymatic activity of Proteinase K was not suboptimal. Another study used the protease trypsin to prove that the majority of Aβ is present on the EV membrane [466], but failed to include a control to confirm that EV membranes were not broken and/or permeabilized, thus allowing trypsin to get access to luminal proteins in addition to surface ones. Similarly, a study that used trypsin along with the detergent saponin to permeabilize the EV membrane reported the presence of α-

synuclein in exosomes to be both membranal as well as luminal, with its abundance being higher in the membrane fractions [356]. In another study, after EV treatment with Na_2CO_3 to break EV membranes and release soluble luminal proteins, α-synuclein was found to be present in higher amounts in the exosomal membrane fraction than in the luminal soluble protein fraction [345]. Alix, which is a *bona fide* luminal EV marker [436, 437], was also present in the membrane fraction. Although both Alix [467] and α-synuclein [468] could potentially associate with the luminal leaflet of EV membranes, this study did not address whether α-synuclein could associate with the surface of EVs *after* its secretion. On the other hand, by performing a Proteinase K protection assay with saponin-mediated permeabilization as well as by using increasing concentrations of NaCl to remove peripheral membrane-associated tau, Wang et al. reported that tau is located within exosomes [437]. Of note, misfolded proteins can associate with the surface of EVs in the extracellular milieu [296, 469], after they have been secreted in a naked form, and this interaction can influence their biological properties and modulate their interactions with recipient cells [389, 392]. For instance, Yuyama et al. previously reported that extracellular Aβ binds to glycosphingolipid clusters on membranes of exosomes from neuroblastoma cells and undergoes fibrillization [296, 469]. Interestingly, neuroblastoma cell-derived exosomes injected *in vivo* into transgenic APP-expressing mouse brains trapped Aβ and were subsequently internalized by microglia for degradation [469]. My data indicates that mHTT in EVs is mainly luminal, which suggests that this pool of mHTT remains separate from the mHTT that might be secreted in a naked form by the unconventional secretion pathway

[365]. Whether gangliosides can also affect mHTT secretion through this pathway was not investigated in this thesis.

Other important questions that remain to be answered are whether there is a preferential secretion of mHTT over wtHTT upon cell treatment with GM1, and whether secretion of mHTT within EVs is sufficient to decrease cellular mHTT. The first question can be addressed by co-transfecting both *wtHTT* as well as *mHTT* in cells and observing their levels in EVs and parent cells upon GM1 treatment. Since *in vivo* treatment with GM1 decreased mHTT but not wtHTT levels in the brains of heterozygous HD mice [256], mHTT might be preferentially secreted in response to GM1 treatment. In my studies, using human HD fibroblasts, I observed a decrease in cellular mHTT levels concomitantly with an increase in EV secretion (although mHTT levels in EV fractions could not be determined). However, N2a 72Q cells pre-incubated with GM1 failed to recapitulate the effect in their cellular mHTT levels. This could be attributed to several reasons. Firstly, the cells used in my studies overexpress the mHTT cDNA under control of the strong and stable cytomegalovirus (CMV) promoter. Thus, any GM1-mediated export of mHTT may have been compensated by the continuous, steady-state supply of mHTT, preventing a significant and detectable decrease of its intracellular levels. Secondly, treatment with GM1 for 6 – 18 h may have been insufficient to significantly reduce cellular mHTT levels in this cell line, and a prolonged treatment may be necessary. Finally, it is also plausible that a more sensitive method than immunoblotting, such as ELISA, might be required to detect small mHTT changes intracellularly over a short period of time. Some of these issues can be addressed in the future by determining the effects of GM1 in the inducible rat

pheochromocytoma PC12 cells expressing mHTT where the transgene expression can be controlled by ponasterone-A [470], thus preventing potential confounding effects caused by constitutive overexpression. In addition, primary neurons from Q140 mice will be used in the future, to observe whether an increased secretion of EVs carrying mHTT is accompanied by a decrease in total cellular levels of mHTT. Similar studies can be performed using Genz-123346 to further validate whether a decrease in cellular gangliosides causes a decline in mHTT secretion through EVs with a collateral increase in intracellular mHTT accumulation.

Future studies will also confirm the effects of gangliosides on EV secretion in mouse models *in vivo*.

Although GM1 promotes the secretion of EVs, the underlying mechanism/(s) behind these effects are still unclear. Cell treatment with GM1 increases its content in EVs, yet surprisingly, it does not affect the size distribution of EVs as shown by data generated using NTA and DLS. This finding suggests that some of the incorporated GM1 might be in the EV lumen, and future studies can test this by performing immunogold labelling for GM1. Furthermore, the size range of EVs affected by the treatment is broadly between 70nm and 150nm, which overlaps with the size ranges of exosomes and microvesicles [264, 471], making it difficult to discriminate whether GM1 affects a specific subpopulation of EVs based on size. Nevertheless, some clues on its activity to stimulate EV secretion can also be obtained from our preliminary proteomics analysis on WT and HD mice brains treated with GM1 (compared to untreated controls) *in vivo*, which showed that several proteins involved in EV biogenesis are increased in the brains of animals treated with GM1 (preliminary data,

not shown). These include CD81 (a tetraspanin marker of EVs that interacts with lipid rafts and participates in the recruitment of proteins into EVs) [288], Rab11b and Rab35 (GTPases involved in endocytic recycling) [293, 472-474], EH domain-containing protein (EHD4) (ATPase that associates with the membrane and participates in membrane tubulation and fission) [475, 476], among others. All these proteins have a common feature, in that, they bind to membranes, the composition of which (i.e. the specific enrichment in cholesterol, sphingomyelin, and glycosphingolipids) modulates their association and activity [477-480]. Thus, membrane enrichment with gangliosides might facilitate the recruitment of proteins involved in EV biogenesis. Moreover, several studies have highlighted the enrichment of cholesterol in EVs as compared to their parent cells [477], and the important role of cholesterol in EV biogenesis [477]. In GM2/GD2 synthase KO mice, Ohmi et al. found that both cholesterol and sphingomyelin are decreased, concomitantly with the lack of complex gangliosides [481]. Whether changes in ganglioside levels in the models used in this thesis are associated with changes in cholesterol and sphingomyelin levels was not investigated but could be an important information to obtain in future studies.

Characterizing and phenotyping EVs based on the expression of their protein markers – which can be achieved by immunoblotting or flow cytometry analyses, among others - may also provide hints about their biogenesis, mechanism of secretion and functional role [333, 482]. As an example, GM1 might increase the externalization of PS on EV membranes, which, as discussed before, would function as an ‘eat-me-signal’ that targets the EVs toward uptake and degradation by phagocytic cells [315]. Levels of PS can be measured by exploiting its binding to Annexin V [316].

Furthermore, pharmacological inhibitors that target specific pathways of EV biogenesis and secretion can be employed to determine whether GM1 affects one or more pathways. For instance, manumycin A, a cell-permeable, selective and potent inhibitor of Ras GTPase activity, can be employed to determine whether GM1-mediated effects on EV secretion rely on the ESCRT machinery [483, 484]. Similarly, the neutral sphingomyelinase inhibitor, GW4869, can be used to investigate if the mechanism is ceramide-dependent [38, 483]. Finally, the potential GM1-mediated impact on microvesicle release can be studied using Y27632, a competitive inhibitor of Rho-associated protein kinases (ROCK), which are serine-threonine kinases involved in cytoskeleton reorganisation and microvesicle production [483].

Of note, the pharmacological inhibitors discussed above can also be used to block EV secretion in HD cells in order to determine whether EV secretion is, in fact, a necessary pathway in HD cells without which their survival would be compromised. For this, due consideration must be given to determining the optimal concentrations of inhibitors that can reduce EV secretion without causing non-specific, drug-induced cytotoxicity, to avoid confounding results.

A general synopsis of my findings which also includes the hypothesis we are currently working on in our lab is shown in the form of a diagrammatic model in **Fig. 34**. As discussed before, EVs, considered to be a double-edged sword in neurodegenerative diseases, can contribute to increasing disease pathogenesis by carrying toxic proteins and facilitating their transcellular spreading [348-350]. However, some studies also point out that EVs may decrease cellular proteotoxic stress [348, 351, 352] by

exporting toxic proteins and targeting them to phagocytic cells like microglia for subsequent degradation [296, 469]. Thus, investigating the fate of EVs carrying mHTT post-GM1 treatment is of paramount importance. As GM1 administration was shown to have profound therapeutic effects in HD models *in vivo*, it is unlikely that GM1-mediated increase in EVs and mHTT secretion would promote disease spreading. Instead, GM1 might modify the properties of the secreted EVs to promote their clearance by microglia and other brain cells. It is plausible that the enrichment of the EV surface with GM1, as it occurs upon cell treatment with the ganglioside, might serve as a 'code' to preferentially target EVs to microglia for degradation. Future studies in our lab will address this hypothesis. Microglia are indeed a primary target of EVs in the CNS [296, 485], but what drives preferential EV uptake by microglia or by other brain cells is currently unclear [296]. PS exposed on the surface of N2a-derived EVs was found to be crucial for microglial uptake of exosomes carrying Aβ, while blocking GM1 found on exosomes by cholera toxin B subunit had no effect on microglial internalization of Aβ with exosomes [296]. However, our studies in collaboration with Ms. Anissa Viveiros (data not shown, Viveiros et al., manuscript in preparation) suggests that only a small fraction of EVs secreted by N2a cells externalize PS, suggesting that additional molecules might mediate EV uptake. Furthermore, in the context of neurodegenerative conditions, the uptake of EVs by microglia can trigger inflammatory microglia activation that can contribute to neuronal damage [359]. EV enrichment with GM1, as shown in my studies, might play an important role on the response of microglia upon EV uptake. Recently, data from our lab have revealed that exogenous administration of GM1, either in micellar or liposomal form, can decrease

the production of inflammatory cytokines from microglia challenged with pro-inflammatory response-inducing stimuli (like LPS, IL-1β and others) (Galleguillos et al., manuscript in revision, available through BioRxiv). This suggests that GM1 on the surface of EVs might play a similar role and reduce pro-inflammatory microglia activation in the context of neurodegenerative conditions.

In conclusion, while GM1/gangliosides-mediated secretion of EVs might decrease proteotoxic stress in vulnerable neurons in HD, the enrichment of GM1 on the surface of EVs may potentially favour microglial uptake without eliciting a detrimental pro-inflammatory response. Furthermore, the finding that GM1 enhances EV secretion in WT cells suggests that its effects are not specific to HD only. Thus, GM1 can potentially stimulate EV secretion and exert beneficial effects in other protein misfolding diseases like AD and PD.

CHAPTER 5: FIGURES

Fig. 1: Ganglioside biosynthetic pathway

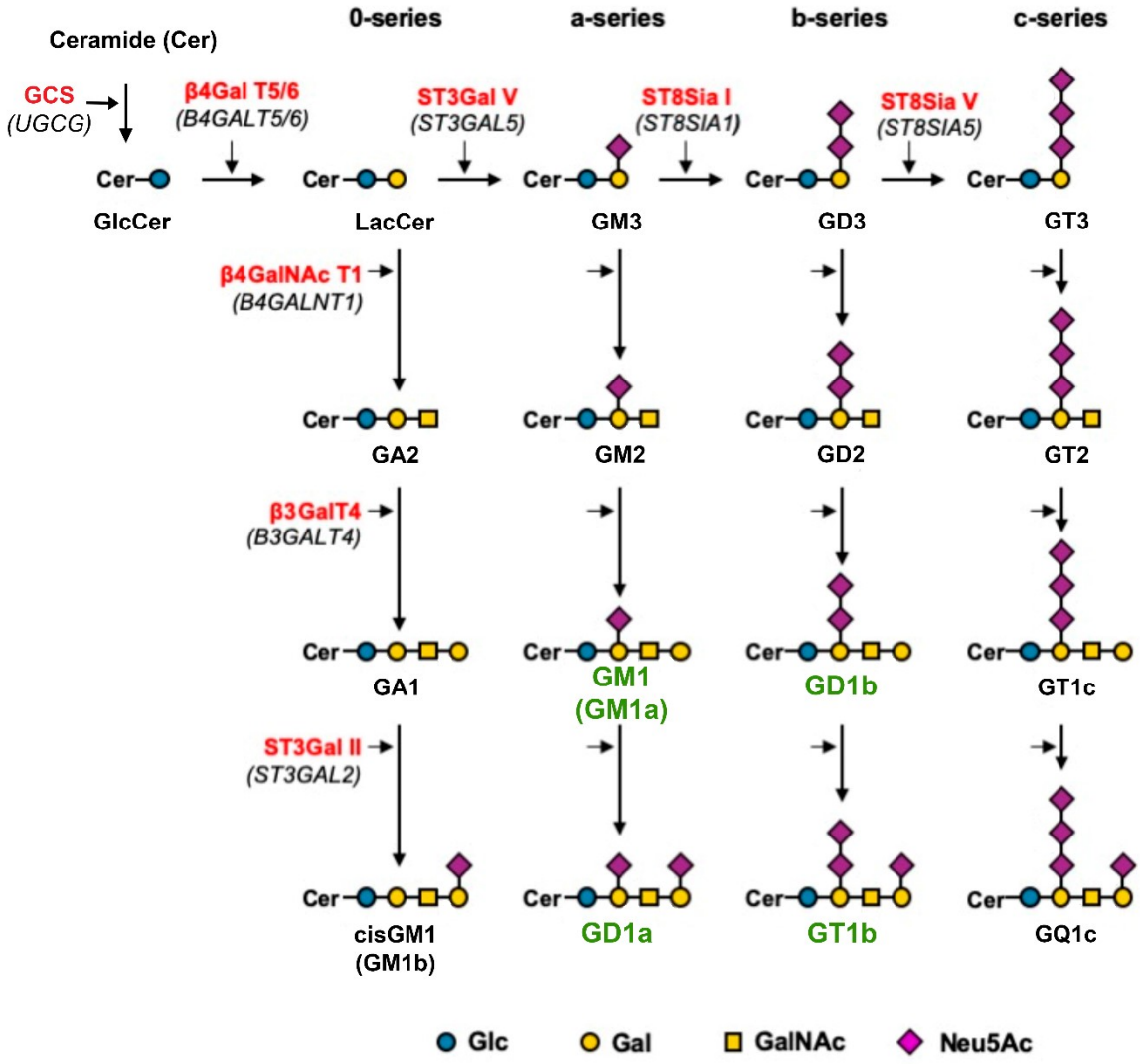

Schematic representation showing the pathway of ganglioside biosynthesis. Ceramide (Cer) is the precursor of gangliosides. It undergoes sequential addition of monosaccharides to synthesize glucosylceramide (GlcCer) followed by lactosylceramide (LacCer), catalysed by enzymes glucosylceramide synthase (GCS) and β-1,4-galactosyltransferase 5 (β4Gal T5/6), respectively. 0-series gangliosides

are synthesized directly from LacCer. Furthermore, precursors of a-, b-, and c- series gangliosides are synthesized from LacCer through the stepwise action of GM3 synthase (ST3Gal V), GD3 synthase (ST8Sia I) and GT3 synthase (ST8Sia V). The genes encoding the glycosyltransferases and sialyltransferases are italicized, indicated in red in parentheses. The major brain gangliosides are indicated in green. Abbreviations used for ganglioside nomenclature are according to Svennerholm [486] Adapted from [487].

Fig. 2: Structure of ganglioside GM1

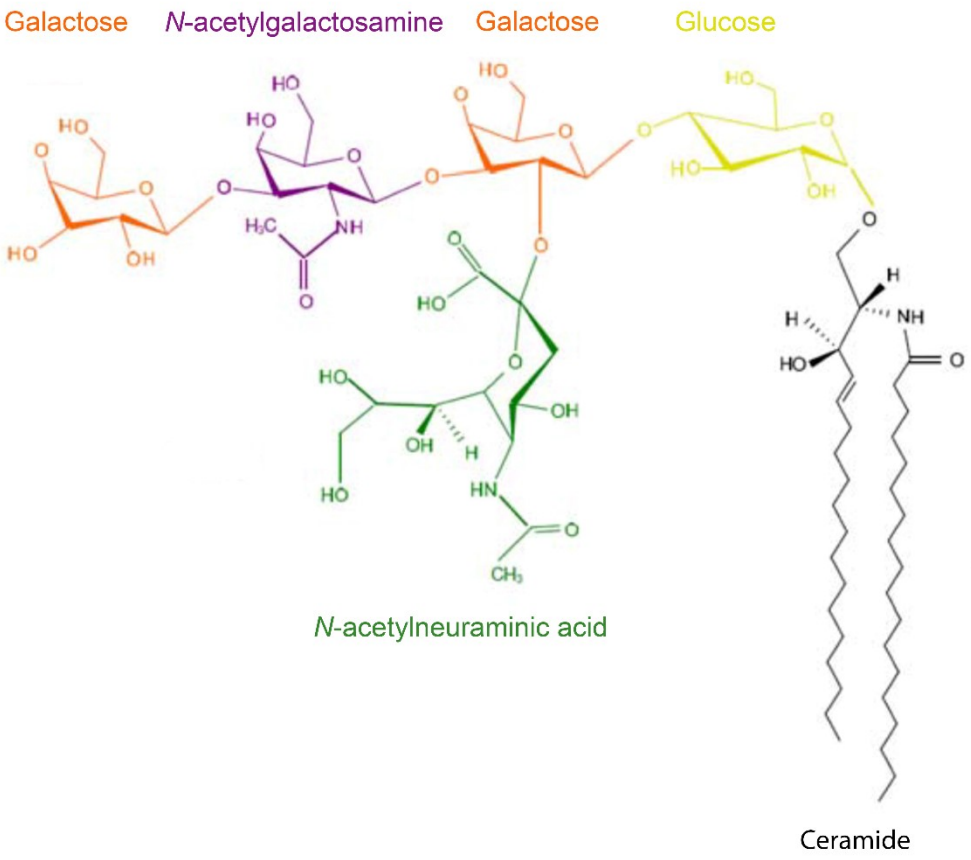

Structure of ganglioside GM1. The ceramide moiety, indicated in black, is anchored to the plasma membrane. The glycan region, with its structures denoted in yellow, orange, purple and green face the extracellular environment. GM1 has only one sialic acid residue, depicted in green. Adapted from [488].

Fig. 3: Schematic of human HTT protein

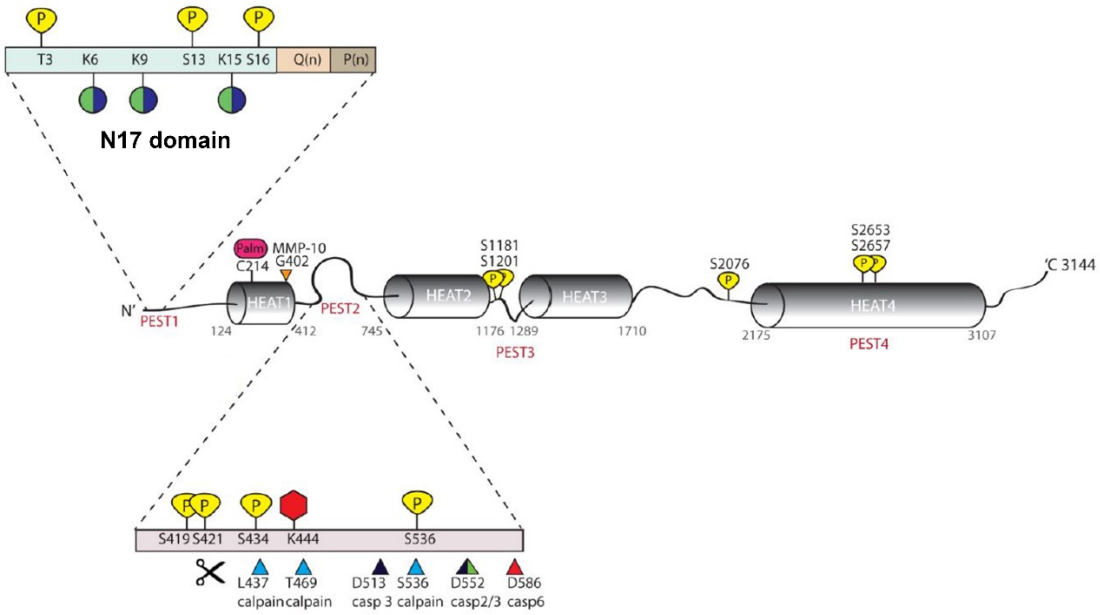

Schematic representation of the HTT protein and its post-translational modifications (PTMs). HTT has four HEAT repeats and four PEST domains, which are marked along its length. PEST 1 domain (containing the first N-terminal 17 amino acids (N17), polyglutamine tract Q(n) and polyproline sequence P(n)) and PEST 2 domain have been magnified to show the large number of clustered PTMs in these regions. Phosphorylation sites at threonine (T) or serine (S) residues are indicated in yellow. Lysines (K) which are modified either by ubiquitination or SUMOylation are denoted by circles in green and purple. Acetylation at lysine (K) 444 is represented as a red hexagon and palmitoylation at cysteine (C) 214 is represented as a pink oval. Protease cleavage sites are marked by triangles; calpain sites are indicated in blue, caspase −2, −3 and −6 sites are indicated by green, black, and red, respectively and matrix metalloproteinase-10 (MMP10) site at 404 is indicated in orange. Adapted from [148].

Fig. 4: Cellular pathogenesis caused by mHTT

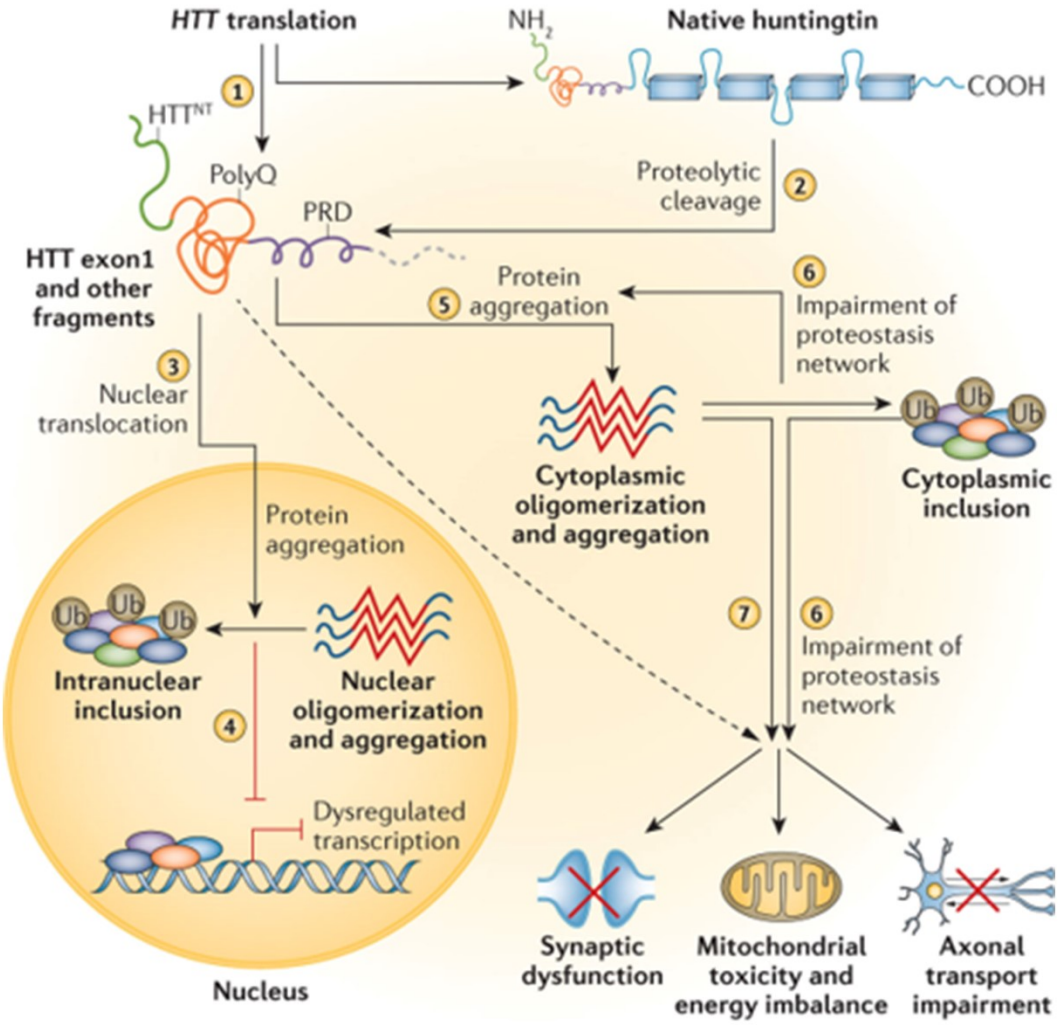

(1) *HTT* encodes the full-length HTT protein. It can also undergo aberrant splicing to encode an N-terminal exon 1 HTT fragment. (2) Full-length HTT is proteolytically cleaved to produce N-terminal HTT fragments among other fragments. (3) mHTT translocates to the nucleus. (4) In the nucleus, these fragments accumulate, oligomerize and aggregate to form inclusion bodies, which then disrupt the transcriptional machinery by sequestrating proteins involved and by other ill-defined mechanisms. (5) These fragments accumulate and aggregate in the cytoplasm to

form inclusions. (6) HD-associated impairment of proteostasis network also increases the tenacity of HTT aggregation, while also leading to other cellular disruptions like synaptic dysfunction, axonal transport dysregulation and mitochondrial impairment. (7) Such disruption of the cellular machinery is also caused by the toxic HTT species. polyQ, polyglutamine; PRD, proline-rich domain; Ub, ubiquitin. Reprinted by permission from Springer Nature [489].

Fig. 5: Prion-like pathology observed in neurodegenerative diseases

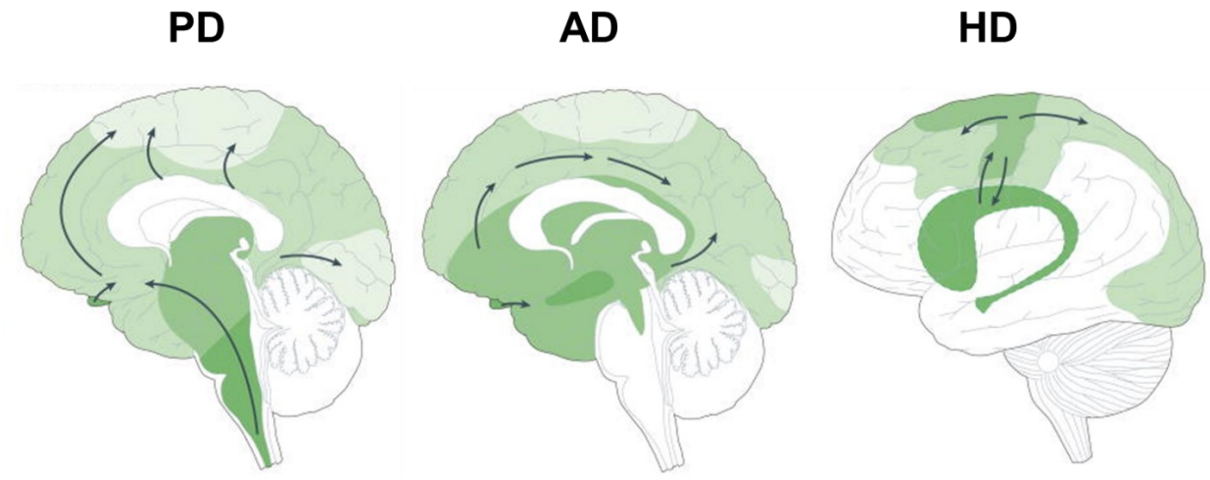

Schematic representation of the spatiotemporal spread of neuropathology observed during disease progression in PD, AD and HD brains, respectively. A mid-sagittal view is shown for PD and AD while a lateral view is shown for HD. The earlier the neuropathology develops in a brain region, the darker its shading in green in the diagram. In PD, Lewy bodies appear first in the dorsal motor nucleus of the vagal nerve in the brainstem and anterior olfactory structures (darkest green). In AD, Aβ neurofibrillary tangles appear first in the hippocampus, nucleus basalis of Meynert and the brainstem (darkest green). In HD, degeneration first occurs in the dorsal striatum (putamen and caudate nucleus) and associated basal ganglia structures (darkest green). Severe atrophy is also observed in primary motor and sensory cortices. After occurrence in these structures, the aggregates spread stereotypically to occupy other regions of the brain (shown in lighter shades of green); the pattern of spreading in each diseased brain is indicated by arrows. Adapted with permission from Springer Nature [490].

Fig. 6: Disease modifying effects of GM1 in HD

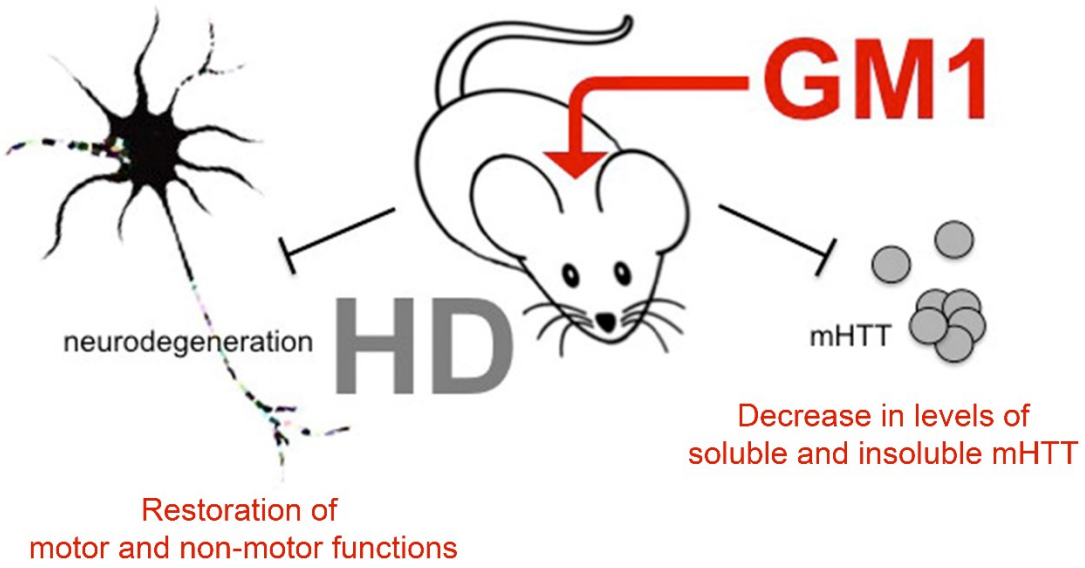

Synopsis describing the disease-modifying effects of GM1 in HD. In mouse models of HD, intracerebroventricular administration of GM1 led to correction of motor and non-motor impairments and slowing down of neurodegeneration. GM1 also decreased brain levels of both soluble and insoluble mHTT in HD mice. Adapted from [256].

Fig. 7: Proteins most significantly affected by treatment with GM1 are involved in the EV pathway

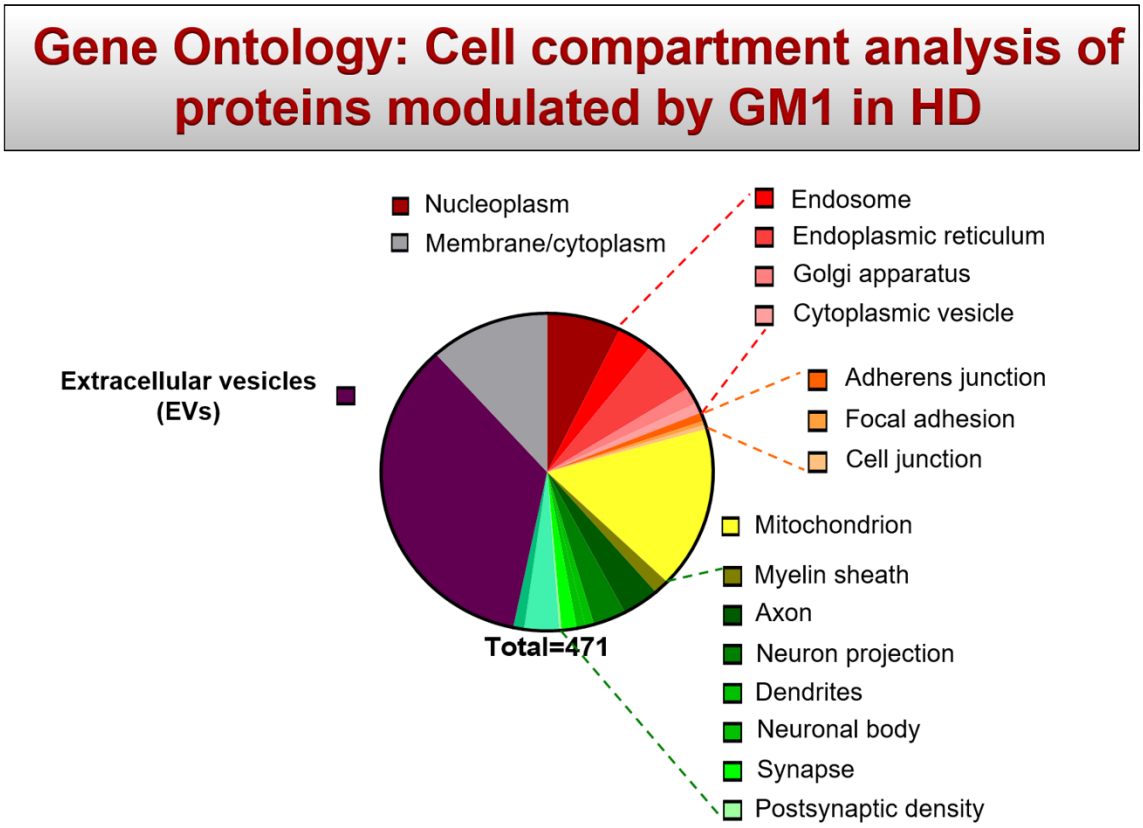

Proteomics and gene ontology analysis of both WT and HD mouse brains treated with GM1 (compared to untreated controls) *in vivo* revealed that the treatment significantly affected the abundance of proteins of the EV pathway (Sipione lab, unpublished data).

Fig. 8: Biogenesis and secretion of EVs

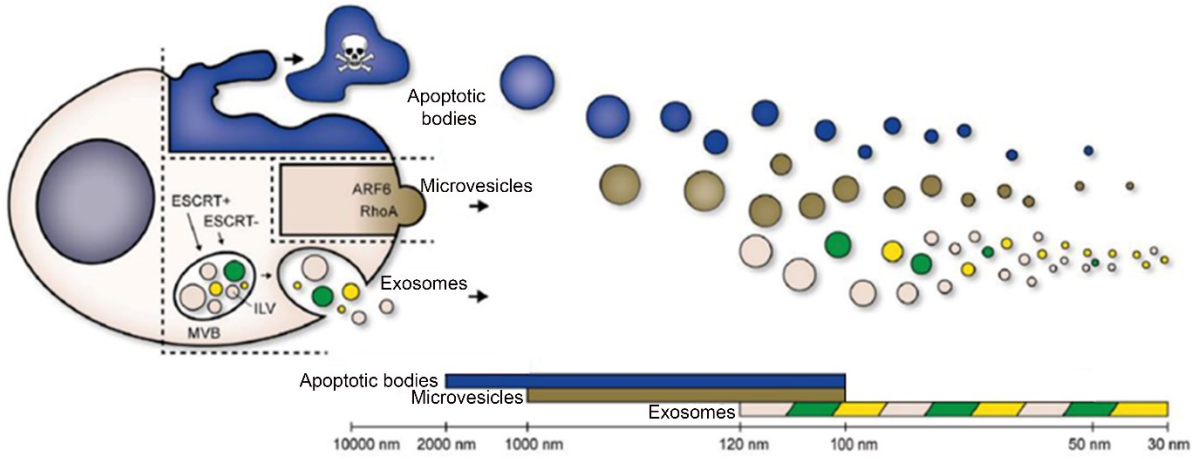

Schematic representation of EV biogenesis and release by eukaryotic cells. EVs consist of exosomes (pink), microvesicles (brown) and apoptotic bodies (blue) and have overlapping sizes. Apoptotic bodies are shed during programmed cell death. Instead, exosomes and microvesicles are shed by living cells. Exosomes are formed by the intraluminal budding of the multivesicular body (MVB), formed from early endosomes, which consequently fuses with the plasma membrane to release the vesicles. Both ESCRT-dependent (ESCRT+) and ESCRT-independent (ESCRT-) pathways are involved in exosome biogenesis. Unique subpopulations of exosomes (as indicated by green and yellow EVs) have been identified. Microvesicles are formed by outward budding and shedding of the plasma membrane, and ARF6 and RhoA are critical players in their biogenesis. Microvesicles can also be formed using the ESCRT machinery (not shown here). EVs are involved in performing several functions, including intercellular communication, synaptic plasticity and are known to carry biomolecules like proteins and nucleic acids. Adapted from [327].

Fig. 9: Experimental design for cell treatment with GM1 and EV collection and analysis

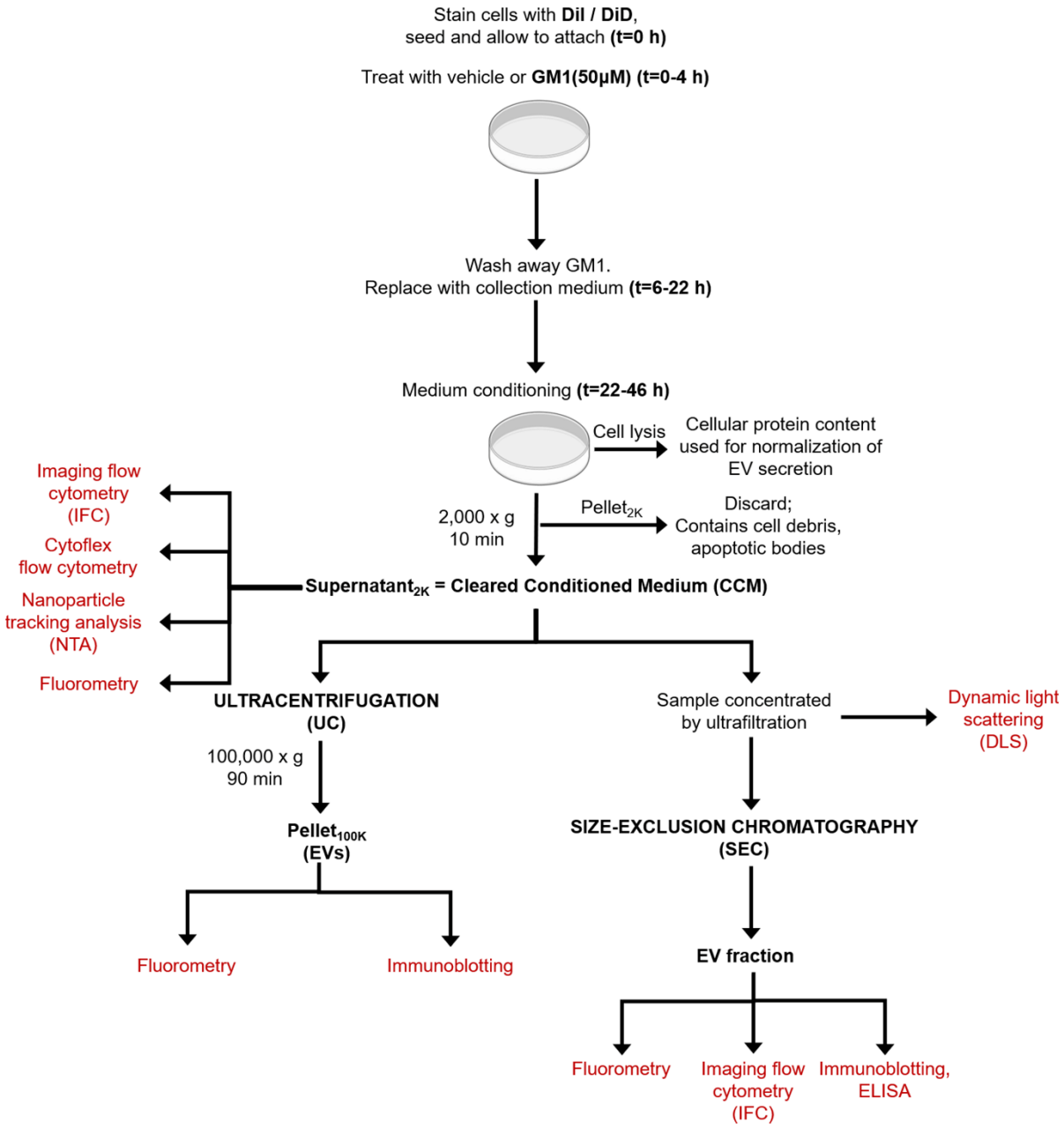

Schematic flowchart showing the general protocol and timeline for cell labelling, GM1 treatment, EV collection, isolation by ultracentrifugation (UC), size-exclusion

chromatography (SEC), and EV analysis by imaging flow cytometry (IFC), nanoparticle tracking analysis (NTA), among others.

Fig. 10: N2a cell treatment with GM1 increases the secretion of EVs as determined by EV isolation by ultracentrifugation

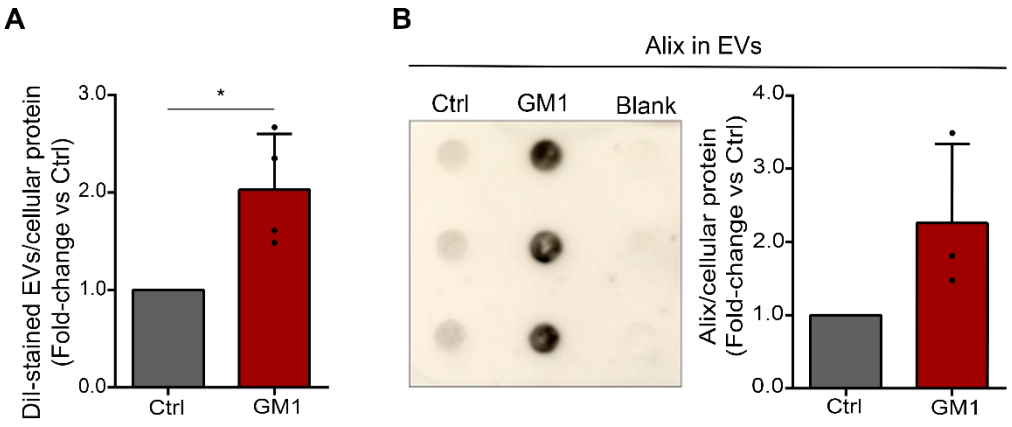

EVs released by N2a cells treated with vehicle (Ctrl) or GM1 for 18 h were collected in medium supplemented with EV-depleted serum (EVD complete medium) for 24 h and isolated by UC.

A. DiI fluorescence measured in the EV pellet was used as a surrogate measure of EV membranes. N=4.

B. Representative dot blot and densitometric analysis for the EV marker Alix in the EV fraction. Equivalent volumes of the EV pellet obtained by UC and resuspended in PBS were loaded in each well in triplicates and the total densitometric signals for Alix were normalized over their corresponding cellular protein contents. The blank is the pellet isolated from unconditioned medium. N=3.

All data are normalized over total cellular protein content and expressed as fold-change over untreated Ctrl. Bars indicate mean values ± SD. N is the number of independent experiments. Two-tailed paired *t*-test, *p<0.05.

Fig. 11: GM1 treatment promotes the secretion of EVs by rat embryonic cortical neurons

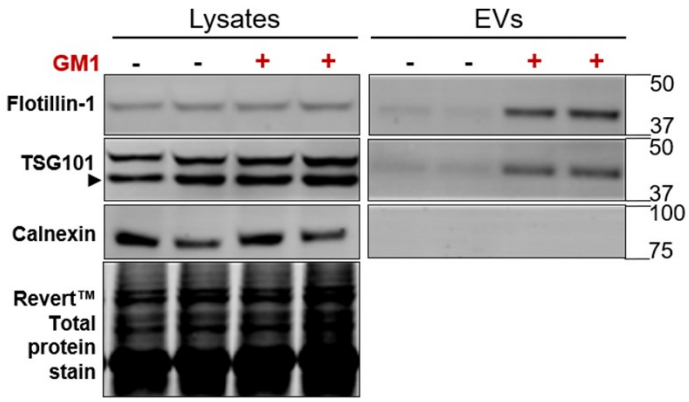

Rat embryonic cortical neurons (WT) were isolated at embryonic day 18 and treated with vehicle or GM1 for 72 h on DIV 15. EVs were collected in neuronal growth medium in the presence of treatment for 72h and were isolated by UC. Equal fractions of the EV pellets were separated by SDS-PAGE. The immunoblots show an enrichment of EV markers TSG101 and Flotillin-1 in EV fractions from two independent cultures treated with GM1 compared to two untreated cultures. Anti-calnexin antibodies were used to control for the purity of the EV fractions (absence of cellular debris and apoptotic bodies). This experiment was performed by Dr. L.C. Morales, a former PhD student in the Sipione lab (unpublished data).

Fig. 12: GM1 treatment increases the secretion of EVs by N2a cells, as measured by imaging flow cytometry

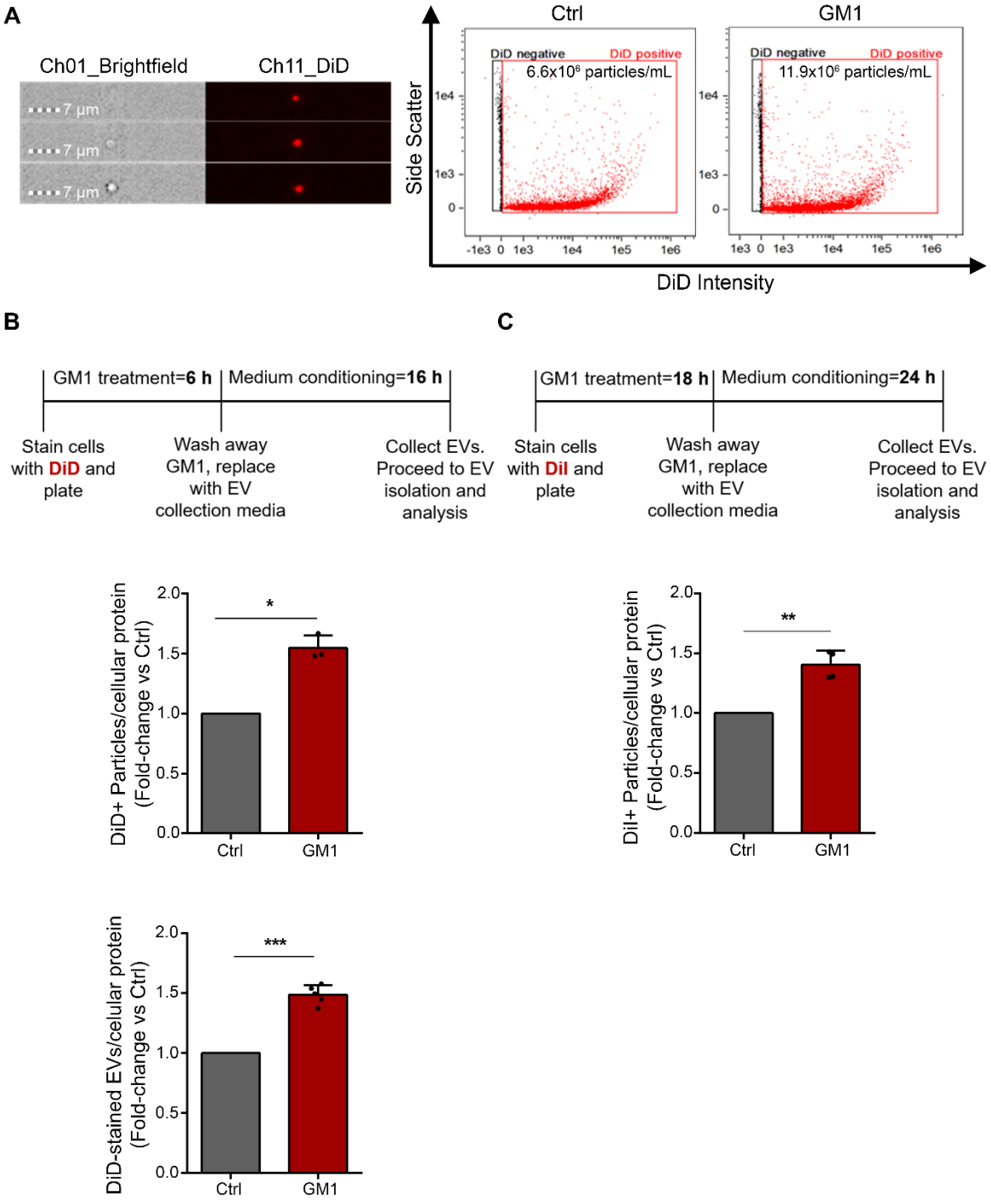

N2a cells were treated with vehicle or GM1 and EVs were collected in serum-free medium supplemented with N2 (SFM+N2) according to the timeline shown in (B) and in (C).

A. Representative imaging flow cytometry (IFC) images and dot plots showing DiD positive particles in the cleared conditioned media (CCM). Data shown refers to the experimental timeline in (B).

B. (**Top**) Experimental timeline, (**middle**) quantification of DiD positive particles present in the CCM by IFC (N=3) and (**bottom**) DiD fluorescence measured in the CCM by fluorometry (N=5).

C. (**Top**) Experimental timeline and (**bottom**) quantification of DiI positive particles present in the CCM by IFC. N=4.

All data are normalized over total cellular protein content and expressed as fold-change over untreated Ctrl. Bars indicate mean values ± SD. N is the number of independent experiments. Two-tailed paired *t*-test, **p*<0.05, ***p*<0.01, ****p*<0.001.

Fig. 13: Isolation of EVs by size-exclusion chromatography further validates that GM1 promotes EV secretion by N2a cells

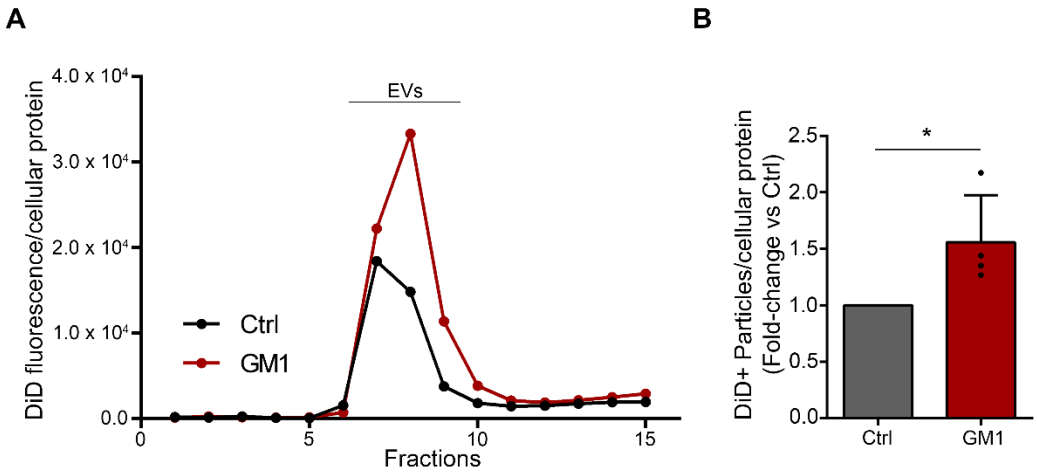

EVs from N2a cells treated with vehicle or GM1 for 6 h and collected in SFM + N2 for 16 h were separated from the CCMs by SEC.

A. Representative size-exclusion chromatogram of the CCMs with the Ctrl and GM1 profiles labelled in black and red, respectively. The DiD fluorescence peak corresponds to the EV fractions.

B. Quantification of DiD positive particles in the EV fractions separated by SEC, measured by IFC. Data are expressed as fold-change over untreated Ctrl. Bars indicate mean values ± SD. N=4.

All data are normalized over total cellular protein content. N is the number of independent experiments. Two-tailed paired *t*-test, *p<0.05.

Fig. 14: N2a 72Q cells exibit lower GM1 levels than N2a cells, and GM1 treatment increases cellular GM1 content in both cell lines to similar levels

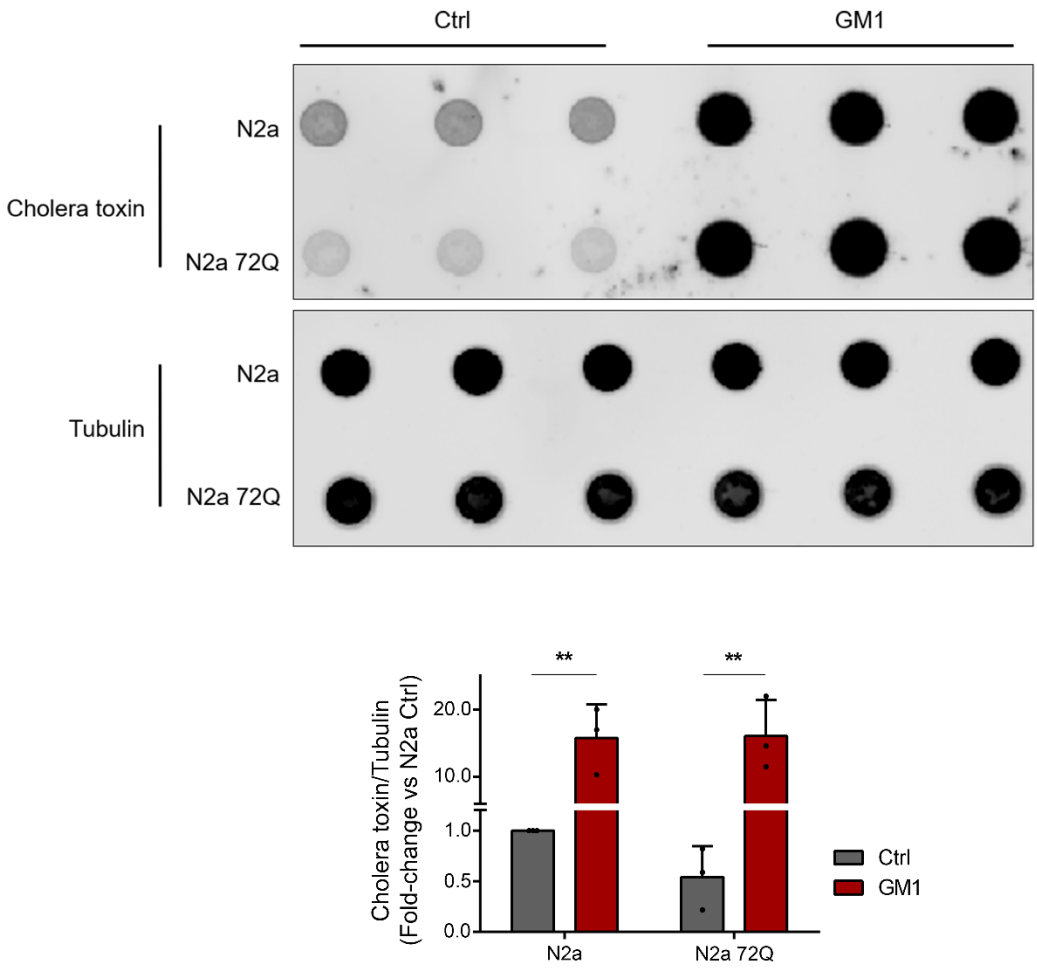

Representative dot blot (**top**) and densitometric analysis (**bottom**) for GM1 in cell lysates of N2a and N2a 72Q cells treated with vehicle or GM1 for 6 h and cultured in SFM+N2 for 16 h before cell lysis. 1µg of cell lysate was loaded per well. GM1 was detected by cholera toxin subunit B. Data were normalized over tubulin and are reported as fold-change over N2a Ctrl. Bars show the mean values ± SD of three independent experiments. Two-way ANOVA with Tukey's test, $^{**}p<0.01$.

Fig. 15: N2a cells exhibit higher EV secretion levels compared to their HD counterpart (N2a 72Q)

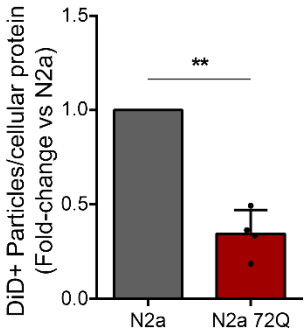

DiD positive EV particles were collected from N2a and N2a 72Q cells in SFM+N2 for 16-24 h and measured in the CCM by IFC. Data are normalized over total cellular protein content and reported as fold-change over N2a. Bars indicate mean values ± SD of four independent experiments. Two-tailed paired *t*-test, $^{**}p<0.01$.

Fig. 16: Treatment of N2a 72Q cells with GM1 promotes EV secretion

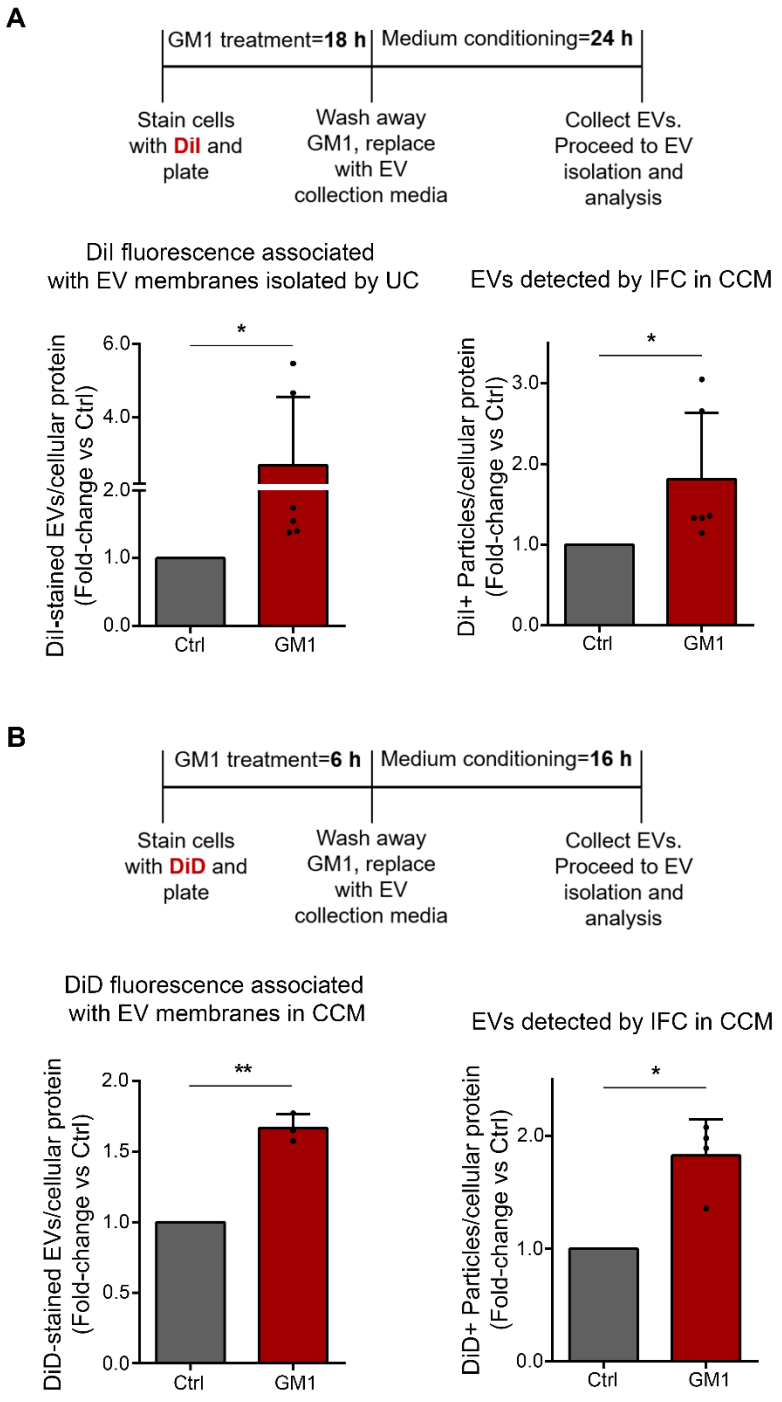

A. Experimental timeline (**top**) for GM1 treatment and EV collection for EVs derived from N2a cells stably expressing Exon1-72Q(mHTT)-eGFP (N2a 72Q cells), (**bottom**

left) DiI fluorescence measured in the EV pellet by UC, N=6 and (**bottom right**) quantification of DiI positive particles present in the CCM by IFC, N=6.

B. (**top**) Experimental timeline, (**bottom left**) DiD fluorescence measured in the CCM, N=3 and (**bottom right**) quantification of DiD positive particles measured in the CCM by IFC, N=4.

All data are normalized over total cellular protein content and reported as fold-change over untreated Ctrl. Bars indicate mean values ± SD. N is the number of independent experiments. Two-tailed paired *t*-test, **p*<0.05, ***p*<0.01.

Fig. 17: EV isolation by size-exclusion chromatography confirms that GM1 increases secretion of EVs in N2a 72Q cells

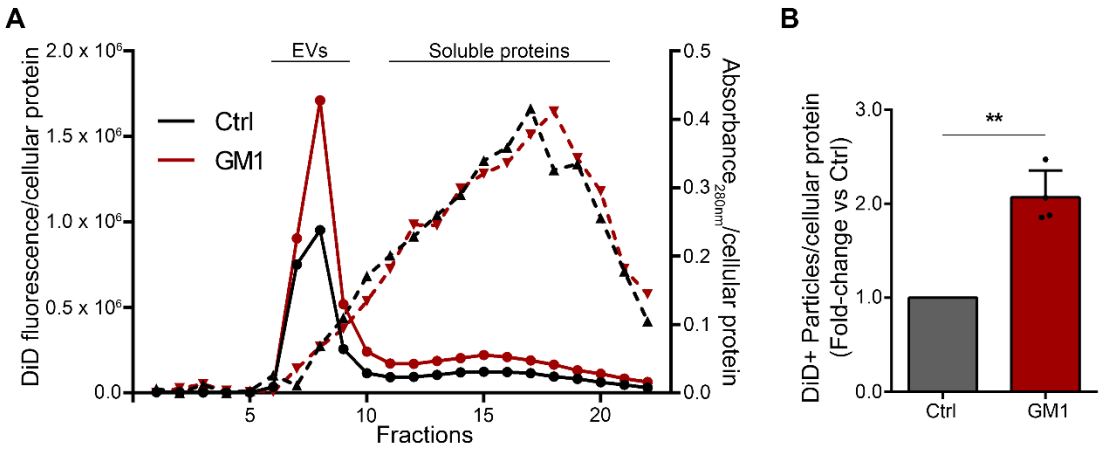

EVs from N2a 72Q cells treated with vehicle or GM1 for 6 h and collected in SFM+N2 for 16 h were separated from the CCMs by SEC.

A. Representative size-exclusion chromatogram of the CCMs separated by SEC with the Ctrl and GM1 profiles labelled in black and red, respectively. The DiD fluorescence peak corresponds to the EV fractions.

B. Quantification of DiD positive particles in the EV fractions separated by SEC, measured by IFC. Data are expressed as fold-change over untreated Ctrl. Bars indicate mean values ± SD from four independent experiments. Two-tailed paired *t*-test, $^{**}p<0.01$.

All data are normalized over total cellular protein content.

Fig. 18: GM1 increases mHTT secretion through EVs

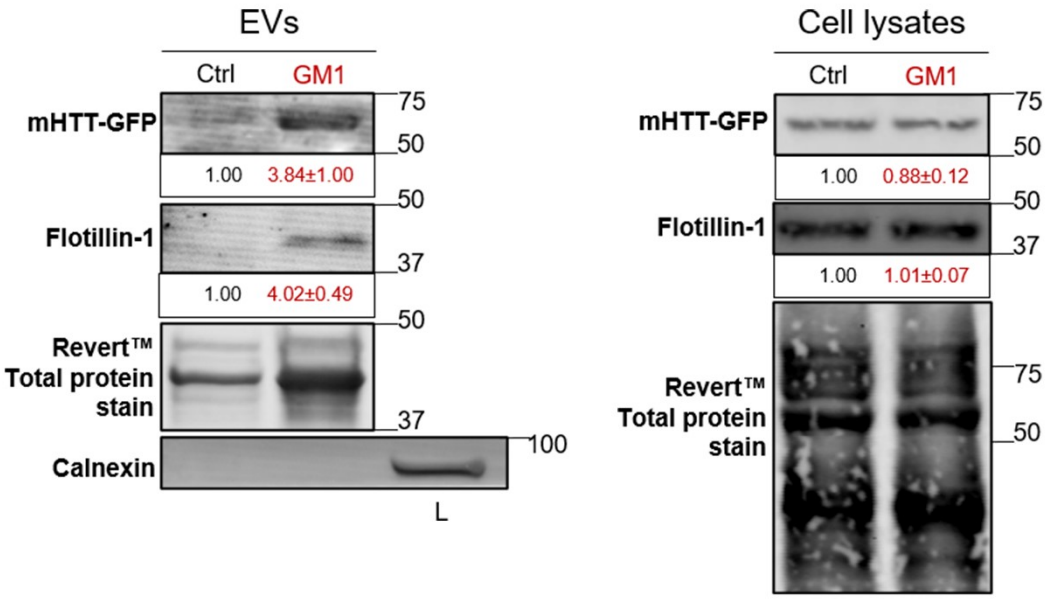

N2a 72Q cells were treated with vehicle or GM1 for 18 h. EVs were collected in EVD complete media for 24 h and isolated by UC. 70% of the total EV pellets and 1.6-1.8% (or 30µg) of the total parent cell lysates were loaded in the gel.

Representative immunoblots for mHTT and the EV marker Flotillin-1 in EVs and in cell lysates. Anti-calnexin antibodies were used to control for the purity of the EV pellet (absence of cellular debris or apoptotic bodies). The values under each blot are averages of densitometric values ± SD from two independent experiments for EVs and three independent experiments for cell lysates. Data are normalized over total cellular protein content for EV fractions or over total protein stain for cell lysates and are expressed as fold-change over untreated Ctrl. L = Total cell lysate control.

Fig. 19: Isolation of EVs by size-exclusion chromatography further corroborates that GM1 promotes the export of mHTT via EVs

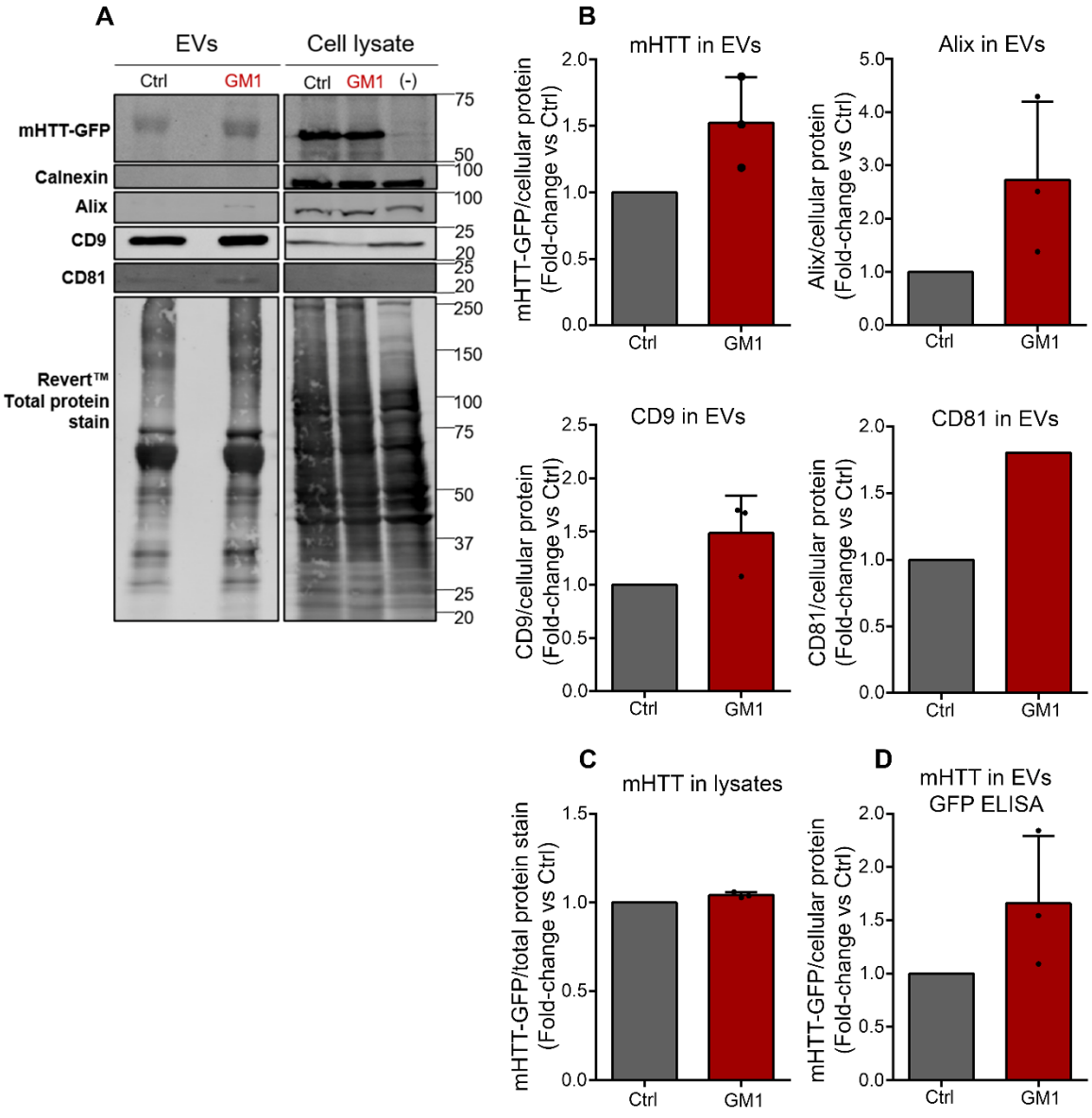

EVs from N2a 72Q cells treated with vehicle or GM1 for 6 h were collected in SFM+N2 for 16 h and isolated by SEC.

A. Representative immunoblots for mHTT and the EV markers Alix, CD9 and CD81 in EVs and cell lysates. 50-75% of the total EV fractions normalized over their

corresponding cellular protein content and 0.5-1.0% (or 60µg) of the total parent cell lysates were loaded in the gel. Anti-calnexin antibodies were used to control for the purity of the EV fractions (absence of cellular debris and apoptotic bodies). (-) is a lysate from non-transfected N2a cells, as a negative control for anti-HTT and anti-GFP antibodies.

B. Densitometric analysis of mHTT and EV markers in EV fractions. Data are normalized over total cellular protein content.

C. Densitometric analysis of mHTT in cell lysates. Data are normalized over total protein stain.

D. mHTT-GFP levels in EV fractions measured by GFP ELISA. Data are normalized over total cellular protein content.

All data are expressed as fold-change over untreated Ctrl. Bars indicate mean values ± SD from three independent experiments for all analyses except for CD81 which is from one experiment.

Fig. 20: GM1 increases the secretion of EVs in human WT and HD fibroblasts,

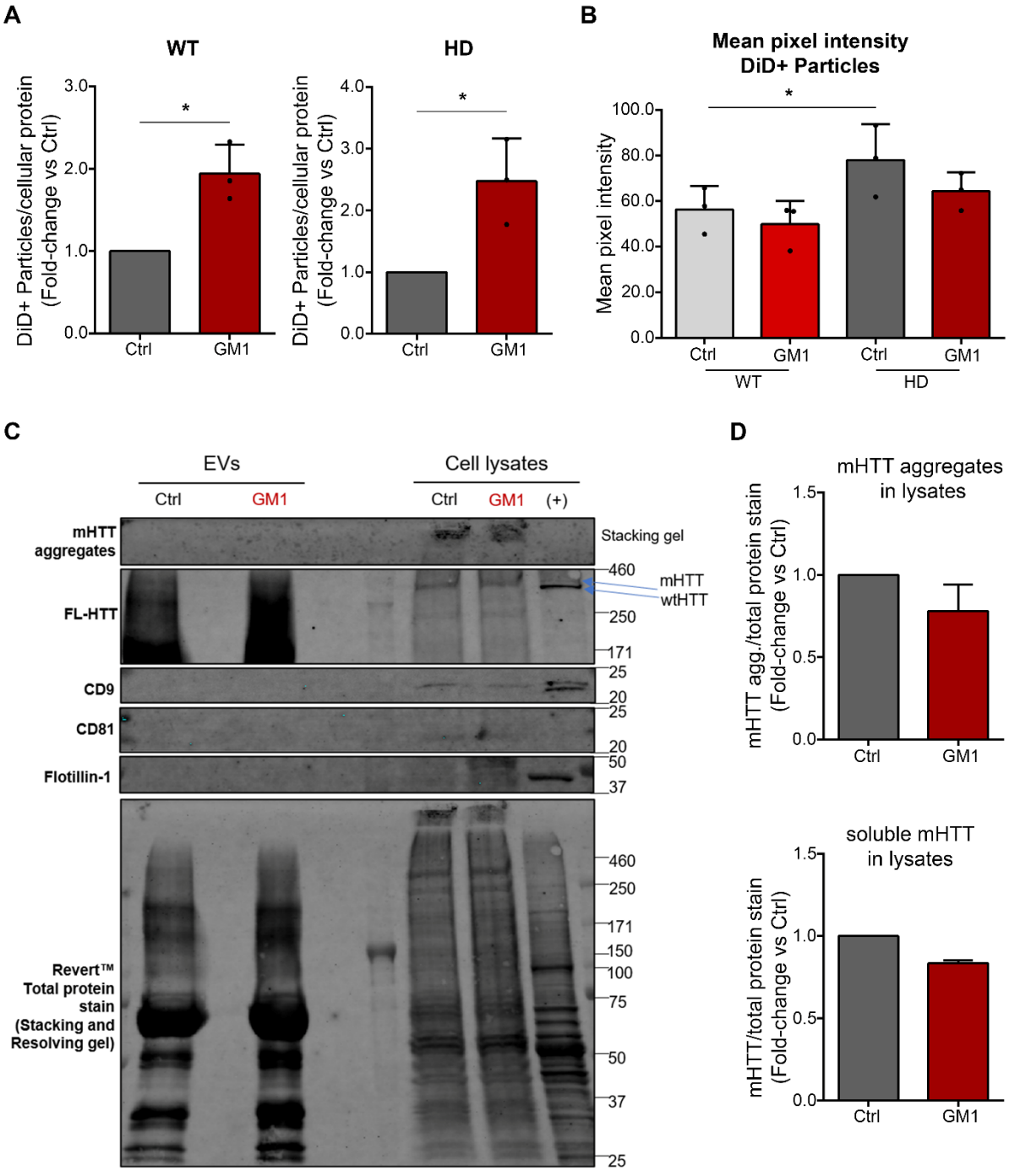

Fibroblasts from 1 HD male patient and an age-matched WT control were treated with vehicle or GM1 for 6 h and allowed to condition SFM+N2 media for 16 h for EV collection and isolation by SEC.

A. DiD positive particles in the CCM of WT and HD fibroblasts, measured by IFC. Data are normalized over total cellular protein content and expressed as fold-change over untreated Ctrl. Bars indicate mean values ± SD from three independent experiments for each genotype. Two-tailed paired *t*-test, **p*<0.05.

B. Mean pixel intensity of DiD positive particles detected by IFC in the CCM of WT and HD fibroblasts treated with vehicle or GM1. Bars indicate mean values ± SD from three independent experiments for each genotype. Two-way ANOVA with Tukey's test, **p*<0.05.

C. Representative immunoblot for HTT and the EV markers Flotillin-1, CD9 and CD81 in EVs and cell lysates of HD fibroblasts treated with vehicle or GM1. EVs were isolated by SEC. (+) is a positive control striatal tissue lysate from a heterozygous Q7/Q140 HD mouse. 100% of the total EV fractions normalized over their corresponding cellular protein content and 50% (or 60µg) of the total parent cell lysates were loaded in the gel. FL-HTT: Full-length HTT.

D. Densitometric analysis of soluble and insoluble (aggregated) mHTT in cell lysates. Data are normalized over total protein stain and are expressed as fold-change over untreated Ctrl. Bars indicate mean values ± SD from two independent experiments.

Fig. 21: The majority of mHTT associated with EVs is located in the EV lumen

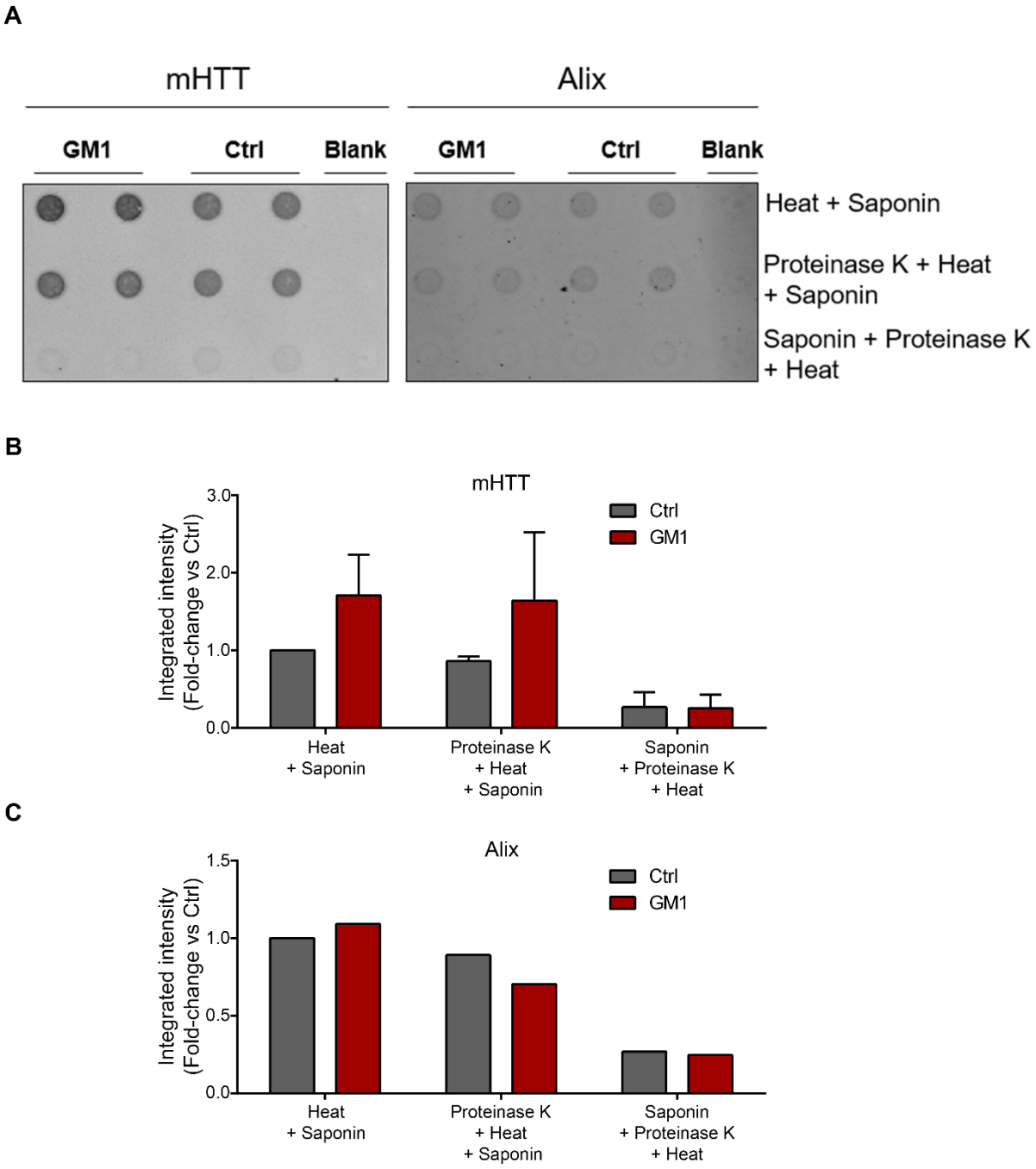

EVs from N2a 72Q cells were treated with vehicle or GM1 for 6 h and collected in SFM+N2 for 16 h prior to isolation by SEC. 5µg of EV protein was loaded per well for each treatment group. EVs were subjected to proteinase K digestion (0.02µg/µg of

EVs) before or after EV membrane permeabilization with saponin (0.1%). Proteinase K was heat-inactivated at 95°. In the absence of prior saponin permeabilization, proteinase K will only digest proteins on the membrane and not in the lumen.

A. Representative dot blot to show levels of mHTT and Alix in EVs. Alix is a cytosolic marker and hence is used as a control for proteinase K digestion. The blank is PBS (used to resuspend EVs) alone. The experiment was repeated twice with similar results.

B. Densitometric analysis for mHTT in EVs, expressed as fold-change vs undigested Ctrl (heat + saponin group). Bars indicate mean values ± SD of two independent experiments.

C. Densitometric analysis for Alix in EVs, expressed as fold-change vs undigested Ctrl (heat + saponin group). The experiment was repeated one more time with similar results, but due to the high signal intensity variability, data for Alix from the second experiment were not combined.

Fig. 22: Cell treatment with GM1 does not affect the size distribution of EVs as determined by nanoparticle tracking analysis

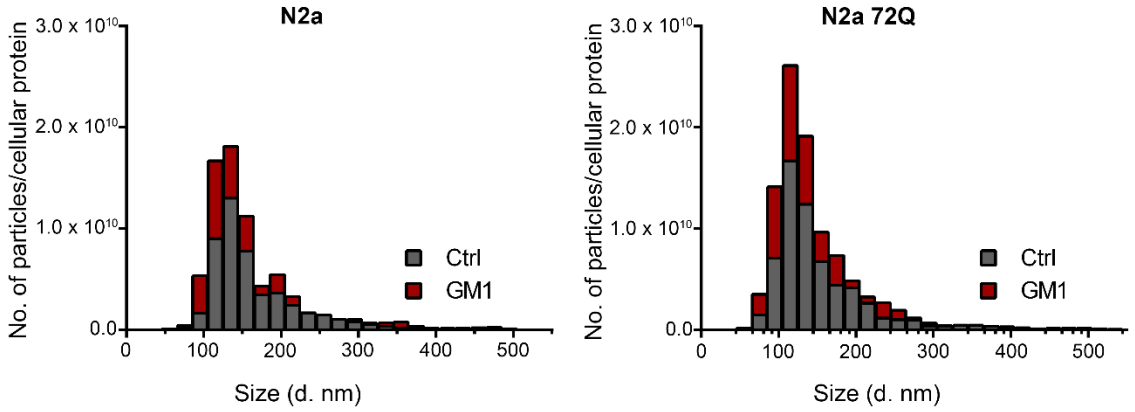

N2a	Ctrl (nm)	GM1 (nm)
Mean	130.65 ± 3.23	134.84 ± 4.53
Median	131.1 ± 4.30	133.69 ± 6.41
Mode	132.0 ± 6.50	131.38 ± 11.43

N2a 72Q	Ctrl (nm)	GM1 (nm)
Mean	119.36 ± 3.98	127.62 ± 8.83
Median	117.11 ± 3.43	123.45 ± 8.47
Mode	112.60 ± 7.74	115.12 ± 14.80

Particle size distribution profile of EVs from the CCM of N2a and N2a 72Q cells treated with vehicle or GM1 for 18 h and collected in SFM+N2 for 24 h. Data were obtained by nanoparticle tracking analysis (NTA) and were normalized over total cellular protein content. For each sample, the average of 5 replicates is plotted. The tables below the histograms report the mean, median and mode values ± SD for each group. The experiment was performed once.

Fig. 23: Dynamic light scattering results show that GM1 does not cause significant differences in the size distribution of EVs

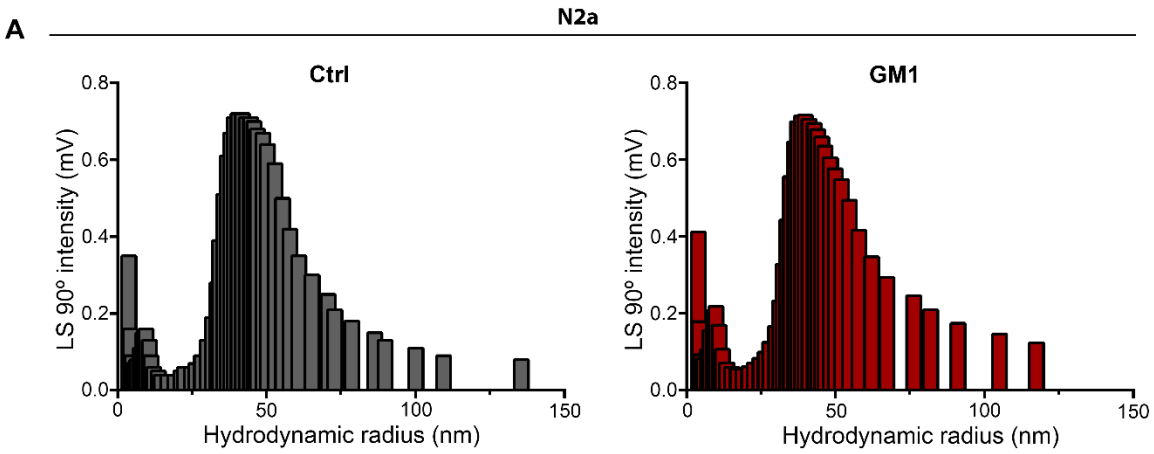

N2a	Ctrl (nm)	GM1 (nm)
Mean	47.65 ± 0.73	48.00 ± 2.00
Median	43.89 ± 0.72	44.13 ± 3.03
Mode	43.89 ± 2.03	44.16 ± 4.36

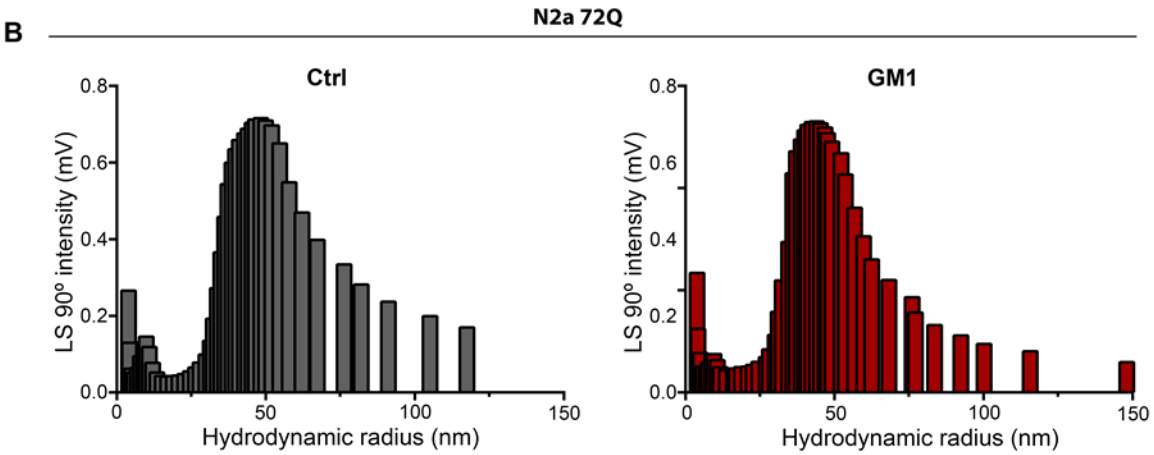

N2a 72Q	Ctrl (nm)	GM1 (nm)
Mean	49.31 ± 2.31	46.50
Median	45.16 ± 0.22	43.97
Mode	47.17 ± 1.15	43.97

Representative histograms of dynamic light scattering (DLS) analysis of EVs in the retentate (CCM concentrate) of **A**. N2a and **B**. N2a 72Q cells treated with vehicle or GM1 for 18 h and collected in SFM+N2 for 24 h. The histograms show the hydrodynamic radii distribution of EVs. The experiment was performed a second time for all groups except for EVs from N2a 72Q cells treated with GM1, and similar results were obtained. The tables below the histograms report the mean, median and mode values ± SD for each group.

Fig. 24: Cell treatment with GM1 increases levels of GM1 in EVs

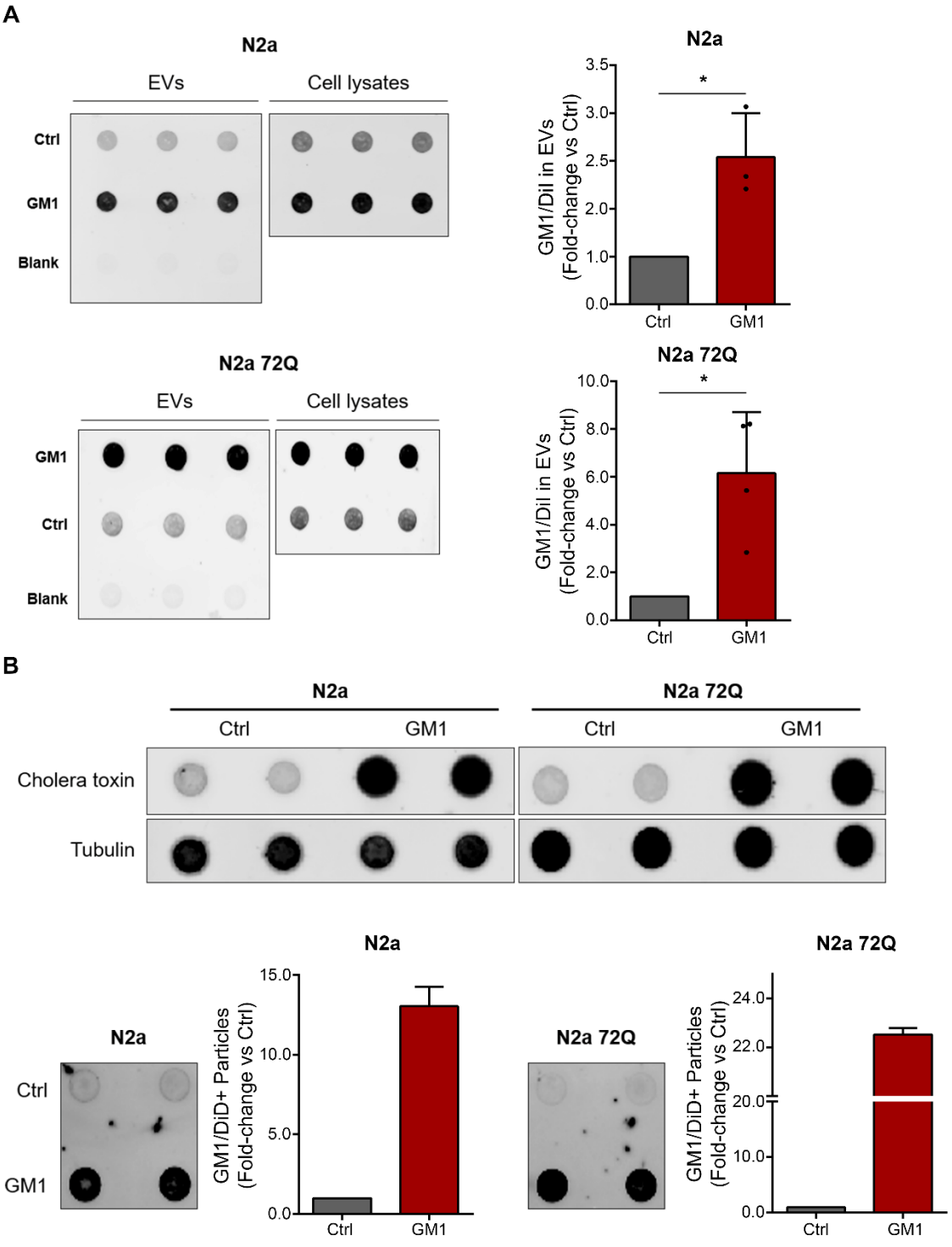

A. EVs from N2a and N2a 72Q cells treated with vehicle or GM1 for 18 h and collected in EVD complete media for 24 h were isolated by UC. (**Left**) Representative dot blot for GM1 in EVs and cell lysates from N2a and N2a 72Q cells. The blank represents the EV pellet of unconditioned medium loaded as a negative control. 1µg of cell lysate was loaded per well. (**Right**) Relative quantitation of GM1 levels in EVs from N2a and N2a 72Q cells normalized to their DiI fluorescence, reported as fold-change over untreated Ctrl. Bars indicate mean values ± SD. N=3 for N2a, N=4 for N2a 72Q.

B. EVs from N2a and N2a 72Q cells treated with vehicle or GM1 for 6 h and collected in SFM+N2 for 16 h were isolated by SEC. (**Top**) Representative dot blot showing levels of GM1 in cell lysates of N2a and N2a 72Q. 1µg of cell lysate was loaded per well. Tubulin was used as a loading control. (**Bottom)** Representative dot blot and relative quantitation of GM1 levels in EVs from N2a and N2a 72Q cells. Data are normalized to DiD positive particles in the EV fractions measured by IFC and are reported as fold-change over untreated Ctrl. N=1 for N2a where bars indicate mean values ± SD of duplicates from the same experiment. N=2 for N2a 72Q.

Signal for GM1 was detected by cholera toxin subunit B. N is the number of independent experiments. Two-tailed paired *t*-test, $*p<0.05$.

Fig. 25: Schematic outline of the experimental design for Genz treatment

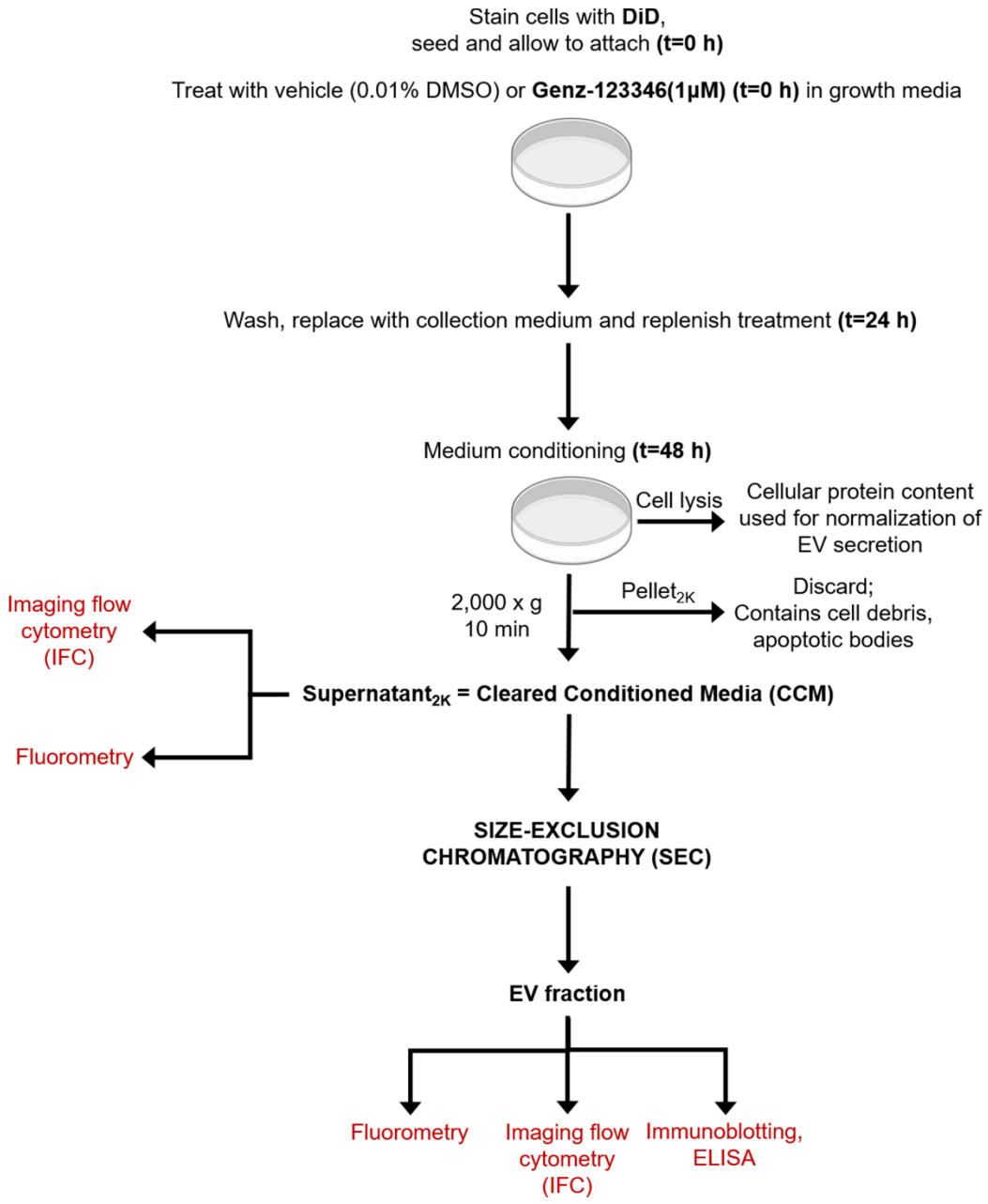

Schematic flowchart showing the procedure for cell labelling, treatment with vehicle or Genz-123346, EV collection and isolation by size-exclusion chromatography (SEC) and the downstream EV analyses performed.

Fig. 26: Genz-123346 effectively decreases GM1 levels in N2a and N2a 72Q cells

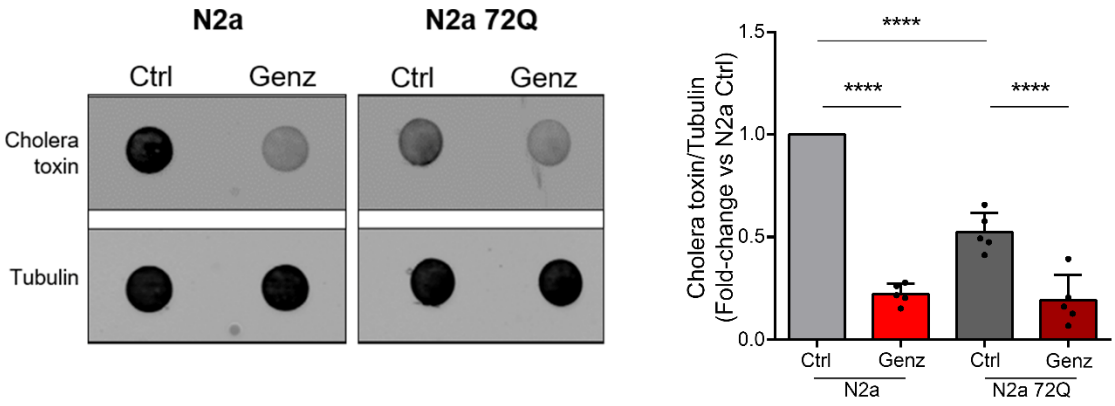

Representative dot blot and densitometric analysis for GM1 in cell lysates of N2a and N2a 72Q cells treated with vehicle (0.01% DMSO) or Genz-123346 for 48 h. 1µg of cell lysate was loaded per well. GM1 was detected by cholera toxin subunit B. Tubulin was used as a loading control. Data are reported as fold-change over N2a vehicle Ctrl. Bars show mean values ± SD of five independent experiments. Two-way ANOVA with Tukey's test, ****p< 0.0001.

Fig. 27: Pharmacological inhibition of ganglioside synthesis decreases cell secretion of EVs

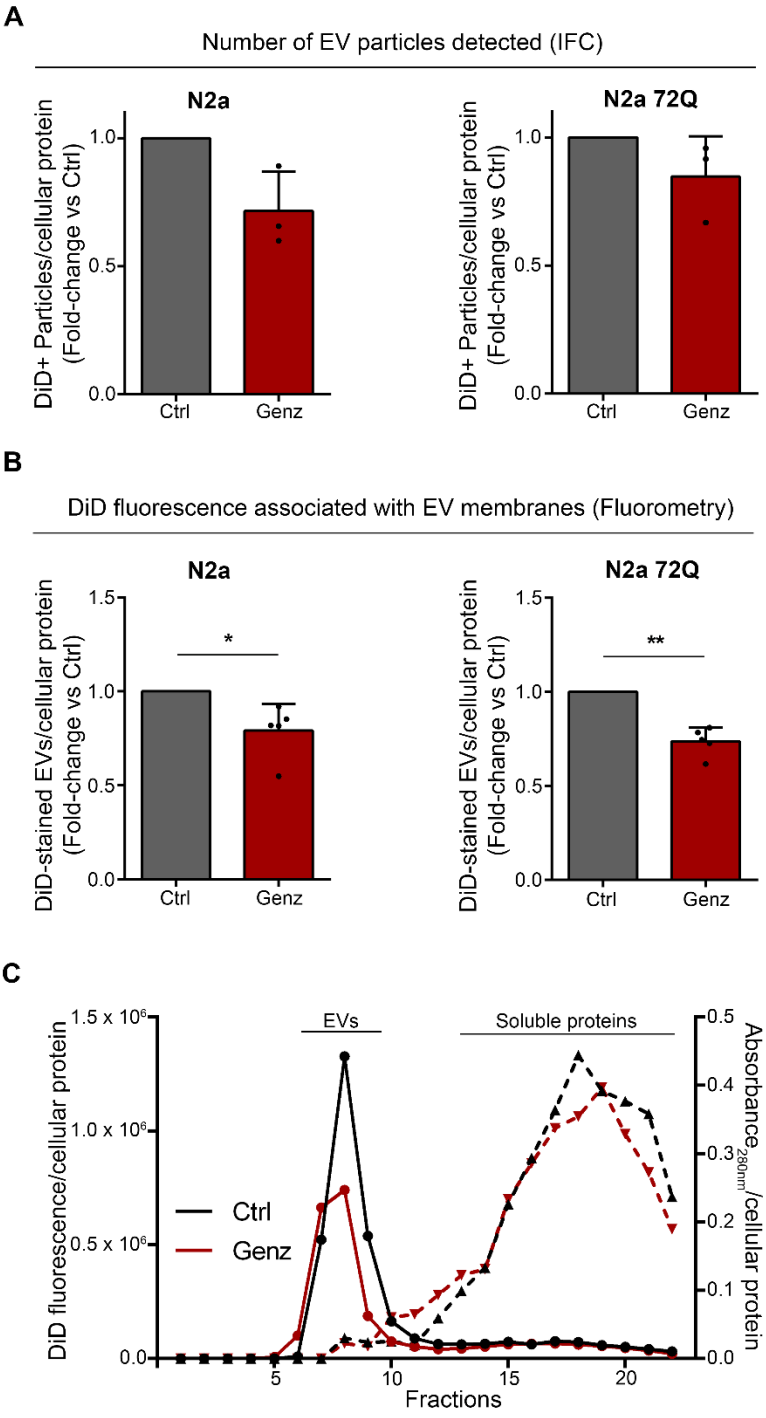

A. DiD positive particles in the CCM of N2a and N2a 72Q cells treated with vehicle or Genz-123346 for 48 h, measured by IFC. EVs were collected in SFM+N2 in the presence of the treatment for 24 h. Data are normalized over total cellular protein content and expressed as fold-change over vehicle Ctrl. Bars indicate mean values ± SD. N=3.

B. DiD fluorescence measured in the CCM of N2a and N2a 72Q cells treated and collected as in (**A**), measured by fluorometry. Data are normalized over total cellular protein content and expressed as fold-change over vehicle Ctrl. Bars indicate mean values ± SD. N=5.

C. EVs from N2a and N2a 72Q cells treated and collected as in (**A**) and separated by SEC. Size-exclusion chromatogram of the CCMs with the vehicle Ctrl and Genz-123346 profiles labelled in black and red, respectively. The DiD fluorescence peak corresponds to the EV fractions. Data are normalized over total cellular protein content.

N is the number of independent experiments. Two-tailed paired *t*-test, **p*<0.05, ***p*<0.01.

Fig. 28: Genetic inhibition of gangliosides decreases cellular GM1 levels

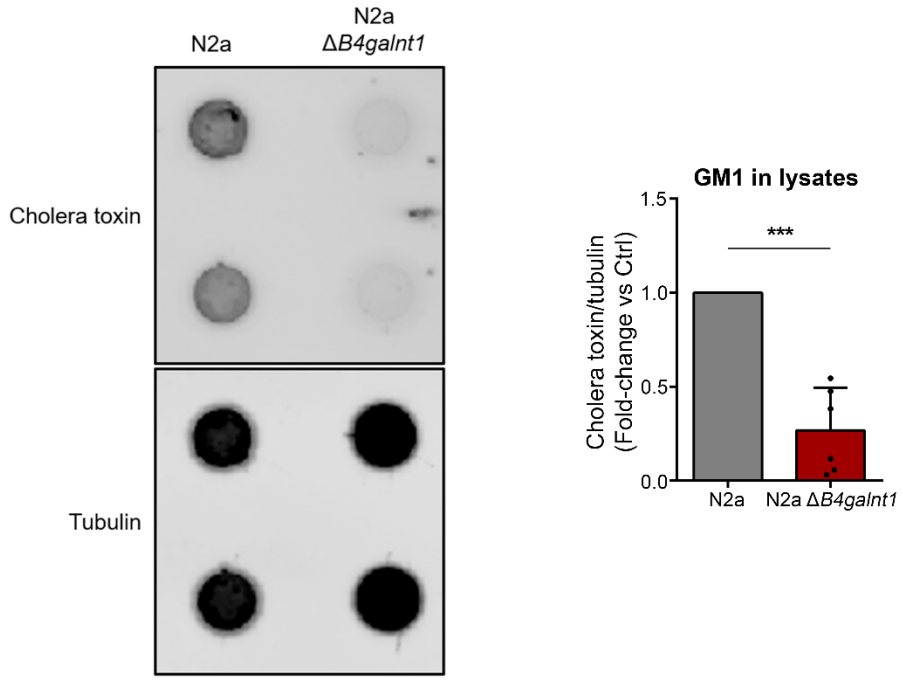

Representative dot blot and densitometric analysis for GM1 in cell lysates of N2a and N2a Δ*B4galnt1* cells cultured in SFM+N2 for 22-24 h before cell lysis. 1µg of cell lysate was loaded per well. GM1 was detected by cholera toxin subunit B. Tubulin was used as a loading control. Data are reported as fold-change over N2a. Bars show the average values ± SD of six independent experiments. Two-tailed paired *t*-test, ****p*<0.001.

Fig. 29: Genetic inhibition of ganglioside synthesis results in decreased secretion of EVs

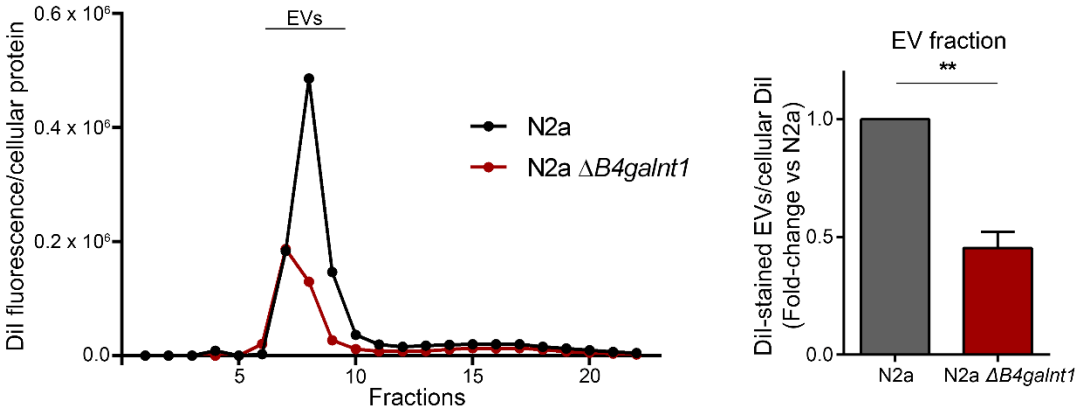

Representative size-exclusion chromatogram (**left**) of the CCMs of SFM+N2 media conditioned by N2a (black) and N2a *ΔB4galnt1* (red) cells for 24 h. The DiI fluorescence peak corresponds to EV fractions. Data are normalized over total cellular protein content. The graph on the r**ight** shows the quantification of DiI fluorescence in EV fractions from N2a and N2a *ΔB4galnt1* cells. Data are normalized over total cellular DiI content and are expressed as fold-change over N2a. Bars indicate mean values ± SD of three independent experiments. Two-tailed paired *t*-test, $^{**}p<0.01$.

Fig. 30: Cell treatment with GM1 restores normal cellular GM1 levels and increases EV secretion in a neuronal GM2/GD2 synthase knock-out model

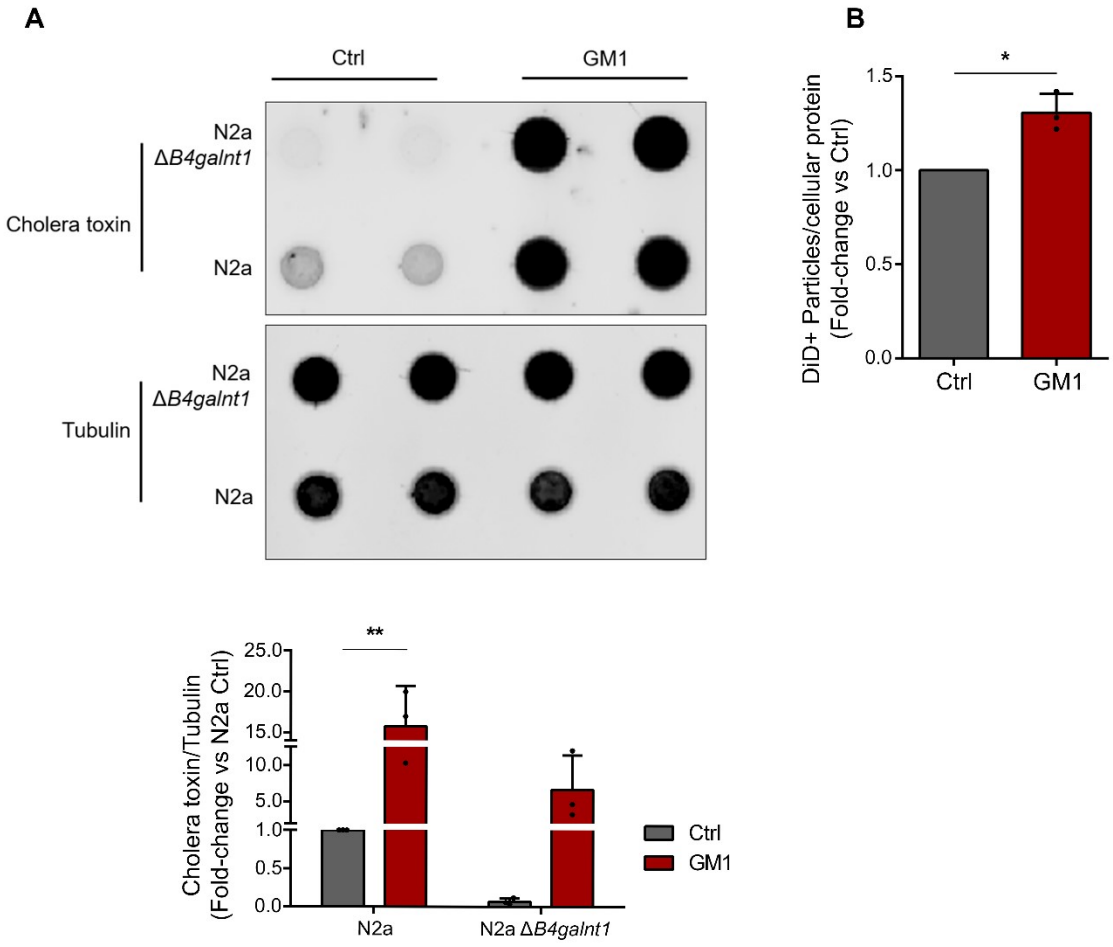

A. (**Top**) Representative dot blot and (**bottom**) densitometric analysis for GM1 in cell lysates of N2a and N2a Δ*B4galnt1* cells treated with vehicle or GM1 for 6 h and cultured in SFM+N2 for 16 h before cell lysis. 1µg of cell lysate was loaded per well. GM1 was detected by cholera toxin subunit B. Tubulin was used as a loading control. Data are reported as fold-change over N2a Ctrl. N=3. Two-way ANOVA with Tukey's test, $^{**}p<0.01$.

B. Quantification of DiD positive particles in the CCM of N2a cells treated with vehicle or GM1 for 6 h and collected in SFM+N2 for 16 h, measured by IFC. Data are expressed as fold-change over untreated Ctrl. N=3. Two-tailed paired *t*-test, *$p<0.05$

All data are normalized over total cellular protein content. Bars indicate mean values ± SD. N is the number of independent experiments.

Fig. 31: Cellular ganglioside levels positively correlate with EV secretion

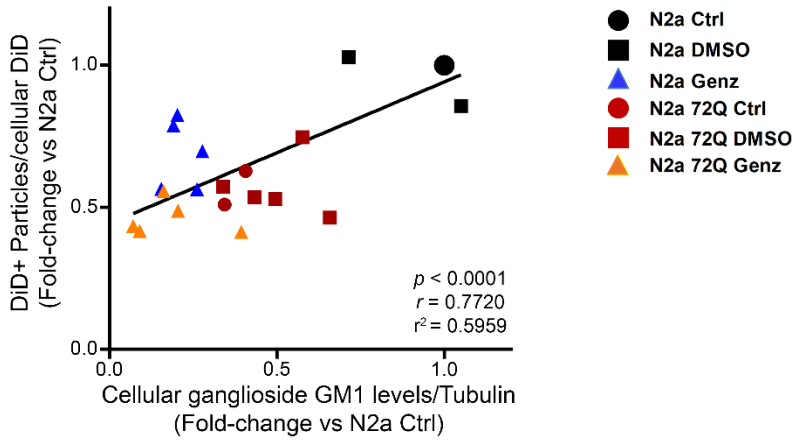

Correlation between cellular GM1 levels and EV secretion in N2a and N2a 72Q cells either untreated or treated with vehicle (DMSO) or Genz-123346 for 48 h. EVs were collected for 24 h in the presence of treatment. EV secretion was measured by IFC and the number of DiD positive particles is normalized over cellular DiD levels measured by fluorometry. Cellular GM1 levels were normalized over cellular Tubulin levels (both measured by immunoblotting). For each experiment, all values are expressed as fold-change over their respective N2a (untreated Ctrl). In the absence of the untreated Ctrl group, fold-change was calculated over the N2a vehicle Ctrl group. N=5 for both genotypes where N is the number of independent experiments, $p < 0.0001$, Pearson correlation coefficient $r = 0.7720$, $r^2 = 0.5959$.

Fig. 32: Inhibition of ganglioside synthesis results in decrease secretion of mHTT via EVs

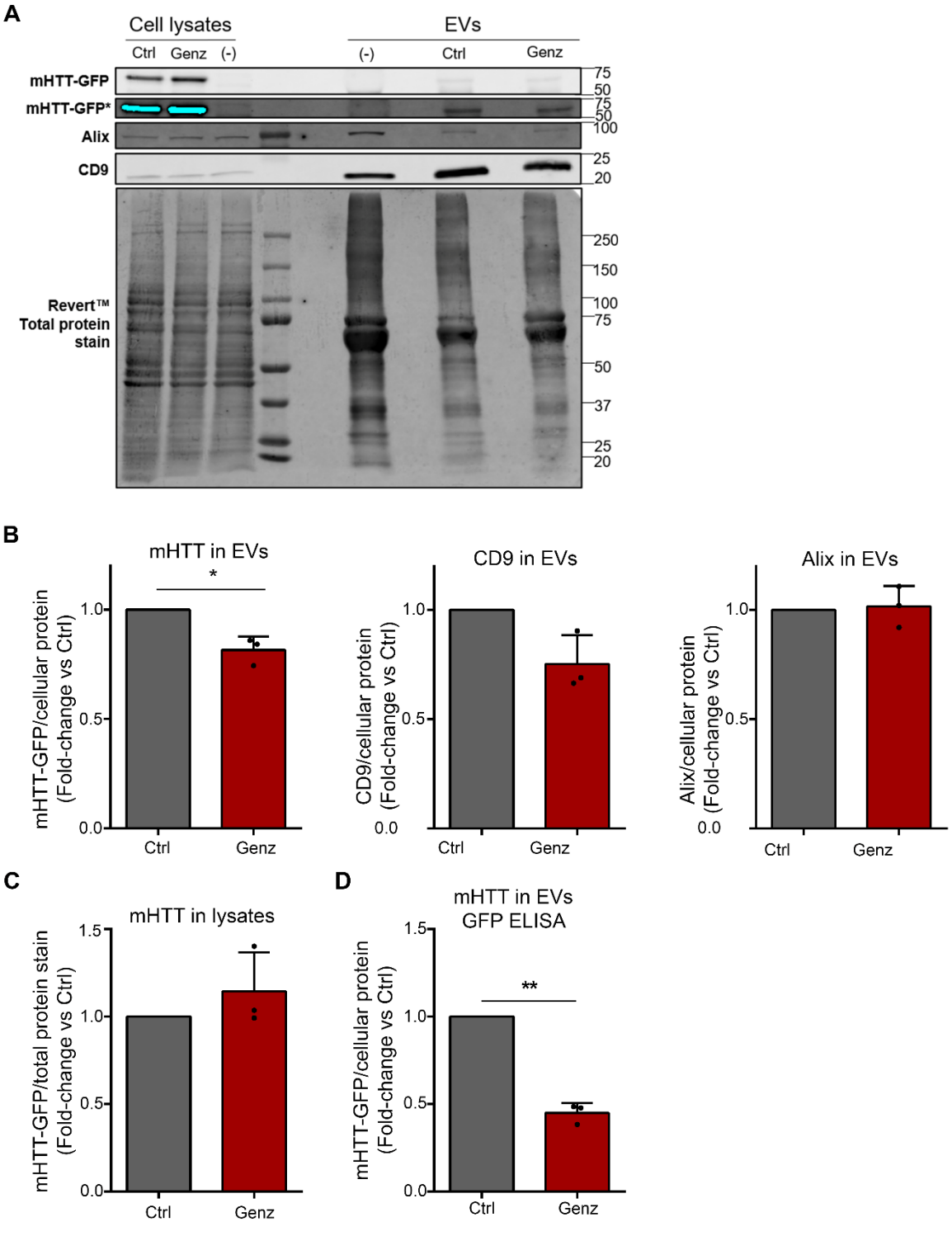

EVs from N2a 72Q cells treated with vehicle or Genz-123346 for 48 h were collected in SFM+N2 for 24 h in the presence of the treatment and separated by SEC.

A. Representative immunoblot for mHTT and the EV markers Alix and CD9 in EV fractions and cell lysates. 50-75% of the total EV fractions normalized over their corresponding cellular protein content and 0.3-0.7% (or 60µg) of the total parent cell lysates were loaded in the gel. (-) denotes either a lysate or EVs isolated by SEC from N2a cells used as negative controls for anti-HTT and anti-GFP antibodies. * indicates an overexposed blot.

B. Densitometric analysis of mHTT and EV markers in EV fractions. Data are normalized over total cellular protein content.

C. Densitometric analysis of mHTT in cell lysates. Data are normalized over total protein stain.

D. mHTT-GFP levels in EV fractions measured by GFP ELISA. Data are normalized over total cellular protein content.

All data are expressed as fold-change over vehicle Ctrl. Bars indicate mean values ± SD of three independent experiments. Two-tailed paired *t*-test, *$p<0.05$, **$p<0.01$.

Fig. 33: Decrease in cellular ganglioside levels also decreases the GM1 content in EVs

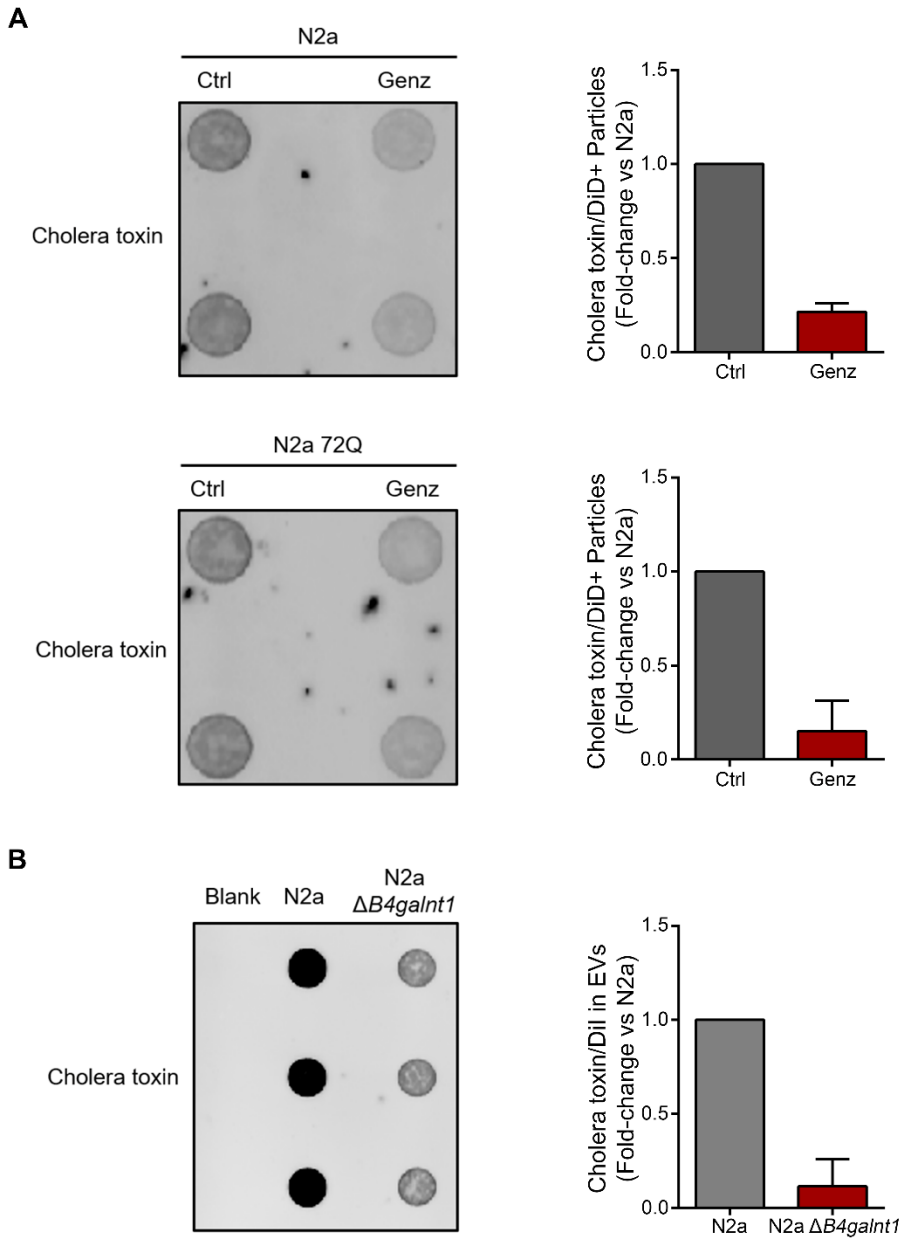

A. Representative dot blot and relative quantification of GM1 levels in EVs from (**top**) N2a cells and (**bottom**) N2a 72Q cells treated with vehicle or Genz-123346 for 48 h, collected in SFM+N2 for 24 h in the presence of the treatment and separated by SEC.

Data are normalized over DiD positive particles measured in the CCM and are reported as fold-change over vehicle Ctrl. N=2 for each genotype.

B. Representative dot blot and relative quantification of GM1 levels in EVs from N2a and N2a *ΔB4galnt1* cells collected in SFM+N2 for 24 h and isolated by SEC. The blank denotes PBS used to resuspend EVs, loaded as a negative control. GM1 was detected by cholera toxin subunit B. Data are normalized to DiI fluorescence in EV fractions and are reported as fold-change over N2a. N=2.

Bars indicate mean values ± SD. N is the number of independent experiments.

Fig. 34: Synopsis and working hypothesis model

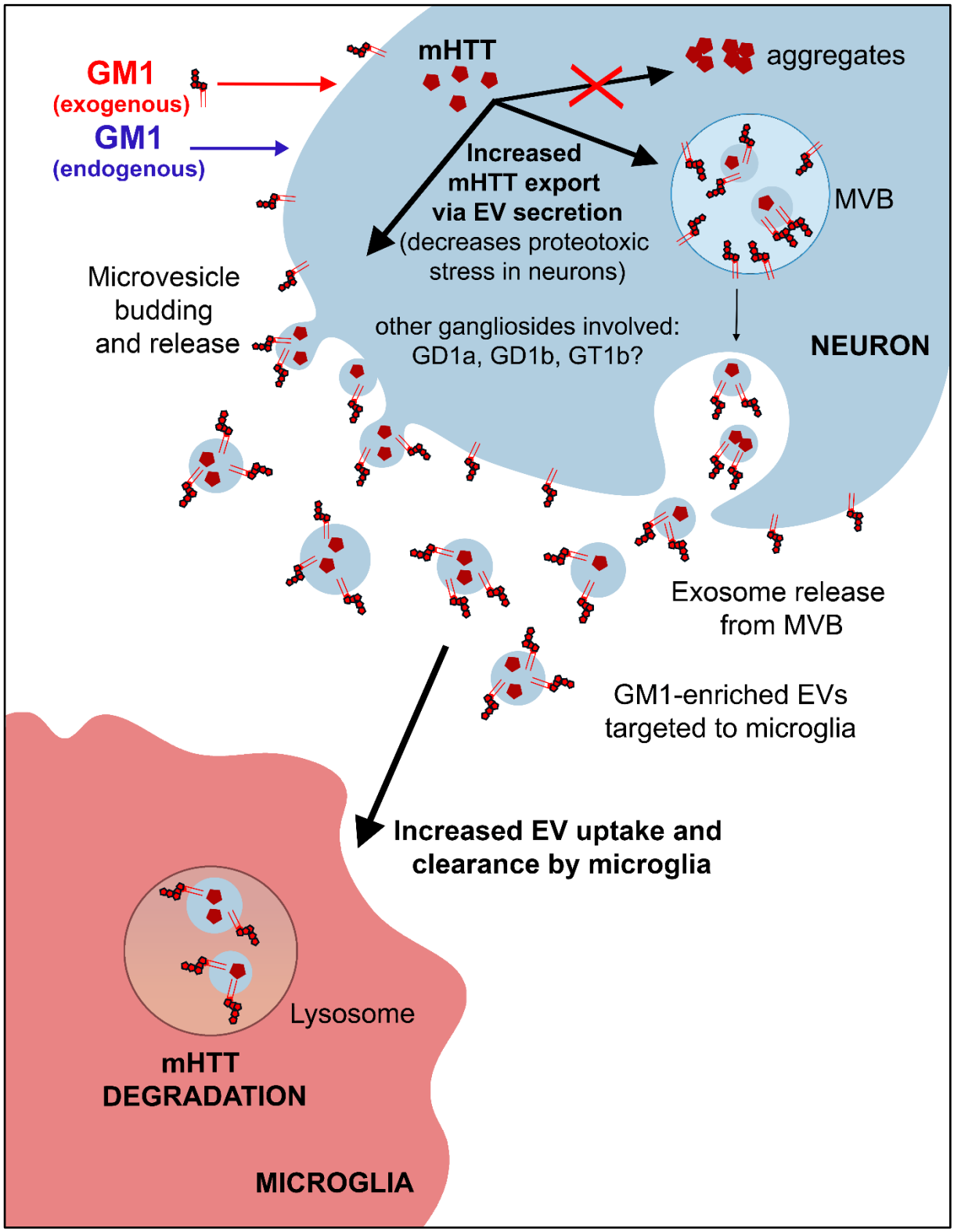

GM1 (both exogenously administered and endogenously synthesized) and potentially other gangliosides promote the secretion of EVs carrying mHTT from neuronal cells. These EVs are enriched with GM1 that may potentially function as a ‘code’ to target them to microglia for subsequent degradation. This may result in mHTT clearance and thus, attenuate cellular proteotoxic burden.

BIBLIOGRAPHY

1. Wickramasinghe, S. and J.F. Medrano, *Primer on genes encoding enzymes in sialic acid metabolism in mammals.* Biochimie, 2011. **93**(10): p. 1641-6.
2. Audry, M., et al., *Current trends in the structure-activity relationships of sialyltransferases.* Glycobiology, 2011. **21**(6): p. 716-26.
3. Yu, R.K., et al., *Structures, biosynthesis, and functions of gangliosides--an overview.* J Oleo Sci, 2011. **60**(10): p. 537-44.
4. Daniotti, J.L. and R. Iglesias-Bartolome, *Metabolic pathways and intracellular trafficking of gangliosides.* IUBMB Life, 2011. **63**(7): p. 513-20.
5. Miller-Podraza, H., R.M. Bradley, and P.H. Fishman, *Biosynthesis and localization of gangliosides in cultured cells.* Biochemistry, 1982. **21**(14): p. 3260-5.
6. Tettamanti, G., *Ganglioside/glycosphingolipid turnover: new concepts.* Glycoconj J, 2004. **20**(5): p. 301-17.
7. Garofalo, T., et al., *Do mitochondria act as "cargo boats" in the journey of GD3 to the nucleus during apoptosis?* FEBS Lett, 2007. **581**(21): p. 3899-903.
8. Lucki, N.C. and M.B. Sewer, *Nuclear sphingolipid metabolism.* Annu Rev Physiol, 2012. **74**: p. 131-51.
9. Ledeen, R. and G. Wu, *New findings on nuclear gangliosides: overview on metabolism and function.* J Neurochem, 2011. **116**(5): p. 714-20.
10. Sonnino, S., et al., *Gangliosides as components of lipid membrane domains.* Glycobiology, 2007. **17**(1): p. 1R-13R.
11. Schengrund, C.L., *Gangliosides: glycosphingolipids essential for normal neural development and function.* Trends Biochem Sci, 2015. **40**(7): p. 397-406.
12. Merrill, A.H., Jr., *Sphingolipid and glycosphingolipid metabolic pathways in the era of sphingolipidomics.* Chem Rev, 2011. **111**(10): p. 6387-422.
13. Vanier, M.T., et al., *Developmental profiles of gangliosides in human and rat brain.* J Neurochem, 1971. **18**(4): p. 581-92.
14. Yu, R.K., Y. Nakatani, and M. Yanagisawa, *The role of glycosphingolipid metabolism in the developing brain.* J Lipid Res, 2009. **50 Suppl**: p. S440-5.

15. Svennerholm, L., *Gangliosides and synaptic transmission.* Adv Exp Med Biol, 1980. **125**: p. 533-44.
16. Kolter, T., *Ganglioside biochemistry.* ISRN Biochem, 2012. **2012**: p. 506160.
17. Svennerholm, L., et al., *Human brain gangliosides: developmental changes from early fetal stage to advanced age.* Biochim Biophys Acta, 1989. **1005**(2): p. 109-17.
18. Tettamanti, G., et al., *A new procedure for the extraction, purification and fractionation of brain gangliosides.* Biochim Biophys Acta, 1973. **296**(1): p. 160-70.
19. Chigorno, V., et al., *Evidence that ganglioside enriched domains are distinct from caveolae in MDCK II and human fibroblast cells in culture.* Eur J Biochem, 2000. **267**(13): p. 4187-97.
20. Iwabuchi, K., K. Handa, and S. Hakomori, *Separation of "glycosphingolipid signaling domain" from caveolin-containing membrane fraction in mouse melanoma B16 cells and its role in cell adhesion coupled with signaling.* J Biol Chem, 1998. **273**(50): p. 33766-73.
21. Schroeder, F., et al., *Membrane cholesterol dynamics: cholesterol domains and kinetic pools.* Proc Soc Exp Biol Med, 1991. **196**(3): p. 235-52.
22. Igbavboa, U., et al., *Transbilayer distribution of cholesterol is modified in brain synaptic plasma membranes of knockout mice deficient in the low-density lipoprotein receptor, apolipoprotein E, or both proteins.* J Neurochem, 1997. **69**(4): p. 1661-7.
23. Patel, D.S., et al., *Influence of Ganglioside GM1 Concentration on Lipid Clustering and Membrane Properties and Curvature.* Biophys J, 2016. **111**(9): p. 1987-1999.
24. Fricke, N. and R. Dimova, *GM1 Softens POPC Membranes and Induces the Formation of Micron-Sized Domains.* Biophys J, 2016. **111**(9): p. 1935-1945.
25. Cantu, L., et al., *Structural aspects of ganglioside-containing membranes.* Biochim Biophys Acta, 2009. **1788**(1): p. 202-8.

26. Dasgupta, R., et al., *The glycolipid GM1 reshapes asymmetric biomembranes and giant vesicles by curvature generation.* Proc Natl Acad Sci U S A, 2018. **115**(22): p. 5756-5761.
27. Roisen, F.J., et al., *Ganglioside stimulation of axonal sprouting in vitro.* Science, 1981. **214**(4520): p. 577-8.
28. Skaper, S.D., A. Leon, and G. Toffano, *Ganglioside function in the development and repair of the nervous system. From basic science to clinical application.* Mol Neurobiol, 1989. **3**(3): p. 173-99.
29. Ledeen, R.W. and G. Wu, *The multi-tasked life of GM1 ganglioside, a true factotum of nature.* Trends Biochem Sci, 2015. **40**(7): p. 407-18.
30. Fanzo, J.C., et al., *CD95 rapidly clusters in cells of diverse origins.* Cancer Biol Ther, 2003. **2**(4): p. 392-5.
31. Nurminen, T.A., et al., *Observation of topical catalysis by sphingomyelinase coupled to microspheres.* J Am Chem Soc, 2002. **124**(41): p. 12129-34.
32. Carrer, D.C. and B. Maggio, *Phase behavior and molecular interactions in mixtures of ceramide with dipalmitoylphosphatidylcholine.* J Lipid Res, 1999. **40**(11): p. 1978-89.
33. Silva, L., et al., *Ceramide-platform formation and -induced biophysical changes in a fluid phospholipid membrane.* Mol Membr Biol, 2006. **23**(2): p. 137-48.
34. Bollinger, C.R., V. Teichgraber, and E. Gulbins, *Ceramide-enriched membrane domains.* Biochim Biophys Acta, 2005. **1746**(3): p. 284-94.
35. Kolesnick, R.N., F.M. Goni, and A. Alonso, *Compartmentalization of ceramide signaling: physical foundations and biological effects.* J Cell Physiol, 2000. **184**(3): p. 285-300.
36. Gulbins, E., et al., *Ceramide, membrane rafts and infections.* J Mol Med (Berl), 2004. **82**(6): p. 357-63.
37. Chiantia, S., et al., *Role of ceramide in membrane protein organization investigated by combined AFM and FCS.* Biochim Biophys Acta, 2008. **1778**(5): p. 1356-64.
38. Trajkovic, K., et al., *Ceramide triggers budding of exosome vesicles into multivesicular endosomes.* Science, 2008. **319**(5867): p. 1244-7.

39. Wu, G., et al., *Cerebellar neurons lacking complex gangliosides degenerate in the presence of depolarizing levels of potassium.* Proc Natl Acad Sci U S A, 2001. **98**(1): p. 307-12.
40. Wu, G. and R.W. Ledeen, *Gangliosides as modulators of neuronal calcium.* Prog Brain Res, 1994. **101**: p. 101-12.
41. Tang, C.M., F. Presser, and M. Morad, *Amiloride selectively blocks the low threshold (T) calcium channel.* Science, 1988. **240**(4849): p. 213-5.
42. Rodriguez, J.A., et al., *Plasma membrane ganglioside sialidase regulates axonal growth and regeneration in hippocampal neurons in culture.* J Neurosci, 2001. **21**(21): p. 8387-95.
43. Zhao, Y., et al., *Gangliosides modulate the activity of the plasma membrane Ca(2+)-ATPase from porcine brain synaptosomes.* Archives of Biochemistry & Biophysics, 2004. **427**(2): p. 204-12.
44. Zhang, J., et al., *Gangliosides activate the phosphatase activity of the erythrocyte plasma membrane Ca2+-ATPase.* Archives of Biochemistry & Biophysics, 2005. **444**(1): p. 1-6.
45. Jiang, L., et al., *Effects of gangliosides on the activity of the plasma membrane Ca2+-ATPase.* Biochimica et Biophysica Acta, 2014. **1838**(5): p. 1255-65.
46. Carlson, R.O., et al., *Endogenous ganglioside GM1 modulates L-type calcium channel activity in N18 neuroblastoma cells.* Journal of Neuroscience, 1994. **14**(4): p. 2272-81.
47. Martinez, A., J. Vitorica, and J. Satrustegui, *Cytosolic free calcium levels increase with age in rat brain synaptosomes.* Neurosci Lett, 1988. **88**(3): p. 336-42.
48. Michaelis, M.L., C.T. Foster, and C. Jayawickreme, *Regulation of calcium levels in brain tissue from adult and aged rats.* Mech Ageing Dev, 1992. **62**(3): p. 291-306.
49. Garcia, M.L. and E.E. Strehler, *Plasma membrane calcium ATPases as critical regulators of calcium homeostasis during neuronal cell function.* Front Biosci, 1999. **4**: p. D869-82.

50. Zaidi, A., et al., *Age-related decrease in brain synaptic membrane Ca2+-ATPase in F344/BNF1 rats.* Neurobiol Aging, 1998. **19**(5): p. 487-95.
51. Michaelis, M.L., K. Johe, and T.E. Kitos, *Age-dependent alterations in synaptic membrane systems for Ca2+ regulation.* Mech Ageing Dev, 1984. **25**(1-2): p. 215-25.
52. Jiang, L., et al., *Decreases in plasma membrane Ca(2)(+)-ATPase in brain synaptic membrane rafts from aged rats.* J Neurochem, 2012. **123**(5): p. 689-99.
53. Huang, E.J. and L.F. Reichardt, *Trk receptors: roles in neuronal signal transduction.* Annu Rev Biochem, 2003. **72**: p. 609-42.
54. Mocchetti, I., *Exogenous gangliosides, neuronal plasticity and repair, and the neurotrophins.* Cell Mol Life Sci, 2005. **62**(19-20): p. 2283-94.
55. Mutoh, T., et al., *Ganglioside GM1 binds to the Trk protein and regulates receptor function.* Proc Natl Acad Sci U S A, 1995. **92**(11): p. 5087-91.
56. Rabin, S.J. and I. Mocchetti, *GM1 ganglioside activates the high-affinity nerve growth factor receptor trkA.* J Neurochem, 1995. **65**(1): p. 347-54.
57. Bachis, A., et al., *Gangliosides prevent excitotoxicity through activation of TrkB receptor.* Neurotox Res, 2002. **4**(3): p. 225-34.
58. Proia, R.L., *Glycosphingolipid functions: insights from engineered mouse models.* Philos Trans R Soc Lond B Biol Sci, 2003. **358**(1433): p. 879-83.
59. Yamashita, T., et al., *A vital role for glycosphingolipid synthesis during development and differentiation.* Proc Natl Acad Sci U S A, 1999. **96**(16): p. 9142-7.
60. Nishie, T., et al., *Beta4-galactosyltransferase-5 is a lactosylceramide synthase essential for mouse extra-embryonic development.* Glycobiology, 2010. **20**(10): p. 1311-22.
61. Kumagai, T., et al., *Early lethality of beta-1,4-galactosyltransferase V-mutant mice by growth retardation.* Biochem Biophys Res Commun, 2009. **379**(2): p. 456-9.

62. Sheikh, K.A., et al., *Mice lacking complex gangliosides develop Wallerian degeneration and myelination defects.* Proc Natl Acad Sci U S A, 1999. **96**(13): p. 7532-7.
63. Chiavegatto, S., et al., *A functional role for complex gangliosides: motor deficits in GM2/GD2 synthase knockout mice.* Exp Neurol, 2000. **166**(2): p. 227-34.
64. Wu, G., et al., *Mice lacking major brain gangliosides develop parkinsonism.* Neurochem Res, 2011. **36**(9): p. 1706-14.
65. Susuki, K., et al., *Gangliosides contribute to stability of paranodal junctions and ion channel clusters in myelinated nerve fibers.* Glia, 2007. **55**(7): p. 746-57.
66. Takamiya, K., et al., *Complex gangliosides are essential in spermatogenesis of mice: possible roles in the transport of testosterone.* Proc Natl Acad Sci U S A, 1998. **95**(21): p. 12147-52.
67. Kawai, H., et al., *Mice expressing only monosialoganglioside GM3 exhibit lethal audiogenic seizures.* J Biol Chem, 2001. **276**(10): p. 6885-8.
68. Tjolsen, A., et al., *The formalin test: an evaluation of the method.* Pain, 1992. **51**(1): p. 5-17.
69. Handa, Y., et al., *GD3 synthase gene knockout mice exhibit thermal hyperalgesia and mechanical allodynia but decreased response to formalin-induced prolonged noxious stimulation.* Pain, 2005. **117**(3): p. 271-9.
70. Tajima, O., et al., *Reduced motor and sensory functions and emotional response in GM3-only mice: emergence from early stage of life and exacerbation with aging.* Behav Brain Res, 2009. **198**(1): p. 74-82.
71. Yoshikawa, M., et al., *Mice lacking ganglioside GM3 synthase exhibit complete hearing loss due to selective degeneration of the organ of Corti.* Proc Natl Acad Sci U S A, 2009. **106**(23): p. 9483-8.
72. Yamashita, T., et al., *Enhanced insulin sensitivity in mice lacking ganglioside GM3.* Proc Natl Acad Sci U S A, 2003. **100**(6): p. 3445-9.
73. Yamashita, T., et al., *Interruption of ganglioside synthesis produces central nervous system degeneration and altered axon-glial interactions.* Proc Natl Acad Sci U S A, 2005. **102**(8): p. 2725-30.

74. Yu, R.K., et al., *Developmental changes in ganglioside composition and synthesis in embryonic rat brain.* J Neurochem, 1988. **50**(6): p. 1825-9.
75. Ngamukote, S., et al., *Developmental changes of glycosphingolipids and expression of glycogenes in mouse brains.* J Neurochem, 2007. **103**(6): p. 2327-41.
76. Ohsawa, T., *Changes of mouse brain gangliosides during aging from young adult until senescence.* Mech Ageing Dev, 1989. **50**(2): p. 169-77.
77. Hilbig, R., G. Lauke, and H. Rahmann, *Brain gangliosides during the life span (embryogenesis to senescence) of the rat.* Dev Neurosci, 1983. **6**(4-5): p. 260-70.
78. Hallett, P.J., et al., *Glycosphingolipid levels and glucocerebrosidase activity are altered in normal aging of the mouse brain.* Neurobiol Aging, 2018. **67**: p. 189-200.
79. Segler-Stahl, K., J.C. Webster, and E.G. Brunngraber, *Changes in the concentration and composition of human brain gangliosides with aging.* Gerontology, 1983. **29**(3): p. 161-8.
80. Huebecker, M., et al., *Reduced sphingolipid hydrolase activities, substrate accumulation and ganglioside decline in Parkinson's disease.* Mol Neurodegener, 2019. **14**(1): p. 40.
81. Blennow, K., et al., *Differences in cerebrospinal fluid gangliosides between "probable Alzheimer's disease" and normal aging.* Aging (Milano), 1992. **4**(4): p. 301-6.
82. Blennow, K., et al., *Gangliosides in cerebrospinal fluid in 'probable Alzheimer's disease'.* Arch Neurol, 1991. **48**(10): p. 1032-5.
83. Wu, G., et al., *Deficiency of ganglioside GM1 correlates with Parkinson's disease in mice and humans.* J Neurosci Res, 2012. **90**(10): p. 1997-2008.
84. Desplats, P.A., et al., *Glycolipid and ganglioside metabolism imbalances in Huntington's disease.* Neurobiol Dis, 2007. **27**(3): p. 265-77.
85. Maglione, V., et al., *Impaired ganglioside metabolism in Huntington's disease and neuroprotective role of GM1.* J Neurosci, 2010. **30**(11): p. 4072-80.

86. Rawlins, M.D., et al., *The Prevalence of Huntington's Disease.* Neuroepidemiology, 2016. **46**(2): p. 144-53.
87. Kay, C., M.R. Hayden, and B.R. Leavitt, *Epidemiology of Huntington disease.* Handb Clin Neurol, 2017. **144**: p. 31-46.
88. Ferrante, R.J., et al., *Morphologic and histochemical characteristics of a spared subset of striatal neurons in Huntington's disease.* J Neuropathol Exp Neurol, 1987. **46**(1): p. 12-27.
89. Reiner, A., et al., *Differential loss of striatal projection neurons in Huntington disease.* Proc Natl Acad Sci U S A, 1988. **85**(15): p. 5733-7.
90. Han, I., et al., *Differential vulnerability of neurons in Huntington's disease: the role of cell type-specific features.* J Neurochem, 2010. **113**(5): p. 1073-91.
91. Sotrel, A., et al., *Morphometric analysis of the prefrontal cortex in Huntington's disease.* Neurology, 1991. **41**(7): p. 1117-23.
92. Hedreen, J.C., et al., *Neuronal loss in layers V and VI of cerebral cortex in Huntington's disease.* Neurosci Lett, 1991. **133**(2): p. 257-61.
93. de la Monte, S.M., J.P. Vonsattel, and E.P. Richardson, Jr., *Morphometric demonstration of atrophic changes in the cerebral cortex, white matter, and neostriatum in Huntington's disease.* J Neuropathol Exp Neurol, 1988. **47**(5): p. 516-25.
94. Rosas, H.D., et al., *Cerebral cortex and the clinical expression of Huntington's disease: complexity and heterogeneity.* Brain, 2008. **131**(Pt 4): p. 1057-68.
95. Aylward, E.H., et al., *Longitudinal change in regional brain volumes in prodromal Huntington disease.* J Neurol Neurosurg Psychiatry, 2011. **82**(4): p. 405-10.
96. Kremer, H.P., et al., *Atrophy of the hypothalamic lateral tuberal nucleus in Huntington's disease.* J Neuropathol Exp Neurol, 1990. **49**(4): p. 371-82.
97. Ahveninen, L.M., et al., *Reduced amygdala volumes are related to motor and cognitive signs in Huntington's disease: The IMAGE-HD study.* Neuroimage Clin, 2018. **18**: p. 881-887.
98. Heinsen, H., et al., *Nerve cell loss in the thalamic mediodorsal nucleus in Huntington's disease.* Acta Neuropathol, 1999. **97**(6): p. 613-22.

99. Kassubek, J., et al., *Thalamic atrophy in Huntington's disease co-varies with cognitive performance: a morphometric MRI analysis.* Cereb Cortex, 2005. **15**(6): p. 846-53.
100. Zweig, R.M., et al., *Linkage to the Huntington's disease locus in a family with unusual clinical and pathological features.* Ann Neurol, 1989. **26**(1): p. 78-84.
101. Rub, U., et al., *Huntington's disease (HD): degeneration of select nuclei, widespread occurrence of neuronal nuclear and axonal inclusions in the brainstem.* Brain Pathol, 2014. **24**(3): p. 247-60.
102. Postert, T., et al., *Basal ganglia alterations and brain atrophy in Huntington's disease depicted by transcranial real time sonography.* J Neurol Neurosurg Psychiatry, 1999. **67**(4): p. 457-62.
103. McNeil, S.M., et al., *Reduced penetrance of the Huntington's disease mutation.* Hum Mol Genet, 1997. **6**(5): p. 775-9.
104. *A novel gene containing a trinucleotide repeat that is expanded and unstable on Huntington's disease chromosomes. The Huntington's Disease Collaborative Research Group.* Cell, 1993. **72**(6): p. 971-83.
105. Arrasate, M. and S. Finkbeiner, *Protein aggregates in Huntington's disease.* Exp Neurol, 2012. **238**(1): p. 1-11.
106. Ross, C.A. and S.J. Tabrizi, *Huntington's disease: from molecular pathogenesis to clinical treatment.* Lancet Neurol, 2011. **10**(1): p. 83-98.
107. Ribai, P., et al., *Psychiatric and cognitive difficulties as indicators of juvenile huntington disease onset in 29 patients.* Arch Neurol, 2007. **64**(6): p. 813-9.
108. Nance, M.A., *Genetic testing of children at risk for Huntington's disease. US Huntington Disease Genetic Testing Group.* Neurology, 1997. **49**(4): p. 1048-53.
109. Andrew, S.E., et al., *The relationship between trinucleotide (CAG) repeat length and clinical features of Huntington's disease.* Nat Genet, 1993. **4**(4): p. 398-403.
110. Genetic Modifiers of Huntington's Disease Consortium. Electronic address, g.h.m.h.e. and C. Genetic Modifiers of Huntington's Disease, *CAG Repeat Not Polyglutamine Length Determines Timing of Huntington's Disease Onset.* Cell, 2019. **178**(4): p. 887-900 e14.

111. Ciosi, M., et al., *A genetic association study of glutamine-encoding DNA sequence structures, somatic CAG expansion, and DNA repair gene variants, with Huntington disease clinical outcomes.* EBioMedicine, 2019. **48**: p. 568-580.
112. Lin, B., et al., *Differential 3' polyadenylation of the Huntington disease gene results in two mRNA species with variable tissue expression.* Hum Mol Genet, 1993. **2**(10): p. 1541-5.
113. Neueder, A., et al., *The pathogenic exon 1 HTT protein is produced by incomplete splicing in Huntington's disease patients.* Sci Rep, 2017. **7**(1): p. 1307.
114. Gipson, T.A., et al., *Aberrantly spliced HTT, a new player in Huntington's disease pathogenesis.* RNA Biol, 2013. **10**(11): p. 1647-52.
115. Sathasivam, K., et al., *Aberrant splicing of HTT generates the pathogenic exon 1 protein in Huntington disease.* Proc Natl Acad Sci U S A, 2013. **110**(6): p. 2366-70.
116. Baxendale, S., et al., *Comparative sequence analysis of the human and pufferfish Huntington's disease genes.* Nat Genet, 1995. **10**(1): p. 67-76.
117. Tartari, M., et al., *Phylogenetic comparison of huntingtin homologues reveals the appearance of a primitive polyQ in sea urchin.* Mol Biol Evol, 2008. **25**(2): p. 330-8.
118. Takano, H. and J.F. Gusella, *The predominantly HEAT-like motif structure of huntingtin and its association and coincident nuclear entry with dorsal, an NF-kB/Rel/dorsal family transcription factor.* BMC Neurosci, 2002. **3**: p. 15.
119. Marques Sousa, C. and S. Humbert, *Huntingtin: here, there, everywhere!* J Huntingtons Dis, 2013. **2**(4): p. 395-403.
120. Hughes, A. and L. Jones, *Huntingtin localisation studies - a technical review.* PLoS Curr, 2011. **3**: p. RRN1211.
121. Strong, T.V., et al., *Widespread expression of the human and rat Huntington's disease gene in brain and nonneural tissues.* Nat Genet, 1993. **5**(3): p. 259-65.
122. Li, S.H., et al., *Huntington's disease gene (IT15) is widely expressed in human and rat tissues.* Neuron, 1993. **11**(5): p. 985-93.

123. Landwehrmeyer, G.B., et al., *Huntington's disease gene: regional and cellular expression in brain of normal and affected individuals.* Ann Neurol, 1995. **37**(2): p. 218-30.
124. DiFiglia, M., et al., *Huntingtin is a cytoplasmic protein associated with vesicles in human and rat brain neurons.* Neuron, 1995. **14**(5): p. 1075-81.
125. Andrade, M.A. and P. Bork, *HEAT repeats in the Huntington's disease protein.* Nat Genet, 1995. **11**(2): p. 115-6.
126. Yoshimura, S.H. and T. Hirano, *HEAT repeats - versatile arrays of amphiphilic helices working in crowded environments?* J Cell Sci, 2016. **129**(21): p. 3963-3970.
127. Saudou, F. and S. Humbert, *The Biology of Huntingtin.* Neuron, 2016. **89**(5): p. 910-26.
128. Thompson, L.M., et al., *IKK phosphorylates Huntingtin and targets it for degradation by the proteasome and lysosome.* J Cell Biol, 2009. **187**(7): p. 1083-99.
129. Steffan, J.S., et al., *SUMO modification of Huntingtin and Huntington's disease pathology.* Science, 2004. **304**(5667): p. 100-4.
130. Maiuri, T., et al., *The huntingtin N17 domain is a multifunctional CRM1 and Ran-dependent nuclear and cilial export signal.* Hum Mol Genet, 2013. **22**(7): p. 1383-94.
131. Atwal, R.S., et al., *Huntingtin has a membrane association signal that can modulate huntingtin aggregation, nuclear entry and toxicity.* Hum Mol Genet, 2007. **16**(21): p. 2600-15.
132. Gu, X., et al., *Serines 13 and 16 are critical determinants of full-length human mutant huntingtin induced disease pathogenesis in HD mice.* Neuron, 2009. **64**(6): p. 828-40.
133. Zheng, Z., et al., *An N-terminal nuclear export signal regulates trafficking and aggregation of Huntingtin (Htt) protein exon 1.* J Biol Chem, 2013. **288**(9): p. 6063-71.
134. Xia, J., et al., *Huntingtin contains a highly conserved nuclear export signal.* Hum Mol Genet, 2003. **12**(12): p. 1393-403.

135. Li, S.H. and X.J. Li, *Aggregation of N-terminal huntingtin is dependent on the length of its glutamine repeats.* Hum Mol Genet, 1998. **7**(5): p. 777-82.
136. Ignatova, Z. and L.M. Gierasch, *Extended polyglutamine tracts cause aggregation and structural perturbation of an adjacent beta barrel protein.* J Biol Chem, 2006. **281**(18): p. 12959-67.
137. Qin, Z.H., et al., *Huntingtin bodies sequester vesicle-associated proteins by a polyproline-dependent interaction.* J Neurosci, 2004. **24**(1): p. 269-81.
138. Warby, S.C., et al., *Activated caspase-6 and caspase-6-cleaved fragments of huntingtin specifically colocalize in the nucleus.* Hum Mol Genet, 2008. **17**(15): p. 2390-404.
139. Tebbenkamp, A.T., et al., *Analysis of proteolytic processes and enzymatic activities in the generation of huntingtin n-terminal fragments in an HEK293 cell model.* PLoS One, 2012. **7**(12): p. e50750.
140. Ratovitski, T., et al., *Mutant huntingtin N-terminal fragments of specific size mediate aggregation and toxicity in neuronal cells.* J Biol Chem, 2009. **284**(16): p. 10855-67.
141. Miller, J.P., et al., *Matrix metalloproteinases are modifiers of huntingtin proteolysis and toxicity in Huntington's disease.* Neuron, 2010. **67**(2): p. 199-212.
142. Lunkes, A., et al., *Proteases acting on mutant huntingtin generate cleaved products that differentially build up cytoplasmic and nuclear inclusions.* Mol Cell, 2002. **10**(2): p. 259-69.
143. Kim, Y.J., et al., *Caspase 3-cleaved N-terminal fragments of wild-type and mutant huntingtin are present in normal and Huntington's disease brains, associate with membranes, and undergo calpain-dependent proteolysis.* Proc Natl Acad Sci U S A, 2001. **98**(22): p. 12784-9.
144. Kim, Y.J., et al., *Lysosomal proteases are involved in generation of N-terminal huntingtin fragments.* Neurobiol Dis, 2006. **22**(2): p. 346-56.
145. Hermel, E., et al., *Specific caspase interactions and amplification are involved in selective neuronal vulnerability in Huntington's disease.* Cell Death Differ, 2004. **11**(4): p. 424-38.

146. Goldberg, Y.P., et al., *Cleavage of huntingtin by apopain, a proapoptotic cysteine protease, is modulated by the polyglutamine tract.* Nat Genet, 1996. **13**(4): p. 442-9.
147. Gafni, J. and L.M. Ellerby, *Calpain activation in Huntington's disease.* J Neurosci, 2002. **22**(12): p. 4842-9.
148. Ehrnhoefer, D.E., L. Sutton, and M.R. Hayden, *Small changes, big impact: posttranslational modifications and function of huntingtin in Huntington disease.* Neuroscientist, 2011. **17**(5): p. 475-92.
149. Schilling, G., et al., *Intranuclear inclusions and neuritic aggregates in transgenic mice expressing a mutant N-terminal fragment of huntingtin.* Hum Mol Genet, 1999. **8**(3): p. 397-407.
150. Mangiarini, L., et al., *Exon 1 of the HD gene with an expanded CAG repeat is sufficient to cause a progressive neurological phenotype in transgenic mice.* Cell, 1996. **87**(3): p. 493-506.
151. Hodgson, J.G., et al., *A YAC mouse model for Huntington's disease with full-length mutant huntingtin, cytoplasmic toxicity, and selective striatal neurodegeneration.* Neuron, 1999. **23**(1): p. 181-92.
152. Barbaro, B.A., et al., *Comparative study of naturally occurring huntingtin fragments in Drosophila points to exon 1 as the most pathogenic species in Huntington's disease.* Hum Mol Genet, 2015. **24**(4): p. 913-25.
153. Schilling, G., et al., *Characterization of huntingtin pathologic fragments in human Huntington disease, transgenic mice, and cell models.* J Neuropathol Exp Neurol, 2007. **66**(4): p. 313-20.
154. Gutekunst, C.A., et al., *Nuclear and neuropil aggregates in Huntington's disease: relationship to neuropathology.* J Neurosci, 1999. **19**(7): p. 2522-34.
155. DiFiglia, M., et al., *Aggregation of huntingtin in neuronal intranuclear inclusions and dystrophic neurites in brain.* Science, 1997. **277**(5334): p. 1990-3.
156. Davies, S.W., et al., *Formation of neuronal intranuclear inclusions underlies the neurological dysfunction in mice transgenic for the HD mutation.* Cell, 1997. **90**(3): p. 537-48.

157. Benn, C.L., et al., *Contribution of nuclear and extranuclear polyQ to neurological phenotypes in mouse models of Huntington's disease.* Hum Mol Genet, 2005. **14**(20): p. 3065-78.
158. Schulte, J. and J.T. Littleton, *The biological function of the Huntingtin protein and its relevance to Huntington's Disease pathology.* Curr Trends Neurol, 2011. **5**: p. 65-78.
159. Zeitlin, S., et al., *Increased apoptosis and early embryonic lethality in mice nullizygous for the Huntington's disease gene homologue.* Nat Genet, 1995. **11**(2): p. 155-63.
160. Nasir, J., et al., *Targeted disruption of the Huntington's disease gene results in embryonic lethality and behavioral and morphological changes in heterozygotes.* Cell, 1995. **81**(5): p. 811-23.
161. Duyao, M.P., et al., *Inactivation of the mouse Huntington's disease gene homolog Hdh.* Science, 1995. **269**(5222): p. 407-10.
162. Wong, Y.C. and E.L. Holzbaur, *The regulation of autophagosome dynamics by huntingtin and HAP1 is disrupted by expression of mutant huntingtin, leading to defective cargo degradation.* J Neurosci, 2014. **34**(4): p. 1293-305.
163. Liot, G., et al., *Mutant Huntingtin alters retrograde transport of TrkB receptors in striatal dendrites.* J Neurosci, 2013. **33**(15): p. 6298-309.
164. Caviston, J.P., et al., *Huntingtin coordinates the dynein-mediated dynamic positioning of endosomes and lysosomes.* Mol Biol Cell, 2011. **22**(4): p. 478-92.
165. Her, L.S. and L.S. Goldstein, *Enhanced sensitivity of striatal neurons to axonal transport defects induced by mutant huntingtin.* J Neurosci, 2008. **28**(50): p. 13662-72.
166. Colin, E., et al., *Huntingtin phosphorylation acts as a molecular switch for anterograde/retrograde transport in neurons.* EMBO J, 2008. **27**(15): p. 2124-34.
167. Twelvetrees, A.E., et al., *Delivery of GABAARs to synapses is mediated by HAP1-KIF5 and disrupted by mutant huntingtin.* Neuron, 2010. **65**(1): p. 53-65.

168. Gauthier, L.R., et al., *Huntingtin controls neurotrophic support and survival of neurons by enhancing BDNF vesicular transport along microtubules.* Cell, 2004. **118**(1): p. 127-38.
169. Pal, A., et al., *Huntingtin-HAP40 complex is a novel Rab5 effector that regulates early endosome motility and is up-regulated in Huntington's disease.* J Cell Biol, 2006. **172**(4): p. 605-18.
170. Nielsen, E., et al., *Rab5 regulates motility of early endosomes on microtubules.* Nat Cell Biol, 1999. **1**(6): p. 376-82.
171. Li, X., et al., *A function of huntingtin in guanine nucleotide exchange on Rab11.* Neuroreport, 2008. **19**(16): p. 1643-7.
172. Legendre-Guillemin, V., et al., *HIP1 and HIP12 display differential binding to F-actin, AP2, and clathrin. Identification of a novel interaction with clathrin light chain.* J Biol Chem, 2002. **277**(22): p. 19897-904.
173. Engqvist-Goldstein, A.E., et al., *The actin-binding protein Hip1R associates with clathrin during early stages of endocytosis and promotes clathrin assembly in vitro.* J Cell Biol, 2001. **154**(6): p. 1209-23.
174. Waelter, S., et al., *The huntingtin interacting protein HIP1 is a clathrin and alpha-adaptin-binding protein involved in receptor-mediated endocytosis.* Hum Mol Genet, 2001. **10**(17): p. 1807-17.
175. Huang, K., et al., *Huntingtin-interacting protein HIP14 is a palmitoyl transferase involved in palmitoylation and trafficking of multiple neuronal proteins.* Neuron, 2004. **44**(6): p. 977-86.
176. Yanai, A., et al., *Palmitoylation of huntingtin by HIP14 is essential for its trafficking and function.* Nat Neurosci, 2006. **9**(6): p. 824-31.
177. Huganir, R.L. and R.A. Nicoll, *AMPARs and synaptic plasticity: the last 25 years.* Neuron, 2013. **80**(3): p. 704-17.
178. Sun, Y., et al., *Polyglutamine-expanded huntingtin promotes sensitization of N-methyl-D-aspartate receptors via post-synaptic density 95.* J Biol Chem, 2001. **276**(27): p. 24713-8.

179. Fan, J., et al., *P38 MAPK is involved in enhanced NMDA receptor-dependent excitotoxicity in YAC transgenic mouse model of Huntington disease.* Neurobiol Dis, 2012. **45**(3): p. 999-1009.
180. Lilienbaum, A., *Relationship between the proteasomal system and autophagy.* Int J Biochem Mol Biol, 2013. **4**(1): p. 1-26.
181. Kocaturk, N.M. and D. Gozuacik, *Crosstalk Between Mammalian Autophagy and the Ubiquitin-Proteasome System.* Front Cell Dev Biol, 2018. **6**: p. 128.
182. Klionsky, D.J. and S.D. Emr, *Autophagy as a regulated pathway of cellular degradation.* Science, 2000. **290**(5497): p. 1717-21.
183. Dikic, I., *Proteasomal and Autophagic Degradation Systems.* Annu Rev Biochem, 2017. **86**: p. 193-224.
184. Glick, D., S. Barth, and K.F. Macleod, *Autophagy: cellular and molecular mechanisms.* J Pathol, 2010. **221**(1): p. 3-12.
185. Chun, Y. and J. Kim, *Autophagy: An Essential Degradation Program for Cellular Homeostasis and Life.* Cells, 2018. **7**(12).
186. Maday, S., K.E. Wallace, and E.L. Holzbaur, *Autophagosomes initiate distally and mature during transport toward the cell soma in primary neurons.* J Cell Biol, 2012. **196**(4): p. 407-17.
187. Wong, M., *Mammalian target of rapamycin (mTOR) pathways in neurological diseases.* Biomed J, 2013. **36**(2): p. 40-50.
188. Ravikumar, B., et al., *Inhibition of mTOR induces autophagy and reduces toxicity of polyglutamine expansions in fly and mouse models of Huntington disease.* Nat Genet, 2004. **36**(6): p. 585-95.
189. Martinez-Vicente, M., et al., *Cargo recognition failure is responsible for inefficient autophagy in Huntington's disease.* Nat Neurosci, 2010. **13**(5): p. 567-76.
190. Schipper-Krom, S., et al., *Dynamic recruitment of active proteasomes into polyglutamine initiated inclusion bodies.* FEBS Lett, 2014. **588**(1): p. 151-9.
191. Li, X., et al., *Inhibiting the ubiquitin-proteasome system leads to preferential accumulation of toxic N-terminal mutant huntingtin fragments.* Hum Mol Genet, 2010. **19**(12): p. 2445-55.

192. McKinnon, C. and S.J. Tabrizi, *The ubiquitin-proteasome system in neurodegeneration.* Antioxid Redox Signal, 2014. **21**(17): p. 2302-21.
193. Tydlacka, S., et al., *Differential activities of the ubiquitin-proteasome system in neurons versus glia may account for the preferential accumulation of misfolded proteins in neurons.* J Neurosci, 2008. **28**(49): p. 13285-95.
194. Bennett, E.J., et al., *Global changes to the ubiquitin system in Huntington's disease.* Nature, 2007. **448**(7154): p. 704-8.
195. Sugars, K.L. and D.C. Rubinsztein, *Transcriptional abnormalities in Huntington disease.* Trends Genet, 2003. **19**(5): p. 233-8.
196. Landles, C. and G.P. Bates, *Huntingtin and the molecular pathogenesis of Huntington's disease. Fourth in molecular medicine review series.* EMBO Rep, 2004. **5**(10): p. 958-63.
197. Oliveira, J.M., *Nature and cause of mitochondrial dysfunction in Huntington's disease: focusing on huntingtin and the striatum.* J Neurochem, 2010. **114**(1): p. 1-12.
198. Bossy-Wetzel, E., A. Petrilli, and A.B. Knott, *Mutant huntingtin and mitochondrial dysfunction.* Trends Neurosci, 2008. **31**(12): p. 609-16.
199. Prusiner, S.B., *Novel proteinaceous infectious particles cause scrapie.* Science, 1982. **216**(4542): p. 136-44.
200. Caughey, B., R.E. Race, and B. Chesebro, *Detection of prion protein mRNA in normal and scrapie-infected tissues and cell lines.* J Gen Virol, 1988. **69 (Pt 3)**: p. 711-6.
201. Kaufman, S.K. and M.I. Diamond, *Prion-like propagation of protein aggregation and related therapeutic strategies.* Neurotherapeutics, 2013. **10**(3): p. 371-82.
202. Brandner, S., et al., *Normal host prion protein (PrPC) is required for scrapie spread within the central nervous system.* Proc Natl Acad Sci U S A, 1996. **93**(23): p. 13148-51.
203. Prusiner, S.B., *Prions.* Proc Natl Acad Sci U S A, 1998. **95**(23): p. 13363-83.
204. Guo, B.B., S.A. Bellingham, and A.F. Hill, *Stimulating the Release of Exosomes Increases the Intercellular Transfer of Prions.* J Biol Chem, 2016. **291**(10): p. 5128-37.

205. Kanu, N., et al., *Transfer of scrapie prion infectivity by cell contact in culture.* Curr Biol, 2002. **12**(7): p. 523-30.
206. Gousset, K., et al., *Prions hijack tunnelling nanotubes for intercellular spread.* Nat Cell Biol, 2009. **11**(3): p. 328-36.
207. Zhu, S., et al., *Prion aggregates transfer through tunneling nanotubes in endocytic vesicles.* Prion, 2015. **9**(2): p. 125-35.
208. Victoria, G.S., et al., *Astrocyte-to-neuron intercellular prion transfer is mediated by cell-cell contact.* Sci Rep, 2016. **6**: p. 20762.
209. Carija, A., et al., *Protein aggregation into insoluble deposits protects from oxidative stress.* Redox Biol, 2017. **12**: p. 699-711.
210. Nucifora, L.G., et al., *Identification of novel potentially toxic oligomers formed in vitro from mammalian-derived expanded huntingtin exon-1 protein.* J Biol Chem, 2012. **287**(19): p. 16017-28.
211. Arrasate, M., et al., *Inclusion body formation reduces levels of mutant huntingtin and the risk of neuronal death.* Nature, 2004. **431**(7010): p. 805-10.
212. Sanchez, I., C. Mahlke, and J. Yuan, *Pivotal role of oligomerization in expanded polyglutamine neurodegenerative disorders.* Nature, 2003. **421**(6921): p. 373-9.
213. Ross, C.A. and M.A. Poirier, *Opinion: What is the role of protein aggregation in neurodegeneration?* Nat Rev Mol Cell Biol, 2005. **6**(11): p. 891-8.
214. Winner, B., et al., *In vivo demonstration that alpha-synuclein oligomers are toxic.* Proc Natl Acad Sci U S A, 2011. **108**(10): p. 4194-9.
215. Patterson, K.R., et al., *Characterization of prefibrillar Tau oligomers in vitro and in Alzheimer disease.* J Biol Chem, 2011. **286**(26): p. 23063-76.
216. Lasagna-Reeves, C.A., et al., *Identification of oligomers at early stages of tau aggregation in Alzheimer's disease.* FASEB J, 2012. **26**(5): p. 1946-59.
217. Gandy, S., et al., *Days to criterion as an indicator of toxicity associated with human Alzheimer amyloid-beta oligomers.* Ann Neurol, 2010. **68**(2): p. 220-30.
218. Conway, K.A., et al., *Acceleration of oligomerization, not fibrillization, is a shared property of both alpha-synuclein mutations linked to early-onset*

Parkinson's disease: implications for pathogenesis and therapy. Proc Natl Acad Sci U S A, 2000. **97**(2): p. 571-6.

219. Braak, H. and E. Braak, *Neuropathological stageing of Alzheimer-related changes.* Acta Neuropathol, 1991. **82**(4): p. 239-59.
220. Petkova, A.T., et al., *Self-propagating, molecular-level polymorphism in Alzheimer's beta-amyloid fibrils.* Science, 2005. **307**(5707): p. 262-5.
221. Yonetani, M., et al., *Conversion of wild-type alpha-synuclein into mutant-type fibrils and its propagation in the presence of A30P mutant.* J Biol Chem, 2009. **284**(12): p. 7940-50.
222. Frost, B., et al., *Conformational diversity of wild-type Tau fibrils specified by templated conformation change.* J Biol Chem, 2009. **284**(6): p. 3546-51.
223. Clavaguera, F., et al., *Transmission and spreading of tauopathy in transgenic mouse brain.* Nat Cell Biol, 2009. **11**(7): p. 909-13.
224. Iba, M., et al., *Synthetic tau fibrils mediate transmission of neurofibrillary tangles in a transgenic mouse model of Alzheimer's-like tauopathy.* J Neurosci, 2013. **33**(3): p. 1024-37.
225. Liu, L., et al., *Trans-synaptic spread of tau pathology in vivo.* PLoS One, 2012. **7**(2): p. e31302.
226. Stohr, J., et al., *Purified and synthetic Alzheimer's amyloid beta (Abeta) prions.* Proc Natl Acad Sci U S A, 2012. **109**(27): p. 11025-30.
227. Luk, K.C., et al., *Pathological alpha-synuclein transmission initiates Parkinson-like neurodegeneration in nontransgenic mice.* Science, 2012. **338**(6109): p. 949-53.
228. Luk, K.C., et al., *Intracerebral inoculation of pathological alpha-synuclein initiates a rapidly progressive neurodegenerative alpha-synucleinopathy in mice.* J Exp Med, 2012. **209**(5): p. 975-86.
229. Rey, N.L., et al., *Transfer of human alpha-synuclein from the olfactory bulb to interconnected brain regions in mice.* Acta Neuropathol, 2013. **126**(4): p. 555-73.

230. Recasens, A., et al., *Lewy body extracts from Parkinson disease brains trigger alpha-synuclein pathology and neurodegeneration in mice and monkeys.* Ann Neurol, 2014. **75**(3): p. 351-62.
231. Paumier, K.L., et al., *Intrastriatal injection of pre-formed mouse alpha-synuclein fibrils into rats triggers alpha-synuclein pathology and bilateral nigrostriatal degeneration.* Neurobiol Dis, 2015. **82**: p. 185-199.
232. Mougenot, A.L., et al., *Prion-like acceleration of a synucleinopathy in a transgenic mouse model.* Neurobiol Aging, 2012. **33**(9): p. 2225-8.
233. Masuda-Suzukake, M., et al., *Prion-like spreading of pathological alpha-synuclein in brain.* Brain, 2013. **136**(Pt 4): p. 1128-38.
234. Watts, J.C., et al., *Bioluminescence imaging of Abeta deposition in bigenic mouse models of Alzheimer's disease.* Proc Natl Acad Sci U S A, 2011. **108**(6): p. 2528-33.
235. Meyer-Luehmann, M., et al., *Exogenous induction of cerebral beta-amyloidogenesis is governed by agent and host.* Science, 2006. **313**(5794): p. 1781-4.
236. Kane, M.D., et al., *Evidence for seeding of beta -amyloid by intracerebral infusion of Alzheimer brain extracts in beta -amyloid precursor protein-transgenic mice.* J Neurosci, 2000. **20**(10): p. 3606-11.
237. Eisele, Y.S., et al., *Induction of cerebral beta-amyloidosis: intracerebral versus systemic Abeta inoculation.* Proc Natl Acad Sci U S A, 2009. **106**(31): p. 12926-31.
238. Hawkes, C.H., K. Del Tredici, and H. Braak, *Parkinson's disease: the dual hit theory revisited.* Ann N Y Acad Sci, 2009. **1170**: p. 615-22.
239. Hawkes, C.H., K. Del Tredici, and H. Braak, *Parkinson's disease: a dual-hit hypothesis.* Neuropathol Appl Neurobiol, 2007. **33**(6): p. 599-614.
240. Rietdijk, C.D., et al., *Exploring Braak's Hypothesis of Parkinson's Disease.* Front Neurol, 2017. **8**: p. 37.
241. Jansen, A.H., et al., *Visualization of prion-like transfer in Huntington's disease models.* Biochim Biophys Acta Mol Basis Dis, 2017. **1863**(3): p. 793-800.

242. Ren, P.H., et al., *Cytoplasmic penetration and persistent infection of mammalian cells by polyglutamine aggregates.* Nat Cell Biol, 2009. **11**(2): p. 219-25.
243. Tan, Z., et al., *Huntington's disease cerebrospinal fluid seeds aggregation of mutant huntingtin.* Mol Psychiatry, 2015. **20**(11): p. 1286-93.
244. Masnata, M., et al., *Demonstration of prion-like properties of mutant huntingtin fibrils in both in vitro and in vivo paradigms.* Acta Neuropathol, 2019. **137**(6): p. 981-1001.
245. Kazantsev, A., et al., *Insoluble detergent-resistant aggregates form between pathological and nonpathological lengths of polyglutamine in mammalian cells.* Proc Natl Acad Sci U S A, 1999. **96**(20): p. 11404-9.
246. Busch, A., et al., *Mutant huntingtin promotes the fibrillogenesis of wild-type huntingtin: a potential mechanism for loss of huntingtin function in Huntington's disease.* J Biol Chem, 2003. **278**(42): p. 41452-61.
247. Alexandrov, A.I., et al., *Wild type huntingtin toxicity in yeast: Implications for the role of amyloid cross-seeding in polyQ diseases.* Prion, 2016. **10**(3): p. 221-7.
248. Stathopulos, P.B., et al., *Sonication of proteins causes formation of aggregates that resemble amyloid.* Protein Sci, 2004. **13**(11): p. 3017-27.
249. Herrera, F., et al., *Visualization of cell-to-cell transmission of mutant huntingtin oligomers.* PLoS Curr, 2011. **3**: p. RRN1210.
250. Cicchetti, F., et al., *Mutant huntingtin is present in neuronal grafts in Huntington disease patients.* Ann Neurol, 2014. **76**(1): p. 31-42.
251. Pecho-Vrieseling, E., et al., *Transneuronal propagation of mutant huntingtin contributes to non-cell autonomous pathology in neurons.* Nat Neurosci, 2014. **17**(8): p. 1064-72.
252. Jeon, I., et al., *Human-to-mouse prion-like propagation of mutant huntingtin protein.* Acta Neuropathol, 2016. **132**(4): p. 577-92.
253. Slow, E.J., et al., *Selective striatal neuronal loss in a YAC128 mouse model of Huntington disease.* Hum Mol Genet, 2003. **12**(13): p. 1555-67.

254. Di Pardo, A., et al., *Ganglioside GM1 induces phosphorylation of mutant huntingtin and restores normal motor behavior in Huntington disease mice.* Proc Natl Acad Sci U S A, 2012. **109**(9): p. 3528-33.
255. Menalled, L.B., et al., *Time course of early motor and neuropathological anomalies in a knock-in mouse model of Huntington's disease with 140 CAG repeats.* J Comp Neurol, 2003. **465**(1): p. 11-26.
256. Alpaugh, M., et al., *Disease-modifying effects of ganglioside GM1 in Huntington's disease models.* EMBO Mol Med, 2017. **9**(11): p. 1537-1557.
257. Yanez-Mo, M., et al., *Biological properties of extracellular vesicles and their physiological functions.* J Extracell Vesicles, 2015. **4**: p. 27066.
258. Chargaff, E. and R. West, *The biological significance of the thromboplastic protein of blood.* J Biol Chem, 1946. **166**(1): p. 189-97.
259. Wolf, P., *The nature and significance of platelet products in human plasma.* Br J Haematol, 1967. **13**(3): p. 269-88.
260. Aaronson, S., et al., *Ultrastructure of intracellular and extracellular vesicles, membranes, and myelin figures produced by Ochromonas danica.* J Ultrastruct Res, 1971. **35**(5): p. 418-30.
261. Chivet, M., et al., *Emerging role of neuronal exosomes in the central nervous system.* Front Physiol, 2012. **3**: p. 145.
262. Konoshenko, M.Y., et al., *Isolation of Extracellular Vesicles: General Methodologies and Latest Trends.* Biomed Res Int, 2018. **2018**: p. 8545347.
263. Cocucci, E., G. Racchetti, and J. Meldolesi, *Shedding microvesicles: artefacts no more.* Trends Cell Biol, 2009. **19**(2): p. 43-51.
264. Raposo, G. and W. Stoorvogel, *Extracellular vesicles: exosomes, microvesicles, and friends.* J Cell Biol, 2013. **200**(4): p. 373-83.
265. Pan, B.T., et al., *Electron microscopic evidence for externalization of the transferrin receptor in vesicular form in sheep reticulocytes.* J Cell Biol, 1985. **101**(3): p. 942-8.
266. Harding, C., J. Heuser, and P. Stahl, *Receptor-mediated endocytosis of transferrin and recycling of the transferrin receptor in rat reticulocytes.* J Cell Biol, 1983. **97**(2): p. 329-39.

267. Johnstone, R.M., et al., *Vesicle formation during reticulocyte maturation. Association of plasma membrane activities with released vesicles (exosomes).* J Biol Chem, 1987. **262**(19): p. 9412-20.
268. Faure, J., et al., *Exosomes are released by cultured cortical neurones.* Mol Cell Neurosci, 2006. **31**(4): p. 642-8.
269. Zitvogel, L., et al., *Eradication of established murine tumors using a novel cell-free vaccine: dendritic cell-derived exosomes.* Nat Med, 1998. **4**(5): p. 594-600.
270. Raposo, G., et al., *B lymphocytes secrete antigen-presenting vesicles.* J Exp Med, 1996. **183**(3): p. 1161-72.
271. Wolfers, J., et al., *Tumor-derived exosomes are a source of shared tumor rejection antigens for CTL cross-priming.* Nat Med, 2001. **7**(3): p. 297-303.
272. van Niel, G., et al., *Intestinal epithelial cells secrete exosome-like vesicles.* Gastroenterology, 2001. **121**(2): p. 337-49.
273. Leung, K.F., J.B. Dacks, and M.C. Field, *Evolution of the multivesicular body ESCRT machinery; retention across the eukaryotic lineage.* Traffic, 2008. **9**(10): p. 1698-716.
274. Hanson, P.I. and A. Cashikar, *Multivesicular body morphogenesis.* Annu Rev Cell Dev Biol, 2012. **28**: p. 337-62.
275. Hurley, J.H. and P.I. Hanson, *Membrane budding and scission by the ESCRT machinery: it's all in the neck.* Nat Rev Mol Cell Biol, 2010. **11**(8): p. 556-66.
276. Wollert, T. and J.H. Hurley, *Molecular mechanism of multivesicular body biogenesis by ESCRT complexes.* Nature, 2010. **464**(7290): p. 864-9.
277. Schmidt, O. and D. Teis, *The ESCRT machinery.* Curr Biol, 2012. **22**(4): p. R116-20.
278. McCullough, J., et al., *ALIX-CHMP4 interactions in the human ESCRT pathway.* Proc Natl Acad Sci U S A, 2008. **105**(22): p. 7687-91.
279. Katoh, K., et al., *The ALG-2-interacting protein Alix associates with CHMP4b, a human homologue of yeast Snf7 that is involved in multivesicular body sorting.* J Biol Chem, 2003. **278**(40): p. 39104-13.
280. Baietti, M.F., et al., *Syndecan-syntenin-ALIX regulates the biogenesis of exosomes.* Nat Cell Biol, 2012. **14**(7): p. 677-85.

281. Roucourt, B., et al., *Heparanase activates the syndecan-syntenin-ALIX exosome pathway.* Cell Res, 2015. **25**(4): p. 412-28.
282. Wollert, T., et al., *Membrane scission by the ESCRT-III complex.* Nature, 2009. **458**(7235): p. 172-7.
283. Adell, M.A., et al., *Coordinated binding of Vps4 to ESCRT-III drives membrane neck constriction during MVB vesicle formation.* J Cell Biol, 2014. **205**(1): p. 33-49.
284. Stuffers, S., et al., *Multivesicular endosome biogenesis in the absence of ESCRTs.* Traffic, 2009. **10**(7): p. 925-37.
285. Yanez-Mo, M., et al., *Tetraspanin-enriched microdomains: a functional unit in cell plasma membranes.* Trends Cell Biol, 2009. **19**(9): p. 434-46.
286. Hemler, M.E., *Tetraspanin functions and associated microdomains.* Nat Rev Mol Cell Biol, 2005. **6**(10): p. 801-11.
287. Charrin, S., et al., *Lateral organization of membrane proteins: tetraspanins spin their web.* Biochem J, 2009. **420**(2): p. 133-54.
288. Andreu, Z. and M. Yanez-Mo, *Tetraspanins in extracellular vesicle formation and function.* Front Immunol, 2014. **5**: p. 442.
289. Chairoungdua, A., et al., *Exosome release of beta-catenin: a novel mechanism that antagonizes Wnt signaling.* J Cell Biol, 2010. **190**(6): p. 1079-91.
290. van Niel, G., et al., *The tetraspanin CD63 regulates ESCRT-independent and -dependent endosomal sorting during melanogenesis.* Dev Cell, 2011. **21**(4): p. 708-21.
291. Pols, M.S. and J. Klumperman, *Trafficking and function of the tetraspanin CD63.* Exp Cell Res, 2009. **315**(9): p. 1584-92.
292. Savina, A., M. Vidal, and M.I. Colombo, *The exosome pathway in K562 cells is regulated by Rab11.* J Cell Sci, 2002. **115**(Pt 12): p. 2505-15.
293. Savina, A., et al., *Rab11 promotes docking and fusion of multivesicular bodies in a calcium-dependent manner.* Traffic, 2005. **6**(2): p. 131-43.
294. Messenger, S.W., et al., *A Ca(2+)-stimulated exosome release pathway in cancer cells is regulated by Munc13-4.* J Cell Biol, 2018. **217**(8): p. 2877-2890.

295. Taylor, J., et al., *Ca(2+) mediates extracellular vesicle biogenesis through alternate pathways in malignancy.* J Extracell Vesicles, 2020. **9**(1): p. 1734326.
296. Yuyama, K., et al., *Sphingolipid-modulated exosome secretion promotes clearance of amyloid-beta by microglia.* J Biol Chem, 2012. **287**(14): p. 10977-89.
297. Kosaka, N., et al., *Secretory mechanisms and intercellular transfer of microRNAs in living cells.* J Biol Chem, 2010. **285**(23): p. 17442-52.
298. Hoshino, D., et al., *Exosome secretion is enhanced by invadopodia and drives invasive behavior.* Cell Rep, 2013. **5**(5): p. 1159-68.
299. Dreux, M., et al., *Short-range exosomal transfer of viral RNA from infected cells to plasmacytoid dendritic cells triggers innate immunity.* Cell Host Microbe, 2012. **12**(4): p. 558-70.
300. Phuyal, S., et al., *Regulation of exosome release by glycosphingolipids and flotillins.* FEBS J, 2014. **281**(9): p. 2214-27.
301. Colombo, M., et al., *Analysis of ESCRT functions in exosome biogenesis, composition and secretion highlights the heterogeneity of extracellular vesicles.* J Cell Sci, 2013. **126**(Pt 24): p. 5553-65.
302. Milhas, D., et al., *Anterograde and retrograde transport of neutral sphingomyelinase-2 between the Golgi and the plasma membrane.* Biochim Biophys Acta, 2010. **1801**(12): p. 1361-74.
303. Hannun, Y.A. and L.M. Obeid, *The Ceramide-centric universe of lipid-mediated cell regulation: stress encounters of the lipid kind.* J Biol Chem, 2002. **277**(29): p. 25847-50.
304. Laulagnier, K., et al., *Mast cell- and dendritic cell-derived exosomes display a specific lipid composition and an unusual membrane organization.* Biochem J, 2004. **380**(Pt 1): p. 161-71.
305. Ghossoub, R., et al., *Syntenin-ALIX exosome biogenesis and budding into multivesicular bodies are controlled by ARF6 and PLD2.* Nat Commun, 2014. **5**: p. 3477.
306. Kooijman, E.E., et al., *Modulation of membrane curvature by phosphatidic acid and lysophosphatidic acid.* Traffic, 2003. **4**(3): p. 162-74.

307. Hessvik, N.P., et al., *PIKfyve inhibition increases exosome release and induces secretory autophagy.* Cell Mol Life Sci, 2016. **73**(24): p. 4717-4737.
308. Wubbolts, R., et al., *Proteomic and biochemical analyses of human B cell-derived exosomes. Potential implications for their function and multivesicular body formation.* J Biol Chem, 2003. **278**(13): p. 10963-72.
309. Llorente, A., et al., *Molecular lipidomics of exosomes released by PC-3 prostate cancer cells.* Biochim Biophys Acta, 2013. **1831**(7): p. 1302-9.
310. Strauss, K., et al., *Exosome secretion ameliorates lysosomal storage of cholesterol in Niemann-Pick type C disease.* J Biol Chem, 2010. **285**(34): p. 26279-88.
311. Tan, S.S., et al., *Therapeutic MSC exosomes are derived from lipid raft microdomains in the plasma membrane.* J Extracell Vesicles, 2013. **2**.
312. Zwaal, R.F. and A.J. Schroit, *Pathophysiologic implications of membrane phospholipid asymmetry in blood cells.* Blood, 1997. **89**(4): p. 1121-32.
313. Taylor, J. and M. Bebawy, *Proteins Regulating Microvesicle Biogenesis and Multidrug Resistance in Cancer.* Proteomics, 2019. **19**(1-2): p. e1800165.
314. Hugel, B., et al., *Membrane microparticles: two sides of the coin.* Physiology (Bethesda), 2005. **20**: p. 22-7.
315. Pollet, H., et al., *Plasma Membrane Lipid Domains as Platforms for Vesicle Biogenesis and Shedding?* Biomolecules, 2018. **8**(3).
316. Dachary-Prigent, J., et al., *Annexin V as a probe of aminophospholipid exposure and platelet membrane vesiculation: a flow cytometry study showing a role for free sulfhydryl groups.* Blood, 1993. **81**(10): p. 2554-65.
317. Arraud, N., et al., *Extracellular vesicles from blood plasma: determination of their morphology, size, phenotype and concentration.* J Thromb Haemost, 2014. **12**(5): p. 614-27.
318. Connor, D.E., et al., *The majority of circulating platelet-derived microparticles fail to bind annexin V, lack phospholipid-dependent procoagulant activity and demonstrate greater expression of glycoprotein Ib.* Thromb Haemost, 2010. **103**(5): p. 1044-52.

319. van den Bogaart, G., et al., *Membrane protein sequestering by ionic protein-lipid interactions.* Nature, 2011. **479**(7374): p. 552-5.
320. Raucher, D., et al., *Phosphatidylinositol 4,5-bisphosphate functions as a second messenger that regulates cytoskeleton-plasma membrane adhesion.* Cell, 2000. **100**(2): p. 221-8.
321. Logan, M.R. and C.A. Mandato, *Regulation of the actin cytoskeleton by PIP2 in cytokinesis.* Biol Cell, 2006. **98**(6): p. 377-88.
322. Wang, Y., et al., *Loss of PIP5KIgamma, unlike other PIP5KI isoforms, impairs the integrity of the membrane cytoskeleton in murine megakaryocytes.* J Clin Invest, 2008. **118**(2): p. 812-9.
323. Sheetz, M.P., J.E. Sable, and H.G. Dobereiner, *Continuous membrane-cytoskeleton adhesion requires continuous accommodation to lipid and cytoskeleton dynamics.* Annu Rev Biophys Biomol Struct, 2006. **35**: p. 417-34.
324. Bianco, F., et al., *Acid sphingomyelinase activity triggers microparticle release from glial cells.* EMBO J, 2009. **28**(8): p. 1043-54.
325. Wang, J., U.R. Pendurthi, and L.V.M. Rao, *Sphingomyelin encrypts tissue factor: ATP-induced activation of A-SMase leads to tissue factor decryption and microvesicle shedding.* Blood Adv, 2017. **1**(13): p. 849-862.
326. Menck, K., et al., *Neutral sphingomyelinases control extracellular vesicles budding from the plasma membrane.* J Extracell Vesicles, 2017. **6**(1): p. 1378056.
327. Willms, E., et al., *Extracellular Vesicle Heterogeneity: Subpopulations, Isolation Techniques, and Diverse Functions in Cancer Progression.* Front Immunol, 2018. **9**: p. 738.
328. Beer, K.B., et al., *Extracellular vesicle budding is inhibited by redundant regulators of TAT-5 flippase localization and phospholipid asymmetry.* Proc Natl Acad Sci U S A, 2018. **115**(6): p. E1127-E1136.
329. von Schwedler, U.K., et al., *The protein network of HIV budding.* Cell, 2003. **114**(6): p. 701-13.
330. Garrus, J.E., et al., *Tsg101 and the vacuolar protein sorting pathway are essential for HIV-1 budding.* Cell, 2001. **107**(1): p. 55-65.

331. Bieniasz, P.D., *The cell biology of HIV-1 virion genesis.* Cell Host Microbe, 2009. **5**(6): p. 550-8.
332. Nabhan, J.F., et al., *Formation and release of arrestin domain-containing protein 1-mediated microvesicles (ARMMs) at plasma membrane by recruitment of TSG101 protein.* Proc Natl Acad Sci U S A, 2012. **109**(11): p. 4146-51.
333. Kowal, J., et al., *Proteomic comparison defines novel markers to characterize heterogeneous populations of extracellular vesicle subtypes.* Proc Natl Acad Sci U S A, 2016. **113**(8): p. E968-77.
334. Yoshioka, Y., et al., *Comparative marker analysis of extracellular vesicles in different human cancer types.* J Extracell Vesicles, 2013. **2**.
335. Mathivanan, S. and R.J. Simpson, *ExoCarta: A compendium of exosomal proteins and RNA.* Proteomics, 2009. **9**(21): p. 4997-5000.
336. Menzies, F.M., K. Moreau, and D.C. Rubinsztein, *Protein misfolding disorders and macroautophagy.* Curr Opin Cell Biol, 2011. **23**(2): p. 190-7.
337. Levine, B. and G. Kroemer, *Autophagy in the pathogenesis of disease.* Cell, 2008. **132**(1): p. 27-42.
338. Komatsu, M., et al., *Loss of autophagy in the central nervous system causes neurodegeneration in mice.* Nature, 2006. **441**(7095): p. 880-4.
339. Baixauli, F., C. Lopez-Otin, and M. Mittelbrunn, *Exosomes and autophagy: coordinated mechanisms for the maintenance of cellular fitness.* Front Immunol, 2014. **5**: p. 403.
340. Eitan, E., et al., *Impact of lysosome status on extracellular vesicle content and release.* Ageing Res Rev, 2016. **32**: p. 65-74.
341. Miranda, A.M., et al., *Neuronal lysosomal dysfunction releases exosomes harboring APP C-terminal fragments and unique lipid signatures.* Nat Commun, 2018. **9**(1): p. 291.
342. Yang, Y., et al., *Secretory carrier membrane protein 5 is an autophagy inhibitor that promotes the secretion of alpha-synuclein via exosome.* PLoS ONE [Electronic Resource]. **12**(7): p. e0180892.

343. Poehler, A.M., et al., *Autophagy modulates SNCA/alpha-synuclein release, thereby generating a hostile microenvironment.* Autophagy, 2014. **10**(12): p. 2171-92.
344. Lee, J.Y. and H.S. Kim, *Extracellular Vesicles in Neurodegenerative Diseases: A Double-Edged Sword.* Tissue Eng Regen Med, 2017. **14**(6): p. 667-678.
345. Emmanouilidou, E., et al., *Cell-produced alpha-synuclein is secreted in a calcium-dependent manner by exosomes and impacts neuronal survival.* J Neurosci, 2010. **30**(20): p. 6838-51.
346. Rajendran, L., et al., *Alzheimer's disease beta-amyloid peptides are released in association with exosomes.* Proc Natl Acad Sci U S A, 2006. **103**(30): p. 11172-7.
347. Saman, S., et al., *Exosome-associated tau is secreted in tauopathy models and is selectively phosphorylated in cerebrospinal fluid in early Alzheimer disease.* J Biol Chem, 2012. **287**(6): p. 3842-9.
348. Joshi, P., et al., *Extracellular vesicles in Alzheimer's disease: friends or foes? Focus on abeta-vesicle interaction.* Int J Mol Sci, 2015. **16**(3): p. 4800-13.
349. Ghidoni, R., L. Benussi, and G. Binetti, *Exosomes: the Trojan horses of neurodegeneration.* Med Hypotheses, 2008. **70**(6): p. 1226-7.
350. Bellingham, S.A., et al., *Exosomes: vehicles for the transfer of toxic proteins associated with neurodegenerative diseases?* Front Physiol, 2012. **3**: p. 124.
351. Yang, Y., et al., *Secretory carrier membrane protein 5 is an autophagy inhibitor that promotes the secretion of alpha-synuclein via exosome.* PLoS One, 2017. **12**(7): p. e0180892.
352. Ferreira, J.V., et al., *Exosomes and STUB1/CHIP cooperate to maintain intracellular proteostasis.* PLoS One, 2019. **14**(10): p. e0223790.
353. Laulagnier, K., et al., *Amyloid precursor protein products concentrate in a subset of exosomes specifically endocytosed by neurons.* Cell Mol Life Sci, 2017.
354. Polanco, J.C., et al., *Extracellular Vesicles Isolated from the Brains of rTg4510 Mice Seed Tau Protein Aggregation in a Threshold-dependent Manner.* J Biol Chem, 2016. **291**(24): p. 12445-66.

355. Kokubo, H., et al., *Part of membrane-bound Abeta exists in rafts within senile plaques in Tg2576 mouse brain.* Neurobiol Aging, 2005. **26**(4): p. 409-18.
356. Danzer, K.M., et al., *Exosomal cell-to-cell transmission of alpha synuclein oligomers.* Mol Neurodegener, 2012. **7**: p. 42.
357. Ngolab, J., et al., *Brain-derived exosomes from dementia with Lewy bodies propagate alpha-synuclein pathology.* Acta Neuropathol Commun, 2017. **5**(1): p. 46.
358. Lee, H.J., S. Patel, and S.J. Lee, *Intravesicular localization and exocytosis of alpha-synuclein and its aggregates.* J Neurosci, 2005. **25**(25): p. 6016-24.
359. Xia, Y., et al., *Microglia as modulators of exosomal alpha-synuclein transmission.* Cell Death Dis, 2019. **10**(3): p. 174.
360. Kreutzberg, G.W., *Microglia: a sensor for pathological events in the CNS.* Trends Neurosci, 1996. **19**(8): p. 312-8.
361. Ransohoff, R.M. and V.H. Perry, *Microglial physiology: unique stimuli, specialized responses.* Annu Rev Immunol, 2009. **27**: p. 119-45.
362. Kim, Y.S. and T.H. Joh, *Microglia, major player in the brain inflammation: their roles in the pathogenesis of Parkinson's disease.* Exp Mol Med, 2006. **38**(4): p. 333-47.
363. Tansey, M.G. and M.S. Goldberg, *Neuroinflammation in Parkinson's disease: its role in neuronal death and implications for therapeutic intervention.* Neurobiol Dis, 2010. **37**(3): p. 510-8.
364. Zhang, X., et al., *Potential Transfer of Polyglutamine and CAG-Repeat RNA in Extracellular Vesicles in Huntington's Disease: Background and Evaluation in Cell Culture.* Cellular & Molecular Neurobiology. **36**(3): p. 459-70.
365. Trajkovic, K., H. Jeong, and D. Krainc, *Mutant Huntingtin Is Secreted via a Late Endosomal/Lysosomal Unconventional Secretory Pathway.* J Neurosci, 2017. **37**(37): p. 9000-9012.
366. Carra, S., S.J. Seguin, and J. Landry, *HspB8 and Bag3: a new chaperone complex targeting misfolded proteins to macroautophagy.* Autophagy, 2008. **4**(2): p. 237-9.

367. Zhang, X., et al., *Potential Transfer of Polyglutamine and CAG-Repeat RNA in Extracellular Vesicles in Huntington's Disease: Background and Evaluation in Cell Culture.* Cell Mol Neurobiol, 2016. **36**(3): p. 459-70.
368. Diaz-Hidalgo, L., et al., *Transglutaminase type 2-dependent selective recruitment of proteins into exosomes under stressful cellular conditions.* Biochim Biophys Acta, 2016. **1863**(8): p. 2084-92.
369. Braun, J.E., S.M. Wilbanks, and R.H. Scheller, *The cysteine string secretory vesicle protein activates Hsc70 ATPase.* J Biol Chem, 1996. **271**(42): p. 25989-93.
370. Deng, J., et al., *Neurons Export Extracellular Vesicles Enriched in Cysteine String Protein and Misfolded Protein Cargo.* Sci Rep, 2017. **7**(1): p. 956.
371. Fontaine, S.N., et al., *DnaJ/Hsc70 chaperone complexes control the extracellular release of neurodegenerative-associated proteins.* EMBO J, 2016. **35**(14): p. 1537-49.
372. Hong, Y., et al., *Mutant Huntingtin Inhibits alphaB-Crystallin Expression and Impairs Exosome Secretion from Astrocytes.* Journal of Neuroscience. **37**(39): p. 9550-9563.
373. Imura, T., et al., *Differential expression of small heat shock proteins in reactive astrocytes after focal ischemia: possible role of beta-adrenergic receptor.* J Neurosci, 1999. **19**(22): p. 9768-79.
374. Waudby, C.A., et al., *The interaction of alphaB-crystallin with mature alpha-synuclein amyloid fibrils inhibits their elongation.* Biophys J, 2010. **98**(5): p. 843-51.
375. Rekas, A., et al., *Interaction of the molecular chaperone alphaB-crystallin with alpha-synuclein: effects on amyloid fibril formation and chaperone activity.* J Mol Biol, 2004. **340**(5): p. 1167-83.
376. Muchowski, P.J., et al., *Noninvasive measurement of protein aggregation by mutant huntingtin fragments or alpha-synuclein in the lens.* J Biol Chem, 2008. **283**(10): p. 6330-6.

377. Hochberg, G.K., et al., *The structured core domain of alphaB-crystallin can prevent amyloid fibrillation and associated toxicity.* Proc Natl Acad Sci U S A, 2014. **111**(16): p. E1562-70.
378. Gangalum, R.K., et al., *Inhibition of the Expression of the Small Heat Shock Protein alphaB-Crystallin Inhibits Exosome Secretion in Human Retinal Pigment Epithelial Cells in Culture.* J Biol Chem, 2016. **291**(25): p. 12930-42.
379. Lee, M., et al., *Exosomes from adipose-derived stem cells ameliorate phenotype of Huntington's disease in vitro model.* European Journal of Neuroscience. **44**(4): p. 2114-9.
380. Carmo, C., et al., *Mitochondrial Dysfunction in Huntington's Disease.* Adv Exp Med Biol, 2018. **1049**: p. 59-83.
381. St-Pierre, J., et al., *Suppression of reactive oxygen species and neurodegeneration by the PGC-1 transcriptional coactivators.* Cell, 2006. **127**(2): p. 397-408.
382. McGill, J.K. and M.F. Beal, *PGC-1alpha, a new therapeutic target in Huntington's disease?* Cell, 2006. **127**(3): p. 465-8.
383. Tomlinson, P.R., et al., *Identification of distinct circulating exosomes in Parkinson's disease.* Ann Clin Transl Neurol, 2015. **2**(4): p. 353-61.
384. Grey, M., et al., *Acceleration of alpha-synuclein aggregation by exosomes.* J Biol Chem, 2015. **290**(5): p. 2969-82.
385. An, K., et al., *Exosomes neutralize synaptic-plasticity-disrupting activity of Abeta assemblies in vivo.* Mol Brain, 2013. **6**: p. 47.
386. Shao, H., et al., *New Technologies for Analysis of Extracellular Vesicles.* Chem Rev, 2018. **118**(4): p. 1917-1950.
387. Erdbrugger, U. and J. Lannigan, *Analytical challenges of extracellular vesicle detection: A comparison of different techniques.* Cytometry A, 2016. **89**(2): p. 123-34.
388. Margolis, L. and Y. Sadovsky, *The biology of extracellular vesicles: The known unknowns.* PLoS Biol, 2019. **17**(7): p. e3000363.
389. Thery, C., et al., *Minimal information for studies of extracellular vesicles 2018 (MISEV2018): a position statement of the International Society for Extracellular*

Vesicles and update of the MISEV2014 guidelines. J Extracell Vesicles, 2018. **7**(1): p. 1535750.

390. Chiang, C.Y. and C. Chen, *Toward characterizing extracellular vesicles at a single-particle level.* J Biomed Sci, 2019. **26**(1): p. 9.
391. Buzas, E.I., et al., *Single particle analysis: Methods for detection of platelet extracellular vesicles in suspension (excluding flow cytometry).* Platelets, 2017. **28**(3): p. 249-255.
392. Rosa-Fernandes, L., et al., *A Perspective on Extracellular Vesicles Proteomics.* Front Chem, 2017. **5**: p. 102.
393. Gross, J., et al., *Nanoparticle tracking analysis of particle size and concentration detection in suspensions of polymer and protein samples: Influence of experimental and data evaluation parameters.* Eur J Pharm Biopharm, 2016. **104**: p. 30-41.
394. Filipe, V., A. Hawe, and W. Jiskoot, *Critical evaluation of Nanoparticle Tracking Analysis (NTA) by NanoSight for the measurement of nanoparticles and protein aggregates.* Pharm Res, 2010. **27**(5): p. 796-810.
395. Gardiner, C., et al., *Extracellular vesicle sizing and enumeration by nanoparticle tracking analysis.* J Extracell Vesicles, 2013. **2**.
396. Parsons, M.E.M., et al., *A Protocol for Improved Precision and Increased Confidence in Nanoparticle Tracking Analysis Concentration Measurements between 50 and 120 nm in Biological Fluids.* Front Cardiovasc Med, 2017. **4**: p. 68.
397. Szatanek, R., et al., *The Methods of Choice for Extracellular Vesicles (EVs) Characterization.* Int J Mol Sci, 2017. **18**(6).
398. Steen, H.B., *Flow cytometer for measurement of the light scattering of viral and other submicroscopic particles.* Cytometry A, 2004. **57**(2): p. 94-9.
399. Orozco, A.F. and D.E. Lewis, *Flow cytometric analysis of circulating microparticles in plasma.* Cytometry A, 2010. **77**(6): p. 502-14.
400. Inglis, H.C., et al., *Techniques to improve detection and analysis of extracellular vesicles using flow cytometry.* Cytometry A, 2015. **87**(11): p. 1052-63.

401. Inglis, H., P. Norris, and A. Danesh, *Techniques for the analysis of extracellular vesicles using flow cytometry.* J Vis Exp, 2015(97).
402. Freyssinet, J.M. and F. Toti, *Membrane microparticle determination: at least seeing what's being sized!* J Thromb Haemost, 2010. **8**(2): p. 311-4.
403. Lannigan, J. and U. Erdbruegger, *Imaging flow cytometry for the characterization of extracellular vesicles.* Methods, 2017. **112**: p. 55-67.
404. Ortyn, W.E., et al., *Sensitivity measurement and compensation in spectral imaging.* Cytometry A, 2006. **69**(8): p. 852-62.
405. Basiji, D.A., *Principles of Amnis Imaging Flow Cytometry.* Methods Mol Biol, 2016. **1389**: p. 13-21.
406. Erdbrugger, U., et al., *Imaging flow cytometry elucidates limitations of microparticle analysis by conventional flow cytometry.* Cytometry A, 2014. **85**(9): p. 756-70.
407. van der Pol, E., et al., *Single vs. swarm detection of microparticles and exosomes by flow cytometry.* J Thromb Haemost, 2012. **10**(5): p. 919-30.
408. Witwer, K.W., et al., *Standardization of sample collection, isolation and analysis methods in extracellular vesicle research.* J Extracell Vesicles, 2013. **2**.
409. Shantsila, E., et al., *Circulating microparticles: challenges and perspectives of flow cytometric assessment.* Thromb Haemost, 2014. **111**(6): p. 1009-14.
410. Lobb, R.J., et al., *Optimized exosome isolation protocol for cell culture supernatant and human plasma.* J Extracell Vesicles, 2015. **4**: p. 27031.
411. Simonsen, J.B., *A liposome-based size calibration method for measuring microvesicles by flow cytometry.* J Thromb Haemost, 2016. **14**(1): p. 186-90.
412. Stoner, S.A., et al., *High sensitivity flow cytometry of membrane vesicles.* Cytometry A, 2016. **89**(2): p. 196-206.
413. Brittain, G.C.t., et al., *A Novel Semiconductor-Based Flow Cytometer with Enhanced Light-Scatter Sensitivity for the Analysis of Biological Nanoparticles.* Sci Rep, 2019. **9**(1): p. 16039.
414. Lawrence, W.G., et al., *Enhanced red and near infrared detection in flow cytometry using avalanche photodiodes.* Cytometry A, 2008. **73**(8): p. 767-76.

415. Colombo, M., G. Raposo, and C. Thery, *Biogenesis, secretion, and intercellular interactions of exosomes and other extracellular vesicles.* Annu Rev Cell Dev Biol, 2014. **30**: p. 255-89.
416. Li, K., et al., *Cushioned-Density Gradient Ultracentrifugation (C-DGUC): A Refined and High Performance Method for the Isolation, Characterization, and Use of Exosomes.* Methods Mol Biol, 2018. **1740**: p. 69-83.
417. Brakke, M.K., *Zonal separations by density-gradient centrifugation.* Arch Biochem Biophys, 1953. **45**(2): p. 275-90.
418. Yuyama, K., N. Yamamoto, and K. Yanagisawa, *Accelerated release of exosome-associated GM1 ganglioside (GM1) by endocytic pathway abnormality: another putative pathway for GM1-induced amyloid fibril formation.* J Neurochem, 2008. **105**(1): p. 217-24.
419. Skryabin, G.O., et al., *Lipid Rafts in Exosome Biogenesis.* Biochemistry (Mosc), 2020. **85**(2): p. 177-191.
420. Rabesandratana, H., et al., *Decay-accelerating factor (CD55) and membrane inhibitor of reactive lysis (CD59) are released within exosomes during In vitro maturation of reticulocytes.* Blood, 1998. **91**(7): p. 2573-80.
421. Dinkins, M.B., G. Wang, and E. Bieberich, *Sphingolipid-Enriched Extracellular Vesicles and Alzheimer's Disease: A Decade of Research.* J Alzheimers Dis, 2017. **60**(3): p. 757-768.
422. Brewer, G.J., et al., *Optimized survival of hippocampal neurons in B27-supplemented Neurobasal, a new serum-free medium combination.* J Neurosci Res, 1993. **35**(5): p. 567-76.
423. Sciannamblo, M., et al., *Changes of the ganglioside pattern and content in human fibroblasts by high density cell population subculture progression.* Glycoconj J, 2002. **19**(3): p. 181-6.
424. Cromwell, C.R., et al., *Incorporation of bridged nucleic acids into CRISPR RNAs improves Cas9 endonuclease specificity.* Nat Commun, 2018. **9**(1): p. 1448.
425. Thery, C., et al., *Isolation and characterization of exosomes from cell culture supernatants and biological fluids.* Curr Protoc Cell Biol, 2006. **Chapter 3**: p. Unit 3 22.

426. Rauvala, H., *Monomer-micelle transition of the ganglioside GM1 and the hydrolysis by Clostridium perfringens neuraminidase.* Eur J Biochem, 1979. **97**(2): p. 555-64.
427. Lee, K.J., et al., *Modulation of nonspecific binding in ultrafiltration protein binding studies.* Pharm Res, 2003. **20**(7): p. 1015-21.
428. Coleman, B.M., et al., *Prion-infected cells regulate the release of exosomes with distinct ultrastructural features.* FASEB J, 2012. **26**(10): p. 4160-73.
429. Li, P., et al., *Progress in Exosome Isolation Techniques.* Theranostics, 2017. **7**(3): p. 789-804.
430. Carrasco-Ramirez, P., et al., *Podoplanin is a component of extracellular vesicles that reprograms cell-derived exosomal proteins and modulates lymphatic vessel formation.* Oncotarget, 2016. **7**(13): p. 16070-89.
431. Wallace, P.K., et al., *Tracking antigen-driven responses by flow cytometry: monitoring proliferation by dye dilution.* Cytometry A, 2008. **73**(11): p. 1019-34.
432. Momen-Heravi, F., et al., *Current methods for the isolation of extracellular vesicles.* Biol Chem, 2013. **394**(10): p. 1253-62.
433. Mathivanan, S., et al., *ExoCarta 2012: database of exosomal proteins, RNA and lipids.* Nucleic Acids Res, 2012. **40**(Database issue): p. D1241-4.
434. Lotvall, J., et al., *Minimal experimental requirements for definition of extracellular vesicles and their functions: a position statement from the International Society for Extracellular Vesicles.* J Extracell Vesicles, 2014. **3**: p. 26913.
435. Linares, R., et al., *High-speed centrifugation induces aggregation of extracellular vesicles.* J Extracell Vesicles, 2015. **4**: p. 29509.
436. Stoorvogel, W., *Resolving sorting mechanisms into exosomes.* Cell Res, 2015. **25**(5): p. 531-2.
437. Wang, Y., et al., *The release and trans-synaptic transmission of Tau via exosomes.* Mol Neurodegener, 2017. **12**(1): p. 5.
438. Lehrich, B.M., et al., *Fetal Bovine Serum-Derived Extracellular Vesicles Persist within Vesicle-Depleted Culture Media.* Int J Mol Sci, 2018. **19**(11).

439. Shelke, G.V., et al., *Importance of exosome depletion protocols to eliminate functional and RNA-containing extracellular vesicles from fetal bovine serum.* J Extracell Vesicles, 2014. **3**.
440. Beninson, L.A. and M. Fleshner, *Exosomes in fetal bovine serum dampen primary macrophage IL-1beta response to lipopolysaccharide (LPS) challenge.* Immunol Lett, 2015. **163**(2): p. 187-92.
441. Shang, L., et al., *Nutrient starvation elicits an acute autophagic response mediated by Ulk1 dephosphorylation and its subsequent dissociation from AMPK.* Proc Natl Acad Sci U S A, 2011. **108**(12): p. 4788-93.
442. Livshits, M.A., et al., *Isolation of exosomes by differential centrifugation: Theoretical analysis of a commonly used protocol.* Sci Rep, 2015. **5**: p. 17319.
443. Tang, Y.T., et al., *Comparison of isolation methods of exosomes and exosomal RNA from cell culture medium and serum.* Int J Mol Med, 2017. **40**(3): p. 834-844.
444. Gudbergsson, J.M., et al., *Systematic review of factors influencing extracellular vesicle yield from cell cultures.* Cytotechnology, 2016. **68**(4): p. 579-92.
445. Gardiner, C., et al., *Techniques used for the isolation and characterization of extracellular vesicles: results of a worldwide survey.* J Extracell Vesicles, 2016. **5**: p. 32945.
446. Mol, E.A., et al., *Higher functionality of extracellular vesicles isolated using size-exclusion chromatography compared to ultracentrifugation.* Nanomedicine, 2017. **13**(6): p. 2061-2065.
447. Guerreiro, E.M., et al., *Efficient extracellular vesicle isolation by combining cell media modifications, ultrafiltration, and size-exclusion chromatography.* PLoS One, 2018. **13**(9): p. e0204276.
448. Oeyen, E., et al., *Ultrafiltration and size exclusion chromatography combined with asymmetrical-flow field-flow fractionation for the isolation and characterisation of extracellular vesicles from urine.* J Extracell Vesicles, 2018. **7**(1): p. 1490143.
449. Boing, A.N., et al., *Single-step isolation of extracellular vesicles by size-exclusion chromatography.* J Extracell Vesicles, 2014. **3**.

450. Monguio-Tortajada, M., et al., *Extracellular vesicle isolation methods: rising impact of size-exclusion chromatography.* Cell Mol Life Sci, 2019. **76**(12): p. 2369-2382.
451. Campos-Silva, C., et al., *High sensitivity detection of extracellular vesicles immune-captured from urine by conventional flow cytometry.* Sci Rep, 2019. **9**(1): p. 2042.
452. Dodge, J.C., et al., *Glycosphingolipids are modulators of disease pathogenesis in amyotrophic lateral sclerosis.* Proc Natl Acad Sci U S A, 2015. **112**(26): p. 8100-5.
453. Ariga, T., M.P. McDonald, and R.K. Yu, *Role of ganglioside metabolism in the pathogenesis of Alzheimer's disease--a review.* J Lipid Res, 2008. **49**(6): p. 1157-75.
454. Kracun, I., et al., *Human brain gangliosides in development, aging and disease.* Int J Dev Biol, 1991. **35**(3): p. 289-95.
455. Shayman, J.A., *The design and clinical development of inhibitors of glycosphingolipid synthesis: will invention be the mother of necessity?* Trans Am Clin Climatol Assoc, 2013. **124**: p. 46-60.
456. Lee, L., A. Abe, and J.A. Shayman, *Improved inhibitors of glucosylceramide synthase.* J Biol Chem, 1999. **274**(21): p. 14662-9.
457. Zhao, H., et al., *Inhibiting glycosphingolipid synthesis improves glycemic control and insulin sensitivity in animal models of type 2 diabetes.* Diabetes, 2007. **56**(5): p. 1210-8.
458. Hong, Y., et al., *Mutant Huntingtin Inhibits alphaB-Crystallin Expression and Impairs Exosome Secretion from Astrocytes.* J Neurosci, 2017. **37**(39): p. 9550-9563.
459. Gorgens, A., et al., *Optimisation of imaging flow cytometry for the analysis of single extracellular vesicles by using fluorescence-tagged vesicles as biological reference material.* J Extracell Vesicles, 2019. **8**(1): p. 1587567.
460. Volnoukhin, M. and B.P. Brandhorst, *Multispectral labeling of embryonic cells with lipophilic carbocyanine dyes.* Mol Reprod Dev, 2015. **82**(7-8): p. 619-24.

461. Gercel-Taylor, C., et al., *Nanoparticle analysis of circulating cell-derived vesicles in ovarian cancer patients.* Anal Biochem, 2012. **428**(1): p. 44-53.
462. Shen, W., et al., *Inhibition of glucosylceramide synthase stimulates autophagy flux in neurons.* J Neurochem, 2014. **129**(5): p. 884-94.
463. Ciechanover, A. and Y.T. Kwon, *Protein Quality Control by Molecular Chaperones in Neurodegeneration.* Front Neurosci, 2017. **11**: p. 185.
464. Takeuchi, T., et al., *Intercellular chaperone transmission via exosomes contributes to maintenance of protein homeostasis at the organismal level.* Proc Natl Acad Sci U S A, 2015. **112**(19): p. E2497-506.
465. Sardar Sinha, M., et al., *Alzheimer's disease pathology propagation by exosomes containing toxic amyloid-beta oligomers.* Acta Neuropathol, 2018. **136**(1): p. 41-56.
466. Eitan, E., et al., *Extracellular Vesicle-Associated Abeta Mediates Trans-Neuronal Bioenergetic and Ca(2+)-Handling Deficits in Alzheimer's Disease Models.* NPJ Aging Mech Dis, 2016. **2**.
467. Romancino, D.P., et al., *Palmitoylation is a post-translational modification of Alix regulating the membrane organization of exosome-like small extracellular vesicles.* Biochim Biophys Acta Gen Subj, 2018. **1862**(12): p. 2879-2887.
468. Kunadt, M., et al., *Extracellular vesicle sorting of alpha-Synuclein is regulated by sumoylation.* Acta Neuropathol, 2015. **129**(5): p. 695-713.
469. Yuyama, K., et al., *Decreased amyloid-beta pathologies by intracerebral loading of glycosphingolipid-enriched exosomes in Alzheimer model mice.* J Biol Chem, 2014. **289**(35): p. 24488-98.
470. Hands, S., et al., *In vitro and in vivo aggregation of a fragment of huntingtin protein directly causes free radical production.* J Biol Chem, 2011. **286**(52): p. 44512-20.
471. Akers, J.C., et al., *Biogenesis of extracellular vesicles (EV): exosomes, microvesicles, retrovirus-like vesicles, and apoptotic bodies.* J Neurooncol, 2013. **113**(1): p. 1-11.
472. Yeung, V., et al., *Rab35-dependent extracellular nanovesicles are required for induction of tumour supporting stroma.* Nanoscale, 2018. **10**(18): p. 8547-8559.

473. Klinkert, K. and A. Echard, *Rab35 GTPase: A Central Regulator of Phosphoinositides and F-actin in Endocytic Recycling and Beyond.* Traffic, 2016. **17**(10): p. 1063-77.
474. Hsu, C., et al., *Regulation of exosome secretion by Rab35 and its GTPase-activating proteins TBC1D10A-C.* J Cell Biol, 2010. **189**(2): p. 223-32.
475. Sharma, M., N. Naslavsky, and S. Caplan, *A role for EHD4 in the regulation of early endosomal transport.* Traffic, 2008. **9**(6): p. 995-1018.
476. Naslavsky, N. and S. Caplan, *EHD proteins: key conductors of endocytic transport.* Trends Cell Biol, 2011. **21**(2): p. 122-31.
477. Pfrieger, F.W. and N. Vitale, *Cholesterol and the journey of extracellular vesicles.* J Lipid Res, 2018. **59**(12): p. 2255-2261.
478. Moreno-Gonzalo, O., I. Fernandez-Delgado, and F. Sanchez-Madrid, *Post-translational add-ons mark the path in exosomal protein sorting.* Cell Mol Life Sci, 2018. **75**(1): p. 1-19.
479. Liu, Z., et al., *Promotion of bone morphogenetic protein signaling by tetraspanins and glycosphingolipids.* PLoS Genet, 2015. **11**(5): p. e1005221.
480. de Gassart, A., et al., *Lipid raft-associated protein sorting in exosomes.* Blood, 2003. **102**(13): p. 4336-44.
481. Ohmi, Y., et al., *Gangliosides are essential in the protection of inflammation and neurodegeneration via maintenance of lipid rafts: elucidation by a series of ganglioside-deficient mutant mice.* J Neurochem, 2011. **116**(5): p. 926-35.
482. Willms, E., et al., *Cells release subpopulations of exosomes with distinct molecular and biological properties.* Sci Rep, 2016. **6**: p. 22519.
483. Catalano, M. and L. O'Driscoll, *Inhibiting extracellular vesicles formation and release: a review of EV inhibitors.* J Extracell Vesicles, 2020. **9**(1): p. 1703244.
484. Datta, A., et al., *Manumycin A suppresses exosome biogenesis and secretion via targeted inhibition of Ras/Raf/ERK1/2 signaling and hnRNP H1 in castration-resistant prostate cancer cells.* Cancer Lett, 2017. **408**: p. 73-81.
485. Fitzner, D., et al., *Selective transfer of exosomes from oligodendrocytes to microglia by macropinocytosis.* J Cell Sci, 2011. **124**(Pt 3): p. 447-58.

486. Svennerholm, L., *Chromatographic Separation of Human Brain Gangliosides.* J Neurochem, 1963. **10**: p. 613-23.
487. Cavdarli, S., et al., *Profiling of O-acetylated Gangliosides Expressed in Neuroectoderm Derived Cells.* Int J Mol Sci, 2020. **21**(1).
488. Mlinac, K. and S. Bognar, *Role of gangliosides in brain aging and neurodegeneration.* Translational Neuroscience, 2010. **1**(4).
489. Bates, G.P., et al., *Huntington disease.* Nat Rev Dis Primers, 2015. **1**: p. 15005.
490. Brundin, P., R. Melki, and R. Kopito, *Prion-like transmission of protein aggregates in neurodegenerative diseases.* Nat Rev Mol Cell Biol, 2010. **11**(4): p. 301-7.

SUPPLEMENTARY MATERIAL

Fig. S1: Isolation by ultracentrifugation recovers less than 10% of the total EV population in the pellet as determined by imaging flow cytometry.

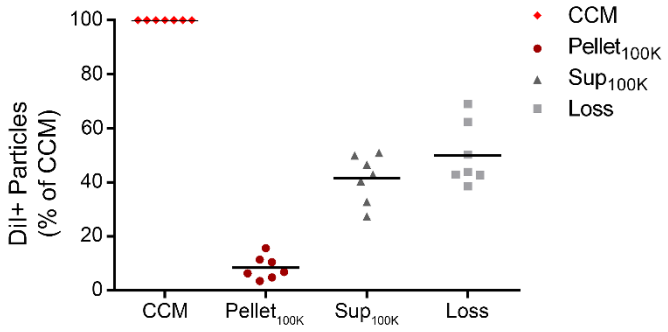

The number of EV particles present in the CCM, in the EV pellet ($Pellet_{100K}$) and in the supernatant (Sup_{100K}) obtained after ultracentrifugation at 100,000 x g were measured by IFC. Data are normalized over the number of DiI positive particles measured in the CCM and reported as its percentage. The percentage of DiI positive particles not recovered in either the $Pellet_{100K}$ or the Sup_{100K} are plotted as 'loss'. N=7 where N is the number of independent experiments. Six experiments have been performed by Anissa Viveiros, a former MSc student in the Posse de Chaves lab.

Fig. S2: Increasing the centrifugation time fails to pellet EVs efficiently

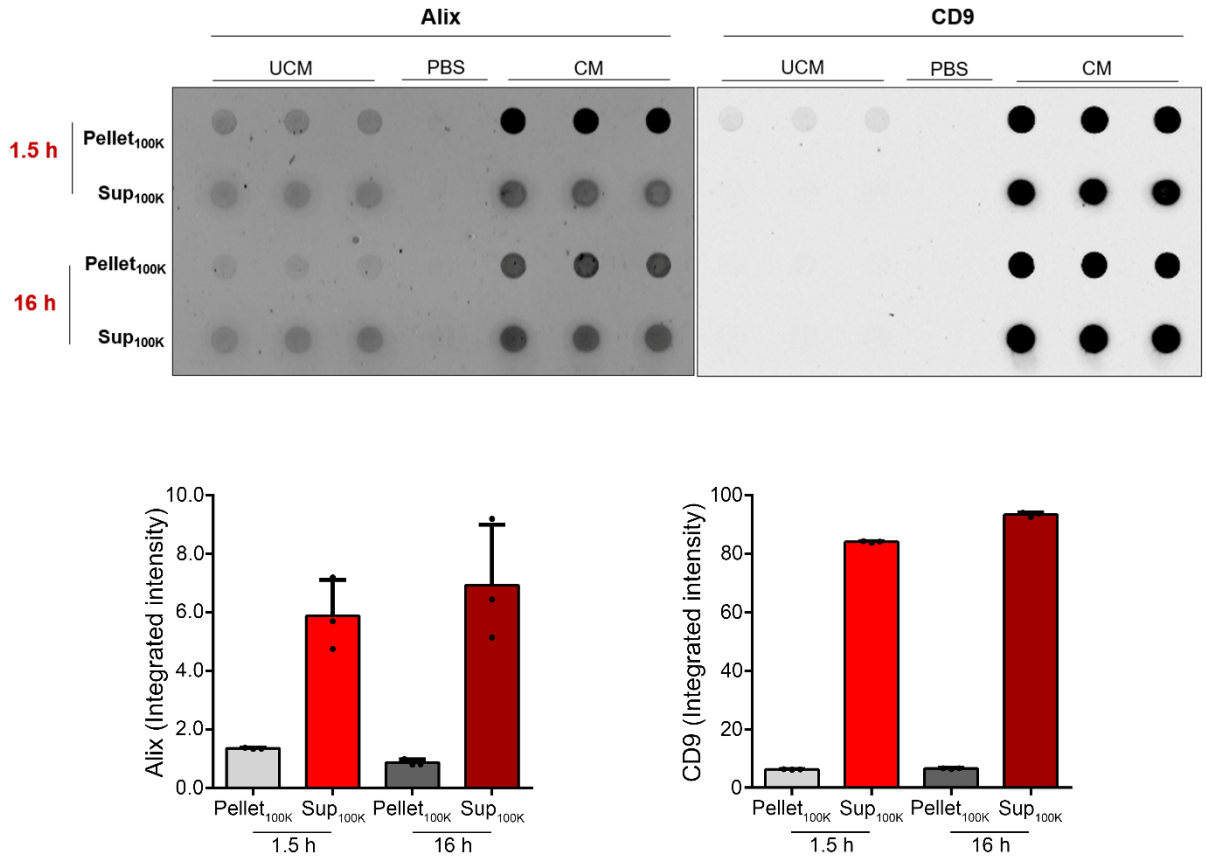

EVs from N2a cells conditioned in EVD complete medium (CM) were isolated by ultracentrifugation for 1.5 h, after which the supernatant recovered (Sup) was further subjected to ultracentrifugation for 16 h to pellet residual EVs. Equal volumes of the unconditioned EVD complete medium (UCM) was also processed in parallel. Dot blot and relative densitometric analyses for the EV markers Alix and CD9 in the EV pellet ($Pellet_{100K}$) and in the supernatant (Sup_{100K}) obtained by ultracentrifugations of the unconditioned medium (UCM) and medium conditioned by N2a cells (CM), both previously centrifuged at 2,000 x g to eliminate debris and apoptotic bodies. Equal fractions of the pellet were loaded in triplicates. Equal volumes of the supernatant

fractions were also loaded in triplicates. Bars show the average values ± SD of triplicates in the same experiment.

Fig. S3: The density of EVs from N2a cells is lower than the mean density of EVs required for efficient pelleting by ultracentrifugation

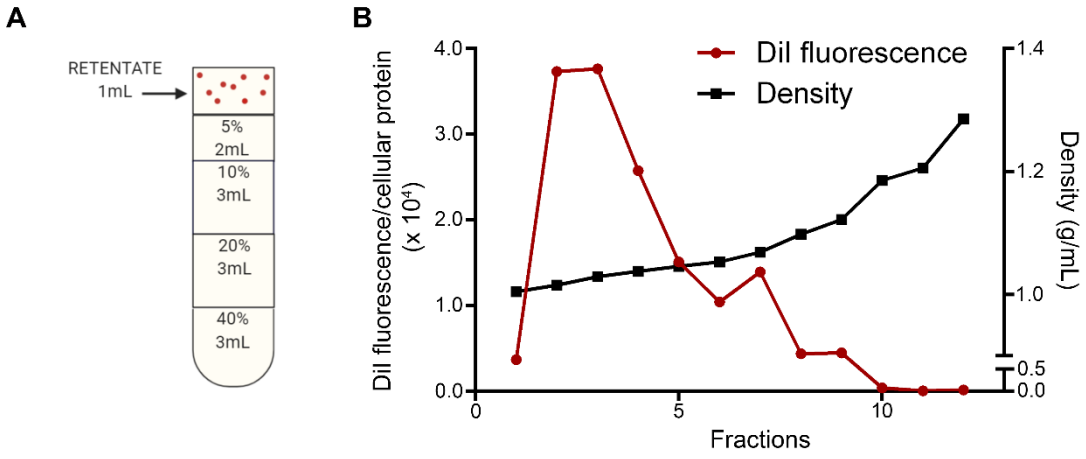

EVs from N2a cells collected in SFM+N2 for 24 h were isolated by OptiPrep™ density gradient centrifugation.

A. Schematic of a discontinuous iodixanol gradient in a polyallomer tube with the retentate loaded on top, used to separate EVs.

B. Representative histogram showing DiI fluorescence and density of fractions isolated by density gradient centrifugation. The experiment was replicated two more times with similar results by Anissa Viveiros, a former MSc student in the Posse de Chaves lab. The density of EVs from N2a cells is between 1.015 and 1.029 g/mL.

Fig. S4: Imaging flow cytometry results show that cell treatment with GM1 does not change the fluorescence signal in EV particles

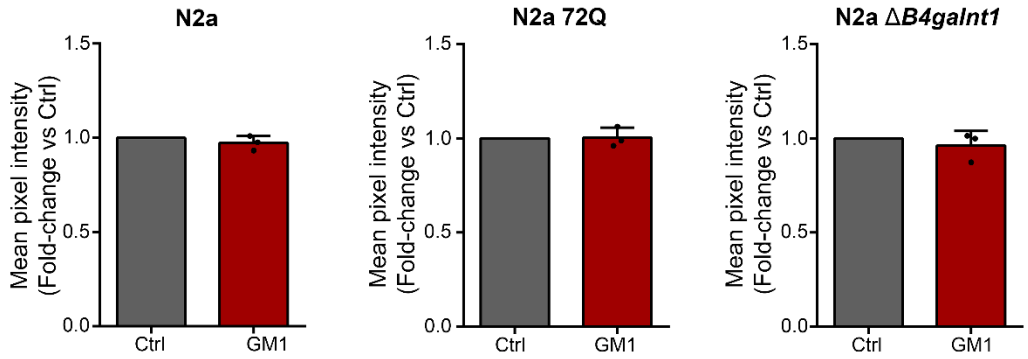

Mean pixel intensity of DiD positive particles in the CCM of N2a, N2a 72Q and N2a Δ*B4galnt1* cells treated with vehicle or GM1 for 6 h and collected in SFM+N2 for 16 h, detected by IFC. All data are expressed as fold-change over untreated Ctrl. Bars indicate mean values ± SD of three independent experiments for each genotype.

Fig. S5: GM1 promotes the secretion of EVs in neuronal cells, as determined by Cytoflex flow cytometry

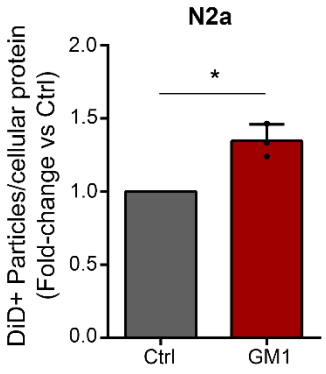

DiD positive particles in the CCM of N2a cells treated with vehicle or GM1 for 6 h and collected in SFM+N2 for 16 h, measured by Cytoflex flow cytometry. All data are normalized over total cellular protein content and are expressed as fold-change over untreated Ctrl. Bars indicate mean values ± SD of three independent experiments. Two-tailed paired *t*-test, *p<0.05.

Fig. S6: GM1 promotes the export of HTT via EVs secreted by transiently transfected N2a cells

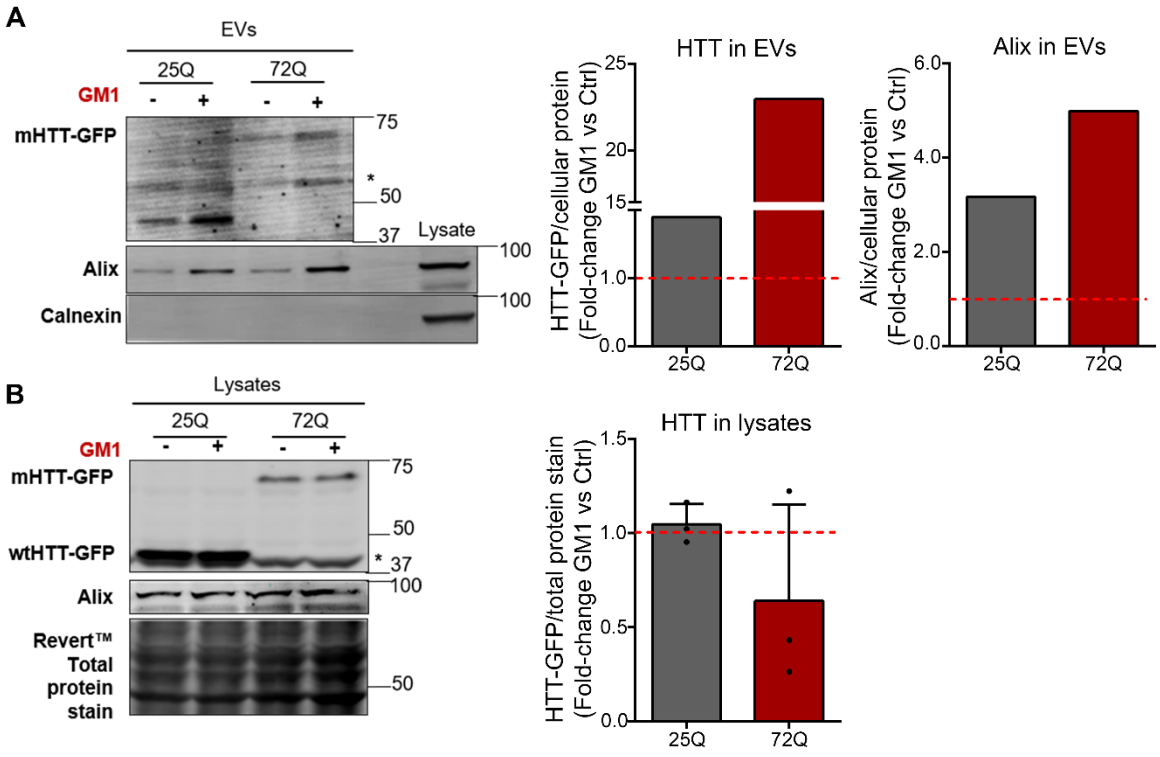

EVs from N2a cells transiently transfected with either HTT-Exon1(25Q)-EGFP (25Q) or HTT-Exon1(72Q)-EGFP (72Q) treated with vehicle or GM1 for 18 h were collected in EVD complete media for 24 h and isolated by UC.

A. Immunoblot for HTT and the EV marker Alix in EVs. Anti-calnexin antibody was used to control for the purity of the EV fractions (absence of cellular debris and apoptotic bodies). All data are normalized over total cellular protein content and expressed as fold-change over untreated Ctrl for each genotype (denoted by the red dotted line). The experiment was performed once.

B. Representative immunoblot and densitometric analysis of HTT and Alix in cell lysates. Data are normalized over total protein stain and expressed as fold-change over untreated Ctrl for each genotype. Bars indicate average densitometric values ± SD of three independent experiments for HTT. Immunoblotting for Alix was performed once.

* indicates a non-specific band. This experiment was performed by Dr. L.C. Morales, a former PhD student in the Sipione lab (unpublished data).

Fig. S7: Imaging flow cytometry results show that pharmacological inhibition of cellular ganglioside synthesis does not affect DiD incorporation into EV membranes

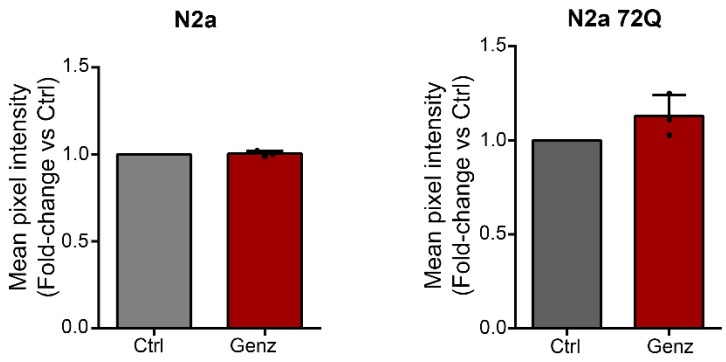

Mean pixel intensity of DiD positive particles detected by IFC in the CCM of N2a and N2a 72Q cells treated with vehicle or Genz-123346 for 48 h and collected in SFM+N2 for 24 h in the presence of the treatment. All data are expressed as fold-change over vehicle Ctrl. Bars indicate mean values ± SD of three independent experiments for each genotype.